NTNU – Trondheim
Norwegian University of
Science and Technology

Dynamic behavior of contact lines for railways with laboratorial model setup according to Norwegian conditions

Arnar Kári Hallgrímsson

Civil and Environmental Engineering (2 year)
Submission date: June 2013
Supervisor: Anders Rönnquist, KT

Norwegian University of Science and Technology
Department of Structural Engineering

Department of Structural Engineering
Faculty of Engineering Science and Technology
NTNU- Norwegian University of Science and Technology

ACCESSIBILITY

MASTER THESIS 2013

SUBJECT AREA:	DATE:	NO. OF PAGES:
Structural dynamics Railway technology	10.06.13	129(88+41)

TITLE:

Dynamic behavior of contact lines for railways with laboratorial model setup according to Norwegian conditions

Dynamisk oppførsel til kontaktledningsanlegg ved laboratoriemodellering etter norske forhold

BY:

Arnar Kári Hallgrímsson

SUMMARY:
Some domestic flight routes in Norway rank among the busiest in Europe. Experience has shown that, in countries such as France and Germany, high velocity trains can be preferable to flying, given that the distance is not too great (usually under 1000km). The domestic flight routes mentioned are all under that limit and therefore, there is great interest for increasing velocities of trains travelling in Norway. The biggest barrier for this purpose is the dynamic behaviour of the catenary--pantograph system, which is the system supplying power to the train. This thesis covers the modelling of that system, experimentally and numerically.

The catenary--pantograph system mainly consists of a messenger wire, contact wire and a pantograph. Electrical power is transmitted from the contact wire through the pantograph to the train's engine. Consistent contact between the pantograph's head and contact wire is vital for the train to operate at high velocities. Too much or too little contact leads to increased wear in the system. In order to examine the performance of the system, the contact force is defined, i.e. the force at the point of contact. This force is one of the most important property of the system and the aim of this thesis is to find out which of the system's parameters affect it. These parameters are related to the overhead wires and the pantograph. Many researches and studies have focused on the pantograph and it is a well defined part of the system, however the overhead lines are less known and will therefore be the main focus of this thesis.

RESPONSIBLE TEACHER: Assoc. prof. Anders Rönnquist

SUPERVISOR(S): Assoc. prof. Anders Rönnquist

CARRIED OUT AT: Department of Structural Engineering (Institutt for Konstruksjonsteknikk

NTNU

Norwegian University of Science and Technology
Faculty of Engineering Science and Technology
Department of Structural Engineering

Masteroppgave for Stud.techn. Arnar K. Hallgrimsson, våren 2013

Dynamisk oppførsel til kontaktledningsanlegg ved laboratoriemodellering etter norske forhold

Dynamic behavior of contact lines for railways with laboratorial model setup according to Norwegian conditions

For strømforsyning til elektriske tog i Norge benyttes en kontaktledning som togenes strømavtaker glir mot. For at denne forsyningen skal være pålitelig og avbruddsfri i høye toghastigheter stilles det strenge statiske og dynamiske krav til kontaktledningsanleggets egenskaper som mekanisk konstruksjon.

Oppgaven skal kartlegge muligheter for å etablere en laboratoriemodell for studier av oppførselen til kontaktledningsanlegg etter norsk bruk. Det legges vekt på enkelhet i oppbygningen men med vurdering av økt kompleksitet, både for praktisk oppbyggende og måling av ønskede parametere. Det kan tenkes at det kun skal fokuseres på kabeloppførsel og ikke et fult kontaktledningssystem. Den numeriske modell må videreutvikles slik at den kan benyttes til å evaluere ulike effekter ved valg av lab konfigurasjon mot full skala. Det er for denne oppgaven også mulig å gå mot full skala målinger og systemidentifikasjon. Det er fra Jernbaneverkets side lovt tilgang til måledata fra deres database og mulig samarbeid med personell som drifter målevogn. Avhengig av eksisterende data med tilhørende systeminformasjon, geografisk og geometrisk data kan statistisk studie gjennomføres og dynamiske systemparametere estimeres. Dette kan også tas inn som en del av utviklingen av laboratorieforsøk. Vurdere hvordan modell, analyse og resultat står i forhold til gjeldende regelverk.

Litteratur studie, numerisk modell og fysisk modell, State-of-the-art:

- Kontaktledningsanleggets mekanisk funksjonalitet og dynamiske egenskaper.
- Pantografens mekaniske funksjonalitet og dynamiske egenskaper.
- Oppdater Matlab skript for beregning av dynamiske egenskaper.
- Studie av eksisterende laboratorieforsøk.
- Vurder skaleringseffekter og overgang mellom numerikk, lab og full skala
- Utvikling av oppsett til lab modell, valg av geometri, material, påføring av last og responsmålinger, hva, hvor og hvordan.
- Dynamiske egenskaper som frekvenser og moder, bølgetransport og refleksjoner i systemet.
- Analyser av samplede resultater for studie av frekvensinnhold og sammenligning mellom ønskede og målte verdier.
- Alternativ utforming og konsekvenser av resultat - typer tiltak som er / kan tenkes bli brukt.

Det vil være opp til kandidaten at selv vektlegge de enkelte delene i oppgaven der oppgaven utføres i henhold til retningslinjer for utførelse av hovedoppgaven ved Institutt for konstruksjonsteknikks gitt på instituttets hjemmesider.

Faglærer: Anders Rönnquist, NTNU

Besvarelsen skal leveres til Institutt for konstruksjonsteknikk innen 10. juni 2013

Address	Org. no. 974 767 880	Location	Phone	Contact person
NO-7491	Email: anders.ronnquist@ntnu.no	Richard Birkelands vei 1a	+ 47 73 59 47 00	Anders Rønnquist
Trondheim	kt-info@ivt.ntnu.no	Gløshaugen	Fax	
Norway	http://www.ivt.ntnu.no/kt/		+ 47 73 59 47 01	Phone: + 47 73 59 46 63

Preface

The following thesis is my final work towards a masters degree in structural engineering at the Norwegian University of Science and Technology (NTNU). It constitutes the work required for completion of the course *TKT4915 BEREGNINGSMEKANIKK* for the spring semester of 2013. The work performed and written about in this thesis is a continuation of the work I carried out in *TKT4511 BEREGN MEKANIKK FDP* during the fall semester of 2012.

The experience gained from the following courses was valuable for finishing this thesis; *TKT4201 KONSTR DYNAMIKK*, *TKT4108 DYNAMIKK VK*, *TKT4192 ELEMENTMET/STYRKE* and *TKT4197 IKKELIN EL ANALYSE*. Participating in these courses, one obtains a set of tools for analysing almost every structural system. In my opinion, it was interesting to take on this project since the catenary–pantograph system is new and different from the systems usually used as examples in the courses for structural dynamics and finite element method. Now that I have finished, I am more confident that I have developed these tools sufficiently to take on more than the normal systems. And so, the experience has been extremely rewarding for me.

Over the course of this spring semester I have been working on this thesis in close relation to my supervisor, Anders Rönnquist, and fellow student colleague, Petter Røe Nåvik. I would like to thank both of them for the help they have given me. I would like to thank Anders specially for the countless hours spent answering my questions and making me ask myself new ones. Additionally I would like to thank Tor Egil Thoresen from the Norwegian national rail administration and the employees of the Trondheim office for helping us obtain measurements of Norwegian systems and giving us information on it.

Trondheim, June 2013
Arnar Kári Hallgrímsson

Abstract–English

Some domestic flight routes in Norway rank among the busiest in Europe. Experience has shown that, in countries such as France and Germany, high velocity trains can be preferable to flying, given that the distance is not too great (usually under $1000km$). The domestic flight routes mentioned are all under that limit and therefore, there is great interest for increasing velocities of trains travelling in Norway. The biggest barrier for this purpose is the dynamic behaviour of the catenary–pantograph system, which is the system supplying power to the train. This thesis covers the modelling of that system, experimentally and numerically.

The catenary–pantograph system mainly consists of a messenger wire, contact wire and a pantograph. Electrical power is transmitted from the contact wire through the pantograph to the train's engine. Consistent contact between the pantograph's head and contact wire is vital for the train to operate at high velocities. Too much or too little contact leads to increased wear in the system. In order to examine the performance of the system, the contact force is defined, i.e. the force at the point of contact. This force is one of the most important property of the system and the aim of this thesis is to find out which of the system's parameters affect it. These parameters are related to the overhead wires and the pantograph. Many researches and studies have focused on the pantograph and it is a well defined part of the system, however the overhead lines are less known and will therefore be the main focus of this thesis.

Abstract–Norwegian

Flyruter i Norge er blant de travleste i Europa. Erfaringer fra land som Frankrike og Tyskland viser at høyhastighetstog kan være et alternativ til fly, dersom avstanden ikke er for stor (under $1000km$). De travleste flyrutene i Norge er alle under $1000km$ og det er derfor stor interesse for å øke hastighetene av tog på de strekninger. Et av problemene ved en slik utbygging er den dynamiske oppførselen til kontaktledningssystemet som forsyner togene med elektrisitet. Denne oppgaven tar for seg modelleringen av et slikt system, både eksperimentelt og numerisk.

Overføring av strøm foregår gjennom kontaktledningssystemet som består av en bæreline, en kontaktledning og en strømavtaker. Elektrisk strøm er overført fra kontakttråden gjennom strømavtakeren til togets motor. Pålitelig kontakt mellom strømavtaker og kontakttråden er viktig for at toget skal kunne operere ved høye hastigheter. For mye eller for lite kontakt fører til økt slitasje i systemet. For å undersøke ytelsen av systemet, blir kontaktkraften definert, dvs. kraften som virker i et kontaktpunkt. Denne kraften er en av de viktigeste egenskapen av systemet. Formålet med denne studien er å bestemme hvilke systemet parametre som påvirker den. Disse parameterne er knyttet til kontakttråden og strømavtakeren. Strømavtakeren er en vel definert del av systemet, men kontakttråden og bærelinen er mindre kjent, og vil derfor være hovedfokus i denne oppgaven.

Contents

List of Figures

List of Tables

Notations

- Vectors and matrices are usually presented by bold symbols, e.g. $\mathbf{M}$
- Time derivative are presented by a dot above the variable, e.g. $\dot{u}$
- Derivative with respect to space is denoted by ', e.g. $\mathbf{N}'$
- Transpose of a vector or matrix is defined by a T, e.g. $\dot{u}^T$.

List of symbols

Abbreviations

DOF – Degree of freedom
FEM – Finite element method

Common subscripts

cw – Contact wire
mw – Messenger wire
m – Mean
e – Element
dr – Dropper
pg – Pantograph
tm – Top mass

fr – Frame

Latin symbols

E – Young's modulus
I – Moment of inertia
P – Axial tension force
v_α – Velocity limit due to reflection
c_p – Wave propagation velocity
r – Reflection coefficient
F – Contact force
v_{tr} – train velocity
A – Cross section area
k – Stiffness
m – Mass
c – Damping
e – Elasticity
F_{pull} – Pull force in elasticity calculations
$unif$ – Uniformity
$\mathbf{M}$ – Global mass matrix
$\mathbf{m}$ – Element mass matrix
$\mathbf{C}$ – Global damping matrix
$\mathbf{c}$ – Element damping matrix
$\mathbf{K}$ – Global stiffness matrix
$\mathbf{k}$ – Global stiffness matrix
$\mathbf{F}$ – Global force vector
$\mathbf{f}$ – Element force vector
$\ddot{\mathbf{d}}$ – acceleration DOF vector
$\dot{\mathbf{d}}$ – velocity DOF vector
$\mathbf{d}$ – displacement DOF vector
u – axial displacement
v – vertical displacement
L – Lagrangian functional
T – Kinetic energy
W_f – Work done by external forces

$\ddot{\mathbf{u}}$ – acceleration time history
$\dot{\mathbf{u}}$ – velocity DOF time history
$\mathbf{u}$ – displacement DOF time history
t – time
V – Volume
S_f - Surface
$\mathbf{N}$ – Shape function matrix
$\mathbf{E}$ – Material constants matrix
N_{el} – Number of elements
$\mathbf{v}$ – Eigenvector
k_c – Contact stiffness
g – Acceleration of gravity
x – Location on x–axes
f – frequency [Hz]
$\mathbf{T}$ – Transformation matrix
C – Direction cosinus
S – Direction sinus

Greek symbols

ρ – mass per unit length
θ – rotational displacement
σ – Standard deviation of contact force
ξ – Critical damping ratio
δ_{disp} – Displacement measured in elasticity calculations
λ – Wavelength
Π – Potential energy
δ – Variational operator
ϱ – mass density
$\boldsymbol{\varepsilon}$ – Strain vector
$\boldsymbol{\sigma}$ – Stresses
$\boldsymbol{\Sigma}$ – Initial stress matrix
ζ – Isoparametric coordinate
ω – Eigenfrequency $[rad/s]$
α & β – Rayleigh damping factors

$\mathbf{\Phi}$ – Matrix of eigenvectors
λ_v – Scaling factor for vertical length
λ_h – Scaling factor for horizontal length
μ – Scaling factor for mass
α_s – Scaling factor for velocity
ϵ – Axial strain
γ – Transversal strain

1 Introduction

Transportation, for both people and goods, has become increasingly important in today's global environment. Travelling by train is a popular transportation mode and is competitive over others like flying or driving when it comes to different factors such as safety, price, environmental effects, comfort and time. Research has shown that it is better to take the train rather than flying or driving, if the distance travelled is under $1000km$ and the train can travel at a velocity of more than $250km/h$ (Wu and Brennan, 1998). Trains travelling over that limit are usually electrically powered. The subject of this thesis is the system that supplies electricity to trains.

The system that supplies electricity to trains is called the catenary–pantograph system, see figure 1.1. The biggest challenge of increasing velocity on the system is its dynamic behaviour. The system mainly consists of the contact wire, messenger wire and the pantograph. On top of the train sits the pantograph, that slides along the contact wire collecting electrical power and delivers it to the train's engine. Contact between the pantograph and the contact wire is an important measure of current collection performance, it is described by a dynamic contact force. Either too low or too high contact force yields negative effects on the system. The aim of this thesis is too study the dynamic behaviour of the system, the parameters that are important to it and how they affect it. Important characteristics of the system include wave propagation velocity in the contact wire, pre–sag of the system, tension in the wires and etc. The thesis deals with the issue generally but a special emphasis is put on Norwegian conditions.

Some domestic flight routes in Norway ranked among the busiest in Europe in 2011; these are Oslo–Trondheim, Oslo–Bergen and Oslo–Stavanger (Aftenbladet, 2011). All three routes are shorter than $1000km$ so there is a good possibility that trains could replace flying for these routes if their velocities are increased. Most trains in Norway run on electricity, but some are still run on diesel oil but the objective is to eventually convert them to run on electricity.

In order to check if the train is the best transportation option a feasibility study was performed for a trip between Trondheim and Oslo. Environmental emissions data was obtained from (Vestlandsforskning, 2013) and time and price data from (SAS, 2013; NSB, 2013; Lavprisekspressen, 2013). Main

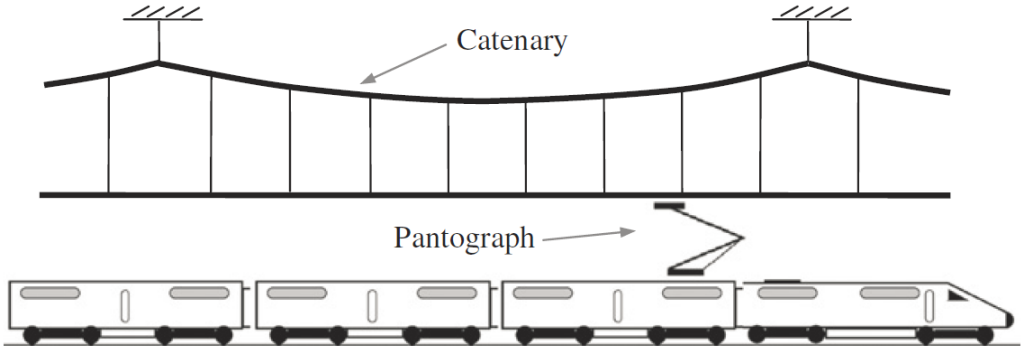

Figure 1.1: The catenary–pantograph system, (Zhou and Zhang, 2011).

assumptions for all options are that the trip is between the central train stations of Trondheim and Oslo and that each transport option is fully utilized. Assumptions for each option are:

Train travelling between Trondheim and Oslo is currently done by so called long distance trains (norsk. Fjerntog) run on electricity. Ticket price and time schedule were given at (NSB, 2013).

Intercity trains are capable of reaching velocities over $250km/h$ and have been proven successful in, e.g. France and Germany. According to (JBV and Railconsult AS, 2012), if one was to be built between Trondheim and Oslo it would take max. $180min$ to travel between the places depending on the route. Since the intercity line does not exist, ticket price is not available, but experience shows that it would be cheaper than a plane ticket.

Car trip time is calculated based on an average velocity of $90km/h$ and a $30min$ food stop; the car uses $7l/100km$ of petrol and the price of petrol is assumed to be $14,5NOK/l$.

Bus price and time estimate is based on information obtained from Lavprisekspressen, (Lavprisekspressen, 2013).

Flying is done with a Boeing 737 and $120km$ of train travelling are added due to trips to and from the airports to the central train stations. The

ticket price contains both the fly ticket and train tickets. Total time is $30+70+55+25+20 = 200min$ due to trips to and from airport ($30min$ and $20min$), flight time ($55min$) and waiting at the airport ($70min$ and $25min$).

Table 1.1: Comparison between different transportation modes for the trip between Trondheim and Oslo.

	Train	Intercity	Car	Bus	Flying
SO_2 [kg]	0	0	0	0	0,02
CO [kg]	0	0	0,08	0,02	0,1
Nox [kg]	0,01	0	0,02	0,2	0,14
CO_2 [kg]	1,71	1,16	21,8	6,64	60,78
NMVOC [kg]	0	0	0,01	0,01	0,01
CH_4 [kg]	0,01	0	0	0	0
PM [kg]	0	0	0,02	0,01	0,01
ECS [kWh]	43,13	28,2	81,05	24,17	193,2
AR/mp	0,48	0,48	1,96	0,34	0,15
EC [NOK]	2,34	1,52	25,86	25,89	74,68
Price [NOK]	399	-	982	429	910
Time [min]	400	130-180	346	510	200

Results can be seen in table 1.1 where $NMVOC$ stands for Non-Methane-Volatile-Organic-Compound, PM for particulate matter, ECS is energy consumption, AR/mp stands for accident risk per million persons and finally EC stands for environmental cost. The table shows that environmental effects from taking the train are significantly lower than for the other options. Although taking the bus is nearly as cheap as taking the train it takes much longer. The only thing standing in the way of trains taking over is that it takes twice the amount of time to travel by train than plane, something that could change with the introduction of intercity train lines or simply by increasing velocity of the current trains. The table shows that planes are safer than trains, however researchers studying this topic disagree between them on which is safer (Koerner, 2004; Brown, 2010). The consensus is though that both options are much safer than using a private car. If the time it takes to travel by train could be reduced, the lower environmental costs and comfort of taking the train would make it the more attractive option.

1.1 Literature survey

The catenary–pantograph system has been popular for research and an abundance of literature exists on the subject. Knowledge of the system has greatly increased since it was first introduced, which has led to significant improvements that mostly relate to increases allowable velocity on the system. The system has been modelled analytically, numerically and in the laboratory. Summary of theories for the system, along with different modelling methods can be found in (Poetsch et al., 1997; Kia et al., 2010).

Simple models are often ideal for learning how a system behaves, in (Wu and Brennan, 1998, 1999) a simple one degree of freedom (DOF) model is developed. The models illustrate dynamic behaviour of the system, but key characteristics are missing, such as wave propagation velocity. Methods used in these simple models for obtaining the stiffness variation of the contact wire have been used for optimization of pantograph models (Park et al., 2003; Kim et al., 2007).

In the absence of complete theoretical understanding researchers turned to scaled laboratory models (Farr et al., 1961; Willets and Edwards, 1966; Willets et al., 1966; Willets and Suddards, 1970). Results from these laboratory studies were distorted because the models were scaled down too much, but dynamic behaviour such as pre–sag and variations in tension force were observed. In (Manabe, 1989; Drugge, 2000), these models were improved upon and the models proved successful in simulating for example wave propagation velocity which is vital to the system. Building a scaled model can be difficult, especially with regard to the overhead lines. Some researchers turned to hybrid modelling, where the overhead lines are modelled mathematically while the pantograph is a physical model (Zhang et al., 2002; Facchinetti and Mauri, 2009; Bruni et al., 2012; Facchinetti and Bruni, 2012).

Nonlinear effects of the system, such as contact loss or slackening of the droppers, cannot be modelled without using numerical modelling. Numerical modelling of the system has increased as computational power increases, most studies use the finite element method for modelling the catenary and a lumped mass model for the pantograph. These studies are for example (Schaub and Simeon, 2001; Cho et al., 2010; Zhou and Zhang, 2011; Jung et al., 2012). Special properties of the system have also been modelled like the initial configuration of the catenary (Lopez-Garcia et al., 2006; Arias

et al., 2009) and nonlinearities due to slackening of droppers (Cho, 2008; Lopez-Garcia et al., 2008).

Additionally, the work carried out here is based largely on the work done previously by the author (Hallgrimsson, 2012), which originated from (Sølvberg, 2008). A textbook from Siemens on contact lines served as a handbook throughout the process as well (Kiessling et al., 2012).

1.2 Objectives and research questions

The main objective of the thesis is to identify parameters that affect the system's dynamic behaviour. That objective is reached by developing a numerical model that is descriptive of the system and is flexible with regard to changing parameters and running. Performing a parameter study will give a good indication of which parameters are important. An additional aim of the thesis is to learn about previously built scaled laboratory models of the system and find out if it is feasible to build one. The numerical model is also supposed to be able to model a scaled down system, that will be checked by implementing a thought up scaled model in the numerical one. The research questions are:

- What parameters of the system are important to its dynamic behaviour?
- How do these parameters affect the system?
- Is it feasible to build a scaled laboratory model?
- Can the numerical model simulate results for scaled down systems?

1.3 Assumptions and organisation of the thesis

The assumptions of the thesis are mostly in regard to the numerical model:

Numerical model

- Modelling spans of different lengths together or in a curvature is not possible.
- The model only accounts for trains with one pantograph.

- Effects from lateral movements are not accounted for, the model is 2D.
- Nonlinear effects from dropper slackening are not included.
- Temperature or weather conditions are not included.
- The system is in perfect condition, no wear is present on the pantograph contact strip or in the contact wire cross section and there are no track irregularities.

In addition full–scale measurements were not obtained and so the numerical model is not validated.

The thesis is setup in the following manner:

Ch. 2 describes the catenary–pantograph system in general, it describes different parts and properties of it. The reference system, that will later on be used in the numerical model, is presented along with the relevant system parameters.

Ch. 3 covers the numerical model developed. The theoretical background necessary to model the system is reviewed along with practical issues related to the modelling itself and results are presented.

Ch. 4 focuses on the scaled laboratory model. Previous scaled models that were built are reviewed and the experience gained from them is summed up in order to suggest a model that could be built in the future. The suggested model is implemented in the numerical model for a simulation of how it will perform.

Ch. 5 lists up the conclusions made from the numerical and scaled model. Ideas for further work are presented.

Appendices are placed at the back with different information relevant to the thesis. Appendix A shows the results obtained for cross section values of the contact wire. Mathematical principles needed for the derivation of the element matrices are found in appendices B and C, while the element matrices themselves are found in appendix D. Integration method steps are presented in appendix E. The model of the pantograph used in the reference system along with values necessary to implement the model are put in appendix F.

Matlab programs that constitute the numerical model and a movie file that shows a run of the model are put into a zip–file that accompanies the thesis electronically, these files are listed up in appendix G.

2 Catenary–pantograph system

The definition of the catenary–pantograph system according to (Kiessling et al., 2012):

> Contact lines are a system of electrical conductors used in conjunction with a sliding current collector to supply electrical energy to vehicles. Contact lines can be overhead contact lines or conductor rail lines.

Overhead contact lines (the catenary system) are the subject of this report along with the sliding current collector (pantograph). Together they make up the catenary–pantograph system. The different parts of the system and physical factors important to its behaviour will be covered in this chapter. This study is done with respect to Norwegian conditions, therefore a span of the Norwegian rail system is chosen as a reference system and will be defined in this chapter.

2.1 General system

The different parts of overhead contact lines or catenary system are: contact and messenger wires, droppers and support poles (registration arms and support brackets) (see figure 2.1). Other important factors that need mention are the pantograph, wave propagation velocity, pre–sag and zig–zag.

2.1.1 Individual parts of the system

Contact wire (cw) and messenger wire (mw) make up most of the catenary system. The contact wire serves as a medium through which electricity is supplied to the train via the pantograph while the messenger wire's purpose is to support the contact wire. The important properties of the wires are mass per unit length (ρ), Young's modulus (E), moment of inertia (I) and the tension force (P). Both mechanical and electrical considerations have to be acknowledged when choosing material and cross section of the contact wire but only mechanical for the messenger wire. The most common material to use for the contact wire is copper, either a solid wire or stranded wire and sometimes with alloy additives such as silver or magnesium (Kiessling et al., 2012). The material chosen for the messenger wire is also often copper.

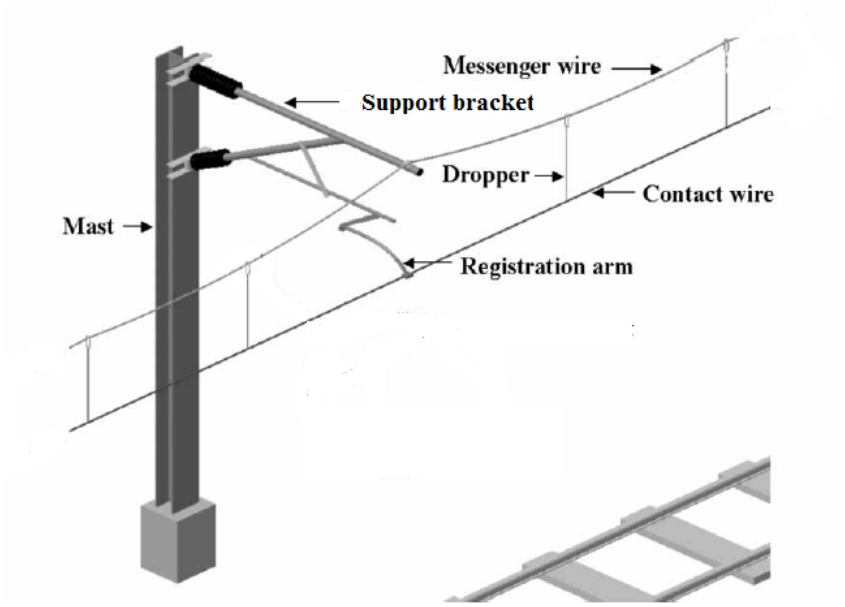

Figure 2.1: Individual parts of the catenary–pantograph system, (Seo et al., 2006).

Typical cross section of a contact wire can be seen in figure 2.2, values for variables shown in the figure can be found in (Kiessling et al., 2012).

Droppers attach the contact wire to the messenger wires. They are designed to carry all loads from the contact wire, horizontal and vertical. Attaching the droppers to the contact wire is usually accomplished through a clasp, see figure 2.3, which is the reason why the contact wire's cross section is shaped as it is. Droppers are a source of stiffness, damping and mass to the system but they also represent a geometric nonlinearity; they slacken as a pantograph passes by and when they are slackened they do not give any resistance to motion. This source of nonlinearity is well recognized and some researchers have tried to include it in the numerical models they develop (Cho, 2008).

Support poles carry horizontal and vertical forces from the catenary system. The messenger wire is extended directly from the pole (called a support bracket), while the contact wire is extended via the registration arm. These

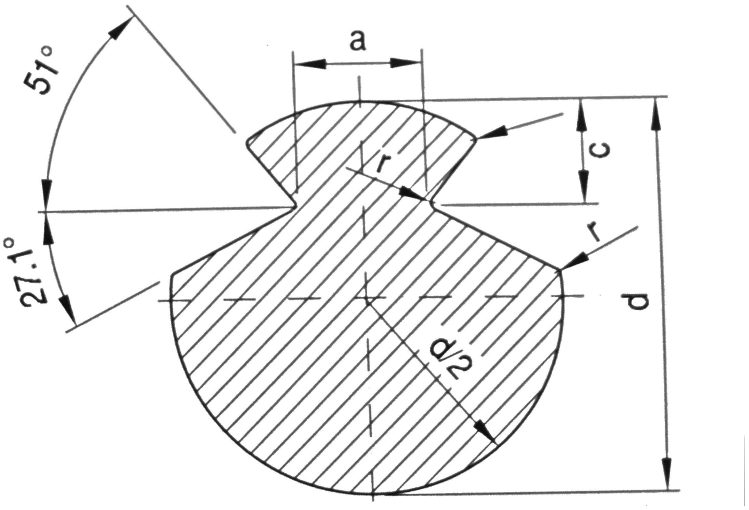

Figure 2.2: Typical contact wire cross section, (Kiessling et al., 2012).

Figure 2.3: Dropper clamped onto the contact wire (Photo: Petter Røe Nåvik).

Figure 2.4: Support pole on a Norwegian track, part of the reference system (Photo: Petter Røe Nåvik).

parts transfer the forces from the catenary system to the support. The registration arm is lighter and more flexible than the support bracket because it cannot influence the stiffness variation of the contact wire too much. Its main purpose is to constrain the contact wire in the lateral direction normal to the train direction. Support brackets are very stiff and constrain movement in all directions. Several different arrangements of these parts exist, one of them can be seen in figure 2.4.

As the train travels along the span the upward lift from the pantograph creates a wave that propagates from the contact point along the span in both directions. Increased stiffness at both dropper and support pole locations will cause the wave to reflect backwards from them towards the pantograph. Amplifications occur in the uplift as the pantograph travels towards the wave, resulting in a condition that limits the allowable train velocity, (Kiessling et al., 2012):

$$v_\alpha = c_{p,cw}\frac{1-r}{1+r} \tag{2.1}$$

where subscript p stands for propagation, $c_{p,cw}$ is the wave propagation ve-

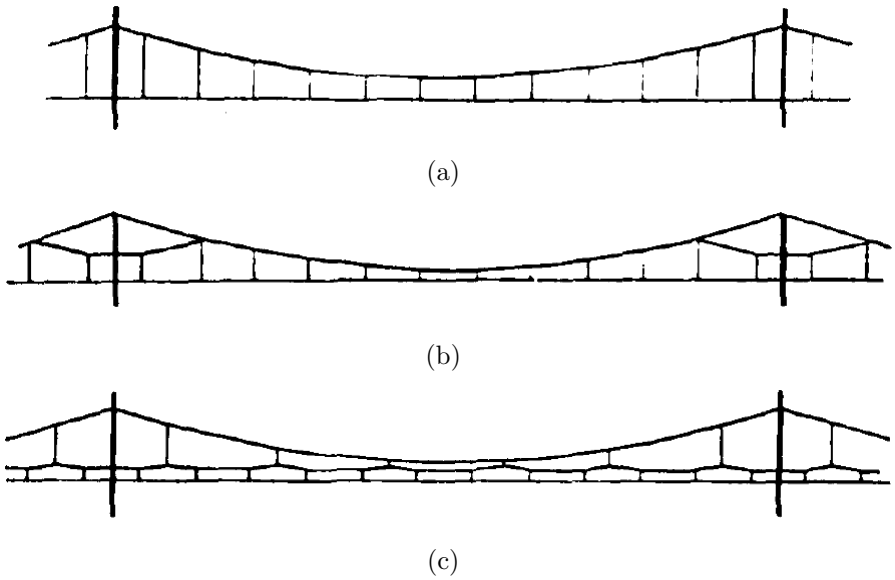

Figure 2.5: Three different types of catenary systems: (a)Simple catenary (b)Stitched catenary (c)Compound catenary, (Farr et al., 1961)

locity (see section 2.1.4) and r is the reflection coefficient expressed as:

$$r = \frac{1}{1 + \sqrt{\frac{P_{cw}\rho_{cw}}{P_{mw}\rho_{mw}}}} \tag{2.2}$$

Complete derivation of these factors can be found in (Kiessling et al., 2012).

2.1.2 Different catenary systems

There are three typical types of catenary systems, see figure 2.5; simple catenary, stitched catenary (often referred to as Y–line) and compound catenary. These three types can furthermore be divided according to the method of producing tension in the wires. Either the wires are fixed at the support poles or weight–tensioning devices are used. If the wires are fixed, pre–sag and tension vary with temperature and therefore it is considered inconvenient for high train velocity (Farr et al., 1961).

The simple catenary arrangement was among the first systems to supply electric power to running trains. Its disadvantage is the large stiffness variation along the span, yielding more dynamic effects in the system because

the pantograph will lift the wire higher in the middle of the span than at the supports. Ideally the vertical height of the pantograph should be uniform as it runs through, to do that the system's stiffness variation must be as small as possible. To counteract this problem, the stitched and compound catenary systems were developed. The stitched catenary is supposed to smooth out the irregularity of the stiffness at the supports. That is accomplished by supporting the contact wire with an additional wire, see figure 2.5. Stitched catenary systems are also commonly used to increase performance of tracks that run in a curvature, where the radius is larger than $700m$ (Sture et al., 1982). In a compound catenary system the contact wire is suspended by droppers from a auxiliary messenger wire, which is suspended by droppers from the main messenger wire. By doing that, the stiffness variations will even out over the whole span. The difference between stitched and compound systems is that the stitch system smooths out stiffness peaks at the supports, while the compound systems creates a more uniform stiffness for the whole span.

2.1.3 Pantograph

The pantograph sits on the top of the train and collects power from the contact wire and transfers it to the train's engine. Different types of the pantograph exist but all of them are basically made up from a head and frame assembly, see figure 2.6. The frame assembly makes sure that the head assembly stays in contact with the contact wire. Both head and frame have a mass that results in inertia of the system as it moves. Due to that mass, the pantograph cannot react instantaneously to changes in stiffness variation of the contact wire and therefore the contact force will vary (Drugge, 2000; Farr et al., 1961). The pantograph's behaviour is velocity dependent, because of its aerodynamic resistance. Due to these effects and the build of the pantograph, its behaviour is often nonlinear.

2.1.4 Wave propagation velocity

The upward force of the pantograph causes waves to propagate in both direction from the contact point. These waves have a propagation velocity that is critical to the behaviour of the system, according to (EN 50119:2001, 2001)

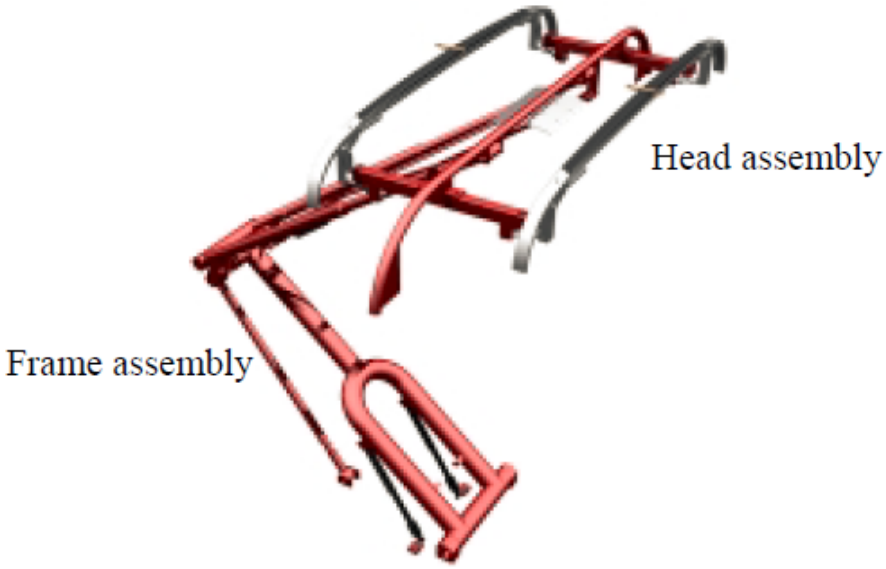

Figure 2.6: The WBL 88 pantograph used for the reference case (Larsson and Drugge, 1998).

the system's velocity should not exceed 70% of the wave propagation velocity which is expressed as:

$$c_p = \sqrt{\frac{P_{cw}}{\rho_{cw}}} \tag{2.3}$$

2.1.5 Pre–sag

Pre–sag is the static displacement of the contact wire due to gravity, it is a factor which significantly influences the degree of variation for the contact force, (Jung et al., 2012) and is therefore vital for the dynamic behaviour of the system. The pre–sag is controlled by the length of the droppers and the tension force in the wires. According to (Cho et al., 2010), optimal pre–sag is obtained by controlling train velocity, span length, uplift force of the pantograph and stiffness variation in the contact wire. The pre–sag should be decreased if train velocity is increased and alternatively increased if any of the other factors mentioned are increased. Using optimal pre–sag at velocities close to the wave propagation velocity does not affect the system because the latter is a governing factor for the system behaviour.

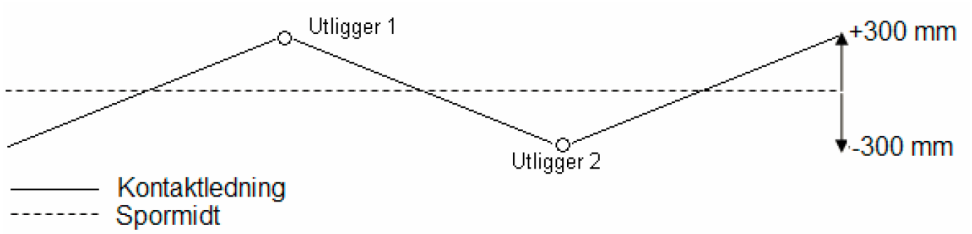

Figure 2.7: Stagger of the catenary system, Contact wire (–) and Middle of the track (- -), (Sølvberg, 2008).

2.1.6 Zig–zag

The catenary system is staggered from one side to the other to reduce the wear on the pantograph, see figure 2.7. In this way the contact point between the pantograph and contact wire moves over the length of the pantograph, typically this length can be $300mm$ from the middle as in figure 2.7. Dynamic effects resulting from the stagger can be great and should preferably be accounted for according to (Facchinetti and Bruni, 2012).

2.1.7 Contact force

The most important and descriptive measurement for the performance of the catenary–pantograph system is the contact force. Too low contact force results in arcing between the contact wire and pantograph, which results in increased wear of the system and could lead to loss of power. If the contact force is too high, unacceptable wear of the contact wire and pantograph will occur. Additionally large vertical displacements of the contact wire could occur if contact force is too high, which would have negative effects on a trailing pantograph in the case of trains that have more than one. The force exerted by the pantograph onto the contact wire when the train is stationary is the static contact force. That force, along with the aerodynamic effects from the pantograph as the train is in motion, is called the aerodynamic contact force. Adding that to the dynamic force components of the system (e.g. inertia of system masses) when the train is moving gives the dynamic contact force or just contact force (F).

2.1.8 System requirements

Requirements are made for the catenary–pantograph system regarding allowable system parameters and setup of the system. The aim of the model developed here is not to simulate a system that is so accurate that it can be used for design, rather be simple and descriptive of system behaviour. Despite that, some of these requirements will be covered here for a frame of reference. International and European standards exist for design and modelling of the system, e.g. (EN 50318:2002, 2002; EN 50119:2001, 2001), from which requirements are obtained and also from various studies. According to (Poetsch et al., 1997) the following key parameters must be observed:

- Mean contact force F_m:
  According to the regulations of the Norwegian national rail administration (`http://www.jernbaneverket.no`, JBV) the requirements for the mean contact force are (in $[N]$), (JD 542, 2004):

$$F_{m,max} = 0,000586v^2 + 70\ [N] \quad \text{for: } 0 \leq v_{tr} \leq 160 \tag{2.4}$$
$$F_{m,max} = 0,00097v^2 + 60,2\ [N] \quad \text{for: } 160 < v_{tr} \leq 250 \tag{2.5}$$
$$F_{m,min} = 0,00096v^2 + 50\ [N] \quad \text{for: } 0 \leq v_{tr} \leq 250 \tag{2.6}$$
$$F_{m,rec} = 0,00104v^2 + 55\ [N] \quad \text{for: } 0 \leq v_{tr} \leq 250 \tag{2.7}$$

  where v_{tr} is the velocity of the train in $[km/h]$ and rec stands for recommended. The first term in these equations represent the aerodynamic force that affects the pantograph, while the second term represents the static uplift force of the pantograph. Figure 2.8 shows these requirements.

- Range of the contact force, $F_m \pm 3\sigma_m$, where σ_m is the contact force standard deviation:
  Standard deviation of the contact force should be within 20% of the maximum mean value for a given velocity, see figure 2.9. Figure 2.10 shows the range, given a maximum standard deviation value. The range is based on a Gaussian distribution, so $99,7\%$ of the values should fall within it. In (EN 50119:2001, 2001) the requirements for this range ($F_m \pm 3\sigma_m$) are given, see table 2.1. According to the table the contact

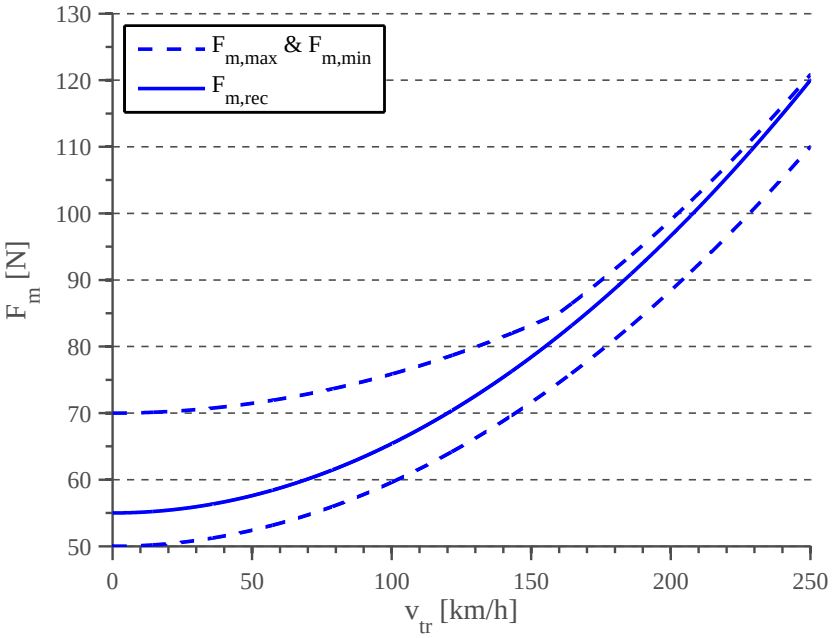

Figure 2.8: Requirements for the mean contact force

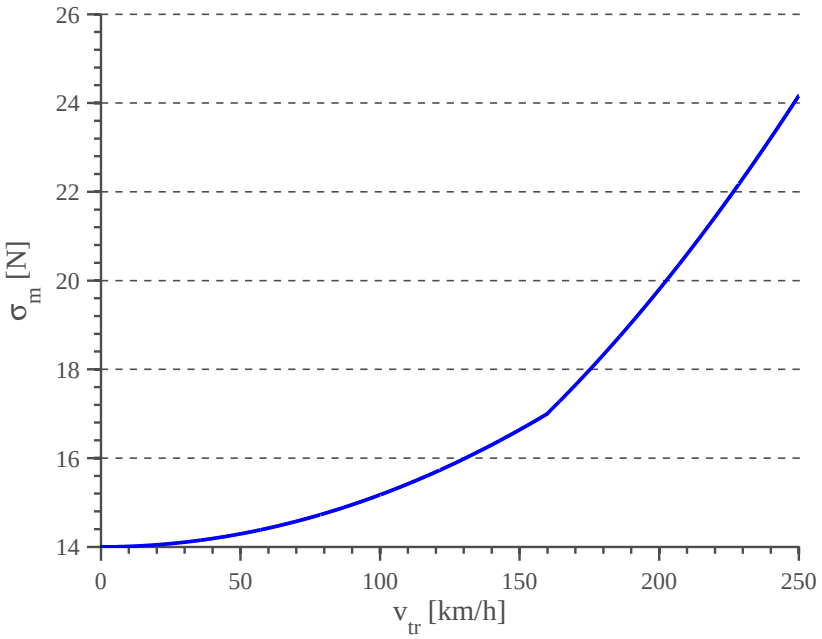

Figure 2.9: Requirements for the standard deviation of the contact force

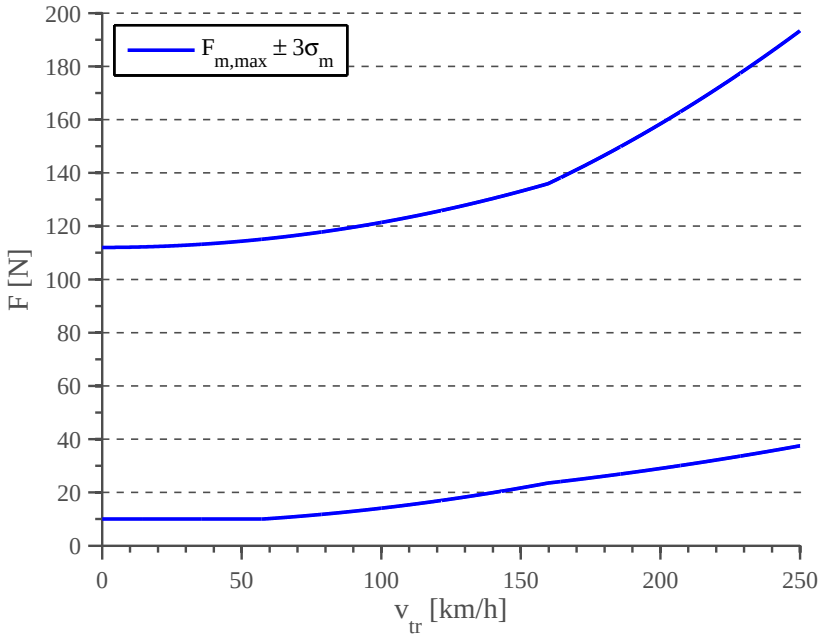

Figure 2.10: Range of contact force, in which $99,7\%$ of all values should fall.

force should not exceed $300N$ and that compares well with figure 2.10. Note that *AC* and *DC* stand for the current system used for the system.

Table 2.1: Requirements for contact force range according to (EN 50119:2001, 2001)

System	v_{tr} [km/h]	Contact force [N] Max.	Min.
AC	≤ 200	300	> 0
AC	> 200	350	> 0
DC	≤ 200	300	> 0
DC	> 200	400	> 0

- Statistical occurrence of contact loss:
  The system should never experience contact loss and therefore it is unacceptable and the statistical occurrence should be zero.

- Statistical occurrence of a contact force below a specified low value:

According to (JD 542, 2004) the critical point of low contact force is $F_m = 10N$, therefore a check will be made of the statistical occurrence below that value. At low velocities, the range of contact force as expressed above will go under $10N$, that was fixed afterwards and the minimum in figure 2.10 is $10N$.

- Maximum contact wire displacement at the registration arm:
  The maximum contact wire displacement at the support as the pantograph passes by was found to be $48 - -55mm$ for a velocity of $250km/h$ and $55 - -65mm$ for a velocity of $300km/h$ for a reference model in (Cho, 2008). Since no other requirements were found, this will be used as a reference.

Maximum static displacement, or pre–sag, is also of interest. Normally the ratio between pre–sag and span length is 1/1000 for the contact wire and 1/100 for the messenger wire (Cho, 2008).

2.2 Reference system

The reference system chosen is a single span between Støren and Soknedal, specifically track nr. 152. Several spans of the track were studied, but the one chosen is the $40m$ long span between masts (support poles) 1277 and 1278. Information on design values for the span were obtained from (Design tables, 2013) and some general system variables for Norway were obtained from (Sølvberg, 2008). The span represents a simple catenary system (no Y–line) and weight–tensioning devices are used to produce the pretensioning in the wires. Table 2.2 lists up the system's parameters necessary for a simulation in the numerical model developed here, except for the time step of the integration method (see section 3.1.5). The parameters in the table that have not been mentioned above are; A-cross section area, ξ-critical damping ratio, k-stiffness, m-mass and c-damping. Some parameters were not obtainable from the sources mentioned, such as information relating to registration arms, support brackets and droppers but they were obtained from (Cho, 2008). The cross section dimensions and moment of inertia for the contact wire were obtained from a fellow colleague (Nåvik, 2013), see appendix A. Only the cross section area of the messenger wire is available, not dimensions

nor moment of inertia. The assumption used to obtain the moment of inertia is that it is half of the contact wire's moment of inertia, since that is the same ratio between their cross section areas. Velocity of the train that the reference system is designed for is $130km/h$.

Field measurements were performed on the system, in order to assess the error that is between actual and design values. A laser distance meter was used to assess different lengths in the system, e.g. length between droppers and their height. Those measurements showed that the system is set up in almost exactly the same way as it is designed. Finding the eigenfrequencies and their accompanying modes is of great interest for every structural system. In order to obtain them, a modal hammer was used. The frequencies of the system are too low for the hammer and its software, and so the results could not be processed.

Tension force A device used to measure the tension force in the wires at arbitrary locations was provided by JBV, see figure 2.11. Great errors between measured values and designed values were observed:

$$P_{cw,measured} = 17,2kN \quad P_{cw,design} = 10kN \quad error = \frac{17,2-10}{10} \cdot 100 = 72\%$$

That is a 72% error from the designed value which is extreme. Several different factors could cause this error, perhaps most likely the measurement device was calibrated in a wrong way. No matter what the cause is, it is important to note that actual values may differ from design values. How much will errors in the system parameters affect the system? The design value will be used in the numerical model.

Elasticity Measuring the elasticity of the contact wire is done by pulling up the wire by a weighing device, which shows how much force is used to pull it, and measuring the corresponding displacement of the wire as it is pulled with a laster distance meter Doing that, the user has the force needed to lift the wire up a certain displacement. The expression for elasticity is:

$$e = \frac{\delta_{disp}}{F_{pull}} \tag{2.8}$$

Table 2.2: Parameters of the reference system based on (Cho, 2008; Sølvberg, 2008; Design tables, 2013).

Droppers	-	1	2	3	4	5	6	-	
Position [m]	0	2,1	9,3	16,4	23,6	30,7	37,9	40	
Model–Position [m]	0	2	9	16,5	23,5	31	38	40	
Height [m]	0,16	0,148	0,136	0,129	0,129	0,136	0,148	0,16	
Parameters	$P[kN]$	$E[N/m^2]$	$\rho[kg/m]$	$I[m^4]$	$A[mm^2]$	$\xi[\%]$	$k[N/m]$	$m[kg]$	$c[Ns/m]$
Contact wire	10	1,24E+11	0,94	9,87E-10	105,7	1	-	-	-
Messenger wire	5	1,13E+11	0,46	4.935E-10	50	1	-	-	-
Droppers	-	-	-	-	-	-	1,00E+05	0,4	5
Registration arm	-	-	-	-	-	-	213	2,6	-
Support bracket	-	-	-	-	-	-	2,00E+06	2,6	-

Figure 2.11: Device used to measure tension in the wires (Photo: Petter Røe Nåvik).

where e represents the elasticity, δ_{disp} the displacement the wire undergoes as it is pulled by a force F_{pull}. Structural engineers prefer to use the reciprocate of the elasticity, i.e. the stiffness. But, since this is commonly used in the railway field it will be used here. The elasticity curve can be seen in figure 2.12. It is important to realize that this method is not accurate, which means that the values may be a little off, but the shape of the curve compares well with what it should be. Recommended properties of the elasticity curve are given in table 2.3 (Kiessling et al., 2012). For the reference span (design velocity of $130km/h$) the elasticity value at mid point is 0,9 which is lower than the table recommends or 1,20. This result is conservative, it would be worse if the value was higher. Uniformity of elasticity for the reference system:

$$unif = 100 * \frac{e_{max} - e_{min}}{e_{max} + e_{min}} = 100 * \frac{0,90 - 0,17}{0,90 + 0,17} \approx 68\% \tag{2.9}$$

Figure 2.12: Measured elasticity curve of the reference system

The uniformity is higher than expected, which is fine, but it could stem from the inaccuracy of the measurement. The more uniform the elasticity curve is the better.

Table 2.3: Recommended values for elasticity at the middle of the span and uniformity of the elasticity curve (Kiessling et al., 2012)

v_{tr} $[km/h]$	e $[mm/N]$	Degree of elasticity uniformity [%]
≤ 100	1,20	50
≤ 160	1,20	30
≤ 200	1,10	20
≤ 280	0,60	10
> 280	0,40	8

3 Numerical modelling

This chapter covers the process of numerically modelling the catenary–pantograph system. The objective of the model is to illustrate the dynamic behaviour of the system and how the parameters defining the system affect it. The theoretical background needed to model the system is reviewed and results are presented. The model is developed using MATLAB.

3.1 Theoretical background

The numerical model of the combined system can be expressed in the following equation of motion:

$$\mathbf{M}\ddot{\mathbf{d}} + \mathbf{C}\dot{\mathbf{d}} + \mathbf{K}\mathbf{d} = \mathbf{F} \tag{3.1}$$

where $\mathbf{M}, \mathbf{C}$ and $\mathbf{K}$ are global system matrices for mass, damping and stiffness respectively, $\mathbf{F}$ is the external force vector and $\mathbf{d}$, $\dot{\mathbf{d}}$, $\ddot{\mathbf{d}}$ are vectors of displacement, velocity and acceleration, respectively. Placing a dot over a variable means that it is the derivative of that variable w.r.t time, double dot means the second derivative w.r.t time. The represented forces in equation 3.1 are inertial-, dissipative-, internal-(elastic-) and external-force in that order from the left.

There are several different methods for solving the equation for the catenary–pantograph system. According to (Poetsch et al., 1997), two common methods used are the finite element method (FEM) for the catenary and a lumped mass model for the pantograph. The majority of studies covered in the literature survey use these methods and also the numerical model described here is based on them. Modelling the contact between these structures is not as straightforward, many different methods have been proposed for that purpose. The one chosen here is based on a model presented in (Zhou and Zhang, 2011) because of its ability to reattach in case of contact loss. These different methods for modelling the catenary, pantograph and the contact between them will be covered in this section.

3.1.1 Catenary model

The catenary is modelled, with the help of FEM, as a pre–tensioned beam model. This section describes the method and the necessary steps that need to be taken to successfully make a discretized model of the catenary wires. Assumptions made for the model are:

- The coordinate system for the model is as follows, x-axes in the direction of the train movement, y-axes vertical direction from the ground up and z-axes normal to the direction of the train.
- Lateral displacements of the wires in the xz-plane are assumed to be negligible. This assumption simplifies the problem and converts it from 3D to 2D. Staggering has been mentioned to be important but in an effort to keep the model simple it is not included, if it were to be included the model would have to be 3D.

FEM steps: The basic steps that characterize every process where FEM is used are, according to (Cook et al., 2001):

- Preprocessing–The parameters of the problem are defined and are applied in the model. These parameters are geometry of the problem, material properties, loading applied and boundary conditions. When all parameters have been defined and implemented, the model is discretized into elements. The size and type of elements must be chosen by the user.
- Numerical analysis–Once the model has been discretized and all problem parameters are in place, the element matrices (stiffness, damping, mass, external loading) can be formed in the local coordinates. These element matrices are then assembled into global matrices (in global coordinates) and the problem can be solved using a time–stepping method.
- Postprocessing–After the equation of motion is solved globally the field variables at each node can be plotted up and analysed. These variables are for example the degrees of freedom at each node, forces etc.

Element type The most commonly chosen model for describing the catenary is a string model; it is common because it is simple and fast (Poetsch et al., 1997). Beam models are more complex but they include important characteristics of the catenary that need to be considered as well. That is why a beam model was chosen for this study. Two different beam elements are proposed: the Euler–Bernoulli that includes bending stiffness and the Timoshenko that also includes shear deformation and rotational inertia effects. According to (Poetsch et al., 1997), many who study the catenary–pantograph system believe that the inclusion of bending stiffness is not important. A study by (Jensen and True, 1998) proposes that as the train's velocity increases, the importance of including the bending stiffness is increased. Since the subject here is high velocity trains, the Euler–Bernoulli beam element was chosen. It is chosen over the Timoshenko element because according to (Poetsch et al., 1997) there is no need to consider shear deformation or rotary inertia effects when the wavelength in the contact wire λ is larger than $5cm$. For the reference system defined in section 2.2:

$$\lambda = 2\pi\sqrt{\frac{EI}{P}} = 2\pi\sqrt{\frac{1,24\text{E}{+}11 \cdot 9,87\text{E-}10}{10000}} = 0,695m \tag{3.2}$$

The wavelength of the reference system is over ten times the minimum and therefore the the Euler–Bernoulli element is judged to be adequate.

The 2D Euler–Bernoulli beam has two nodes with 3 degrees of freedom in each node: vertical, axial and rotational. The elements DOF vector:

$$\mathbf{d}_{cw} = \mathbf{d}_{mw} = [u_1 \quad v_1 \quad \theta_1 \quad u_2 \quad v_2 \quad \theta_2]^T \tag{3.3}$$

where subscripts 1 and 2 represent the node number, u_i is the axial displacement, v_i is the vertical displacement and θ_i the rotational displacement.

Hamilton's principle: The element matrices and the global matrices can be derived using Hamilton's principle (Quek and Liu, 2003; Cook et al., 2001; Wilson, EL., Inc; Langen and Sigbjörnsson, 1979).

For the model derivation, applying Hamilton's principle, the generalized Lagrangian functional is defined as:

$$L = T - \Pi + W_f \tag{3.4}$$

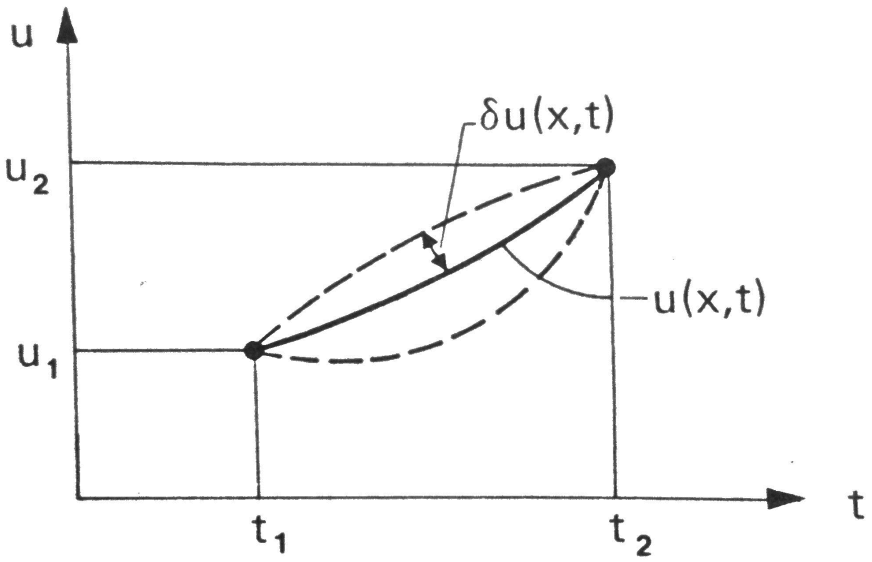

Figure 3.1: Time history of displacement, (Langen and Sigbjörnsson, 1979)

where L is the Lagrangian functional, T is the kinetic energy, Π is the potential energy and W_f is the work done by dissipative and external forces. The terms of equation 3.4 are dependent on time histories of displacement ($\mathbf{u}(x,t)$), velocity ($\dot{\mathbf{u}}(x,t)$) and acceleration ($\ddot{\mathbf{u}}(x,t)$). Let $\bar{\mathbf{u}} = \mathbf{u}(x,t) + \delta u$ be a solution to the functional, δu is a small displacement (virtual displacement). The solution must satisfy compatibility, boundary conditions and given values for $\mathbf{u}(x,t)$ at arbitrary time values t_1 and t_2, see figure 3.1. Hamilton's principle states that for all solutions in the time domain (t_1 and t_2) that satisfy these conditions, the one that makes the Lagrangian functional a minimum yields the most accurate solution:

$$\delta \int_{t_1}^{t_2} L dt = 0 \tag{3.5}$$

This requirement can be used to derive the equation of motion.

Start with the kinetic energy for an arbitrary solid:

$$T = \frac{1}{2} \int_V \varrho \dot{\mathbf{u}}^{\mathbf{T}} \dot{\mathbf{u}} dV \tag{3.6}$$

where V is the solid's volume, ϱ mass density and $\dot{\mathbf{u}}$ is velocity. The displacements and velocities are calculated from nodal DOF:

$$\mathbf{u} = \mathbf{N}\mathbf{d} \Rightarrow \dot{\mathbf{u}} = \mathbf{N}\dot{\mathbf{d}} \tag{3.7}$$

where $\mathbf{N}$ represents the shape functions. The expression for kinetic energy of a single element:

$$T = \frac{1}{2}\int_{V_e} \varrho \dot{\mathbf{d}}_\mathbf{e}^\mathbf{T}\mathbf{N}^\mathbf{T}\mathbf{N}\dot{\mathbf{d}}_\mathbf{e} dV_e = \frac{1}{2}\dot{\mathbf{d}}_\mathbf{e}^\mathbf{T}\Bigg(\underbrace{\int_{V_e} \varrho \mathbf{N}^\mathbf{T}\mathbf{N} dV_e}_{\mathbf{m_e}}\Bigg)\dot{\mathbf{d}}_\mathbf{e}^\mathbf{T} = \frac{1}{2}\dot{\mathbf{d}}_\mathbf{e}^\mathbf{T}\mathbf{m}_\mathbf{e}\dot{\mathbf{d}}_\mathbf{e} \tag{3.8}$$

where V_e is the volume of the element, $\mathbf{d_e}$ are the element nodal DOF and m_e is the element's mass matrix.

The potential energy, in this case the elastic strain energy, for an arbitrary solid is defined as:

$$\Pi = \frac{1}{2}\int_V \boldsymbol{\varepsilon}^\mathbf{T}\boldsymbol{\sigma} dV \tag{3.9}$$

where $\boldsymbol{\varepsilon}$ and $\boldsymbol{\sigma}$ are the strains and stresses of the solid. The stress–strain relation according to Hooke's law for a linearly elastic material with initial stresses (Cook et al., 2001):

$$\boldsymbol{\sigma} = \mathbf{E}\boldsymbol{\varepsilon} + \boldsymbol{\sigma}_0 \tag{3.10}$$

where $\mathbf{E}$ is a matrix of material constants and $\boldsymbol{\sigma}_0$ is the initial stress. Applying Hooke's law, equation 3.9 gives:

$$\int_V \frac{1}{2}\boldsymbol{\varepsilon}^\mathbf{T}\mathbf{E}\boldsymbol{\varepsilon} dV + \int_V \boldsymbol{\varepsilon}^\mathbf{T}\boldsymbol{\sigma}_0 dV \tag{3.11}$$

The first term of the integrand in equation 3.11 is transformed using the usual strain–displacement equations, see appendix C.

$$\boldsymbol{\varepsilon} = \mathbf{B}\mathbf{d} \quad \text{where } \mathbf{B} = \frac{d^2}{dx^2}\mathbf{N} = \mathbf{N}'' \tag{3.12}$$

Using these expression the first term in equation 3.11 becomes:

$$\int_V \frac{1}{2}\boldsymbol{\varepsilon}^\mathbf{T}\mathbf{E}\boldsymbol{\varepsilon} dV = \int_V \frac{1}{2}\mathbf{d}^\mathbf{T}\mathbf{N}''\mathbf{E}\mathbf{N}''\mathbf{d} dV \tag{3.13}$$

The second term, on the other hand, requires a little bit of manipulation. First of all, the second order nonlinear terms have to be added to the strain–displacement relations (see appendix C) and the term becomes (Wilson, EL., Inc):

$$\int_V \boldsymbol{\varepsilon}^{\mathbf{T}} \boldsymbol{\sigma}_0 dV = \frac{1}{2} \int_V [\overline{\mathbf{u}}_{,x}^T \quad \overline{\mathbf{u}}_{,y}^T \quad \overline{\mathbf{u}}_{,z}^T] \boldsymbol{\Sigma} \begin{bmatrix} \overline{\mathbf{u}}_{,x} \\ \overline{\mathbf{u}}_{,y} \\ \overline{\mathbf{u}}_{,z} \end{bmatrix} dV = \frac{1}{2} \int_V \mathbf{g}^{\mathbf{T}} \boldsymbol{\Sigma} \mathbf{g} dV \tag{3.14}$$

where $\boldsymbol{\Sigma}$ is the initial stress matrix:

$$\boldsymbol{\Sigma} = \begin{bmatrix} \boldsymbol{\sigma}_{xx} & \boldsymbol{\sigma}_{xy} & \boldsymbol{\sigma}_{xz} \\ \boldsymbol{\sigma}_{yx} & \boldsymbol{\sigma}_{yy} & \boldsymbol{\sigma}_{yz} \\ \boldsymbol{\sigma}_{zx} & \boldsymbol{\sigma}_{zy} & \boldsymbol{\sigma}_{zz} \end{bmatrix}, \quad \boldsymbol{\sigma}_{rs} = \begin{bmatrix} \mathbf{s}_{ij} & 0 & 0 \\ 0 & \mathbf{s}_{ij} & 0 \\ 0 & 0 & \mathbf{s}_{ij} \end{bmatrix}_0 \tag{3.15}$$

where $r, s \, \epsilon \{x, y, z\}$, $\mathbf{s}$ represent initial stresses and:

$$\mathbf{g} = \mathbf{G}\mathbf{d} \quad \text{where } \mathbf{G} = \frac{d}{dx}\mathbf{N} \tag{3.16}$$

Finally the potential energy of a single element becomes:

$$\Pi = \frac{1}{2}\left(\int_{V_e} \mathbf{d_e^T} (\mathbf{N}'')^{\mathbf{T}} \mathbf{E} \mathbf{N}'' \mathbf{d_e} + \mathbf{d_e^T} (\mathbf{N}')^{\mathbf{T}} \boldsymbol{\Sigma} \mathbf{N}' \mathbf{d_e} dV_e \right) \tag{3.17}$$

$$= \frac{1}{2}\left(\mathbf{d_e^T} \Big(\underbrace{\int_{V_e} (\mathbf{N}'')^{\mathbf{T}} \mathbf{E} \mathbf{N}'' dV_e}_{\mathbf{k_{em}}} \Big) \mathbf{d_e} + \mathbf{d_e^T} \Big(\underbrace{\int_{V_e} (\mathbf{N}')^{\mathbf{T}} \boldsymbol{\Sigma} \mathbf{N}' dV_e}_{\mathbf{k_{eg}}} \Big) \mathbf{d_e} \right) \tag{3.18}$$

$$= \frac{1}{2}(\mathbf{d_e^T k_{em} d_e} + \mathbf{d_e^T k_{eg} d_e}) = \frac{1}{2} \mathbf{d_e^T k_e d_e} \tag{3.19}$$

where $\mathbf{k_{em}}$ and $\mathbf{k_{eg}}$ are the elements material and geometric stiffness matrices, adding them together gives the total element stiffness matrix $\mathbf{k_e}$.

The third and last part of the Lagrangian functional is the work done by external forces on an arbitrary solid:

$$W_f = \int_V \mathbf{u}^{\mathbf{T}} \mathbf{f_b} dV + \int_{S_f} \mathbf{u}^{\mathbf{t}} \mathbf{f_s} dS_f - \frac{1}{2} \int_V \mathbf{u}^{\mathbf{T}} c \dot{\mathbf{u}} dV \tag{3.20}$$

where the first term represents work done on the solid by body forces, the

second term is work done by surface traction and the last term represents work done by dissipative forces. S_f represents the surface of the solid and c damping. For a single element equation 3.20 becomes:

$$\begin{aligned} W_f &= \int_{V_e} \mathbf{d_e^T N^T f_b} dV_e + \int_{S_e} \mathbf{d_e^T N^T f_s} dS_e - \frac{1}{2} \int_{V_e} \mathbf{d_e^T N^T} c \mathbf{N} \dot{\mathbf{d}}_\mathbf{e} dV_e \\ &= \mathbf{d_e^T} \Bigg(\underbrace{\int_{V_e} \mathbf{N^T f_b} dV_e}_{\mathbf{F_b}} \Bigg) + \mathbf{d_e^T} \Bigg(\underbrace{\int_{S_e} \mathbf{N^T f_s} dS_e}_{\mathbf{F_s}} \Bigg) - ... \\ &\quad ... - \frac{1}{2} \mathbf{d_e^T} \Bigg(\underbrace{\int_{V_e} \mathbf{N^T} c \mathbf{N} dV_e}_{\mathbf{c_e}} \Bigg) \dot{\mathbf{d}}_\mathbf{e}^\mathbf{T} \\ &= \mathbf{d_e^T F_b} + \mathbf{d_e^T F_s} - \frac{1}{2} \mathbf{d_e^T c_e} \dot{\mathbf{d}}_\mathbf{e}^\mathbf{T} = \mathbf{d_e^T f_e} - \frac{1}{2} \mathbf{d_e^T c_e} \dot{\mathbf{d}}_\mathbf{e}^\mathbf{T} \end{aligned} \tag{3.21}$$

where $\mathbf{c_e}$ is the elements damping matrix, $\mathbf{F_b}$ and $\mathbf{F_s}$ are element nodal forces, equivalent to the body and surface forces acting on it and. Adding them together yields the total element nodal load vector:

$$\mathbf{f_e} = \mathbf{F_b} + \mathbf{F_s} \tag{3.22}$$

Now that all terms of the Lagrangian functional have been stated for an element, equations 3.8, 3.19 and 3.21 can be inserted into equation 3.5:

$$\delta \int_{t_1}^{t_2} \left(\frac{1}{2} \dot{\mathbf{d}}_\mathbf{e}^\mathbf{T} \mathbf{m_e} \dot{\mathbf{d}}_\mathbf{e} - \frac{1}{2} \mathbf{d_e^T k_e d_e} + \mathbf{d_e^T f_e} - \frac{1}{2} \mathbf{d_e^T c_e} \dot{\mathbf{d}}_\mathbf{e} \right) = 0 \tag{3.23}$$

$$\Rightarrow \int_{t_1}^{t_2} (\delta \dot{\mathbf{d}}_\mathbf{e}^\mathbf{T} \mathbf{m_e} \dot{\mathbf{d}}_\mathbf{e} - \delta \mathbf{d_e^T k_e d_e} + \delta \mathbf{d_e^T f_e} - \delta \mathbf{d_e^T c_e} \dot{\mathbf{d}}_\mathbf{e}) = 0 \tag{3.24}$$

$$\Rightarrow \int_{t_1}^{t_2} \delta \mathbf{d_e^T} (-\mathbf{m_e} \ddot{\mathbf{d}}_\mathbf{e} - \mathbf{c_e} \dot{\mathbf{d}}_\mathbf{e} - \mathbf{k_e d_e} + \mathbf{f_e}) dt = 0 \tag{3.25}$$

Appendix B illustrates how equation 3.24 is obtained from 3.23; the interchangeability of the integration and variation operators is used (Clarke, 2013). The same principle is also used to get from equation 3.24 to 3.25, only with different operators, i.e. between the variation and differentiation

operators:

$$\delta\dot{\mathbf{d}}_\mathbf{e}^\mathbf{T} = \delta\left(\frac{d\mathbf{d}_\mathbf{e}^\mathbf{T}}{dt}\right) = \frac{d}{dt}(\delta\mathbf{d}_\mathbf{e}^\mathbf{T}) \tag{3.26}$$

Using this rule and integrating the first term of equation 3.24 by using integration by parts (Kreyszig, 2010):

$$\int_{t_1}^{t_2} \delta\dot{\mathbf{d}}_\mathbf{e}^\mathbf{T}\mathbf{m_e}\dot{\mathbf{d}}_\mathbf{e}dt = \underbrace{[\delta\mathbf{d}_\mathbf{e}^\mathbf{T}\mathbf{m_e}\dot{\mathbf{d}}_\mathbf{e}]_{t_1}^{t_2}}_{=0} - \int_{t_1}^{t_2} \delta\mathbf{d}_\mathbf{e}^\mathbf{T}\mathbf{m_e}\ddot{\mathbf{d}}_\mathbf{e}dt = -\int_{t_1}^{t_2} \delta\mathbf{d}_\mathbf{e}^\mathbf{T}\mathbf{m_e}\ddot{\mathbf{d}}_\mathbf{e}dt \tag{3.27}$$

The first term after the initial integration is equal to zero because of the conditions that were stated in the beginning that each time history of displacements must satisfy, i.e. $\delta d_e = 0$ at t_1 and t_2. The integration sign in equation 3.25 can be dropped because if the integral is supposed to equal zero then the integrand must also equal zero:

$$\delta\mathbf{d}_\mathbf{e}^\mathbf{T}(-\mathbf{m_e}\ddot{\mathbf{d}}_\mathbf{e} - \mathbf{c_e}\dot{\mathbf{d}}_\mathbf{e} - \mathbf{k}\mathbf{d_e} + \mathbf{f_e}) = 0 \tag{3.28}$$

Since $\delta\mathbf{d}_\mathbf{e}^\mathbf{T}$ is not necessarily equal to zero, the equation inside the parenthesis must equal zero. Finally the equation of motion for a single element is complete:

$$\mathbf{m_e}\ddot{\mathbf{d}}_\mathbf{e} + \mathbf{c_e}\dot{\mathbf{d}}_\mathbf{e} + \mathbf{k_e}\mathbf{d_e} = f_e \tag{3.29}$$

And so Hamilton's principle has been used to derive the equation of motion, along with the element matrices. These matrices for a beam element are:

$$\mathbf{m_e} = \rho\int_{l_{el}} \mathbf{N}^\mathbf{T}\mathbf{N}dx \tag{3.30}$$

$$\mathbf{c_e} = c\int_{l_{el}} \mathbf{N}^\mathbf{T}\mathbf{N}dx \tag{3.31}$$

$$\mathbf{k_{em}} = EI_z\int_{l_{el}} (\mathbf{N}'')^\mathbf{T}\mathbf{N}''dx \tag{3.32}$$

$$\mathbf{k_{eg}} = P\int_{l_{el}} (\mathbf{N}')^\mathbf{T}\mathbf{N}'dx \tag{3.33}$$

where all variables have been defined in chapter 2. Although the element's damping matrix may be calculated according to equation 3.31 it is often better to skip it and formulate the global damping matrix using the global

mass and stiffness matrices (see section 3.1.3), and therefore the element damping matrix is left out for now.

These integrals are calculated for the beam element with 2 DOF at each node with the help of the Hermitian interpolation functions (Cook et al., 2001):

$$N_1 = \frac{1}{4}(1-\zeta)^2(2+\zeta) \tag{3.34}$$

$$N_2 = \frac{1}{8}(1-\zeta)^2(1+\zeta) \tag{3.35}$$

$$N_3 = \frac{1}{4}(1+\zeta)^2(2-\zeta) \tag{3.36}$$

$$N_4 = -\frac{1}{8}(1+\zeta)^2(1-\zeta) \tag{3.37}$$

$$\mathbf{N} = [N_1\ N_2\ N_3\ N_4],\ \mathbf{N}' = [N_1'\ N_2'\ N_3'\ N_4'],\ \mathbf{N}'' = [N_1''\ N_2''\ N_3''\ N_4''] \tag{3.38}$$

where ζ is the isoparametric coordinate. Defined as $-1 \leq \zeta \leq 1$, $\zeta = -1$ represents the left end of the element while $\zeta = 1$ represents the right. The element matrices are presented in appendix D for the 2 DOF element. For the 3 DOF element the rows and columns for the axial DOF are simply added. There are no coupling effects between the axial DOF and the other ones. The entries in the matrices that relate to the axial DOF are calculated in the same manner as the other ones but with different shape functions. Linear shape functions are used:

$$N_1 = 1 - \zeta, \quad N_2 = \zeta \tag{3.39}$$

Once the element matrices have been formulated coordinate transformation is needed to take them from local to global coordinates:

$$\mathbf{M_e} = \mathbf{T'm_eT} \quad \mathbf{K_e} = \mathbf{T'k_eT} \tag{3.40}$$

where $\mathbf{M_e}$ and $\mathbf{K_e}$ are the element matrices in global coordinates and $\mathbf{T}$ is the transformation matrix for the element (see appendix D). Only when that is finished can the element matrices be assembled into the global matrices:

$$\mathbf{K}_{cw} = \sum_{i=1}^{N_{el}} \mathbf{K}_{e,i} \quad \mathbf{M}_{cw} = \sum_{i=1}^{N_{el}} \mathbf{M}_{e,i} \tag{3.41}$$

where and N_{el} for number of elements in the model. Assembly for the messenger wire is the same. These matrices are then introduced to the system's total matrices from equation 3.1.

Registration arm, support bracket and droppers: The mass, damping and stiffness values for each of the main components of the catenary system can be added to the global mass, damping and stiffness matrices individually. Each entry in the matrices corresponds to a DOF at a certain node, therefore it is simply a matter of finding those entries and adding the value to them. The registration arms and support brackets are modelled as mass–springs so they contribute to the mass and stiffness matrices while the droppers are modelled as mass-springs-dashpots so they add to the mass, stiffness and damping matrices.

The droppers couple the contact and messenger wire and so their formulation requires more thought. They are modelled as mass–spring-dashpots and the force in each dropper is:

$$f_{dr,i} = m_{dr}g + k_{dr}(v_{mw} - v_{cw}) + c_{dr}(\dot{v}_{mw} - v_{cw}) \tag{3.42}$$

where the subscript dr is for dropper and g is the gravitational acceleration. The droppers represent a nonlinearity in the catenary system because if it slackens it gives no resistance to the vertical motion of the wire (Cho, 2008). These nonlinear effects will not be included in the model developed here. Values for mass, stiffness and damping of these different parts are given in table 2.2. As an example the following shows how stiffness of a dropper is implemented in the global stiffness matrix:

$$\mathbf{K}_{dr} = \begin{pmatrix} \ddots & \cdots & \cdots & \cdots & \\ \vdots & k_{dr} & \cdots & -k_{dr} & \vdots \\ \vdots & \vdots & \ddots & \vdots & \vdots \\ \vdots & -k_{dr} & \cdots & k_{dr} & \vdots \\ & \cdots & \cdots & \cdots & \ddots \end{pmatrix} \begin{pmatrix} \vdots \\ v_{cw} \\ \vdots \\ v_{mw} \\ \vdots \end{pmatrix} \tag{3.43}$$

3.1.2 Pantograph model

Unlike the catenary, the pantograph is a smaller entity and not a part of a greater system. Due to this, experimentation and research on it is easier and more practical. Several research papers from the literature survey focus on developing an optimized pantograph model, where a sensitivity analysis is performed on the pantograph's design variables (e.g. head mass, head stiffness etc.) (Lee et al., 2012; Kim et al., 2007; Park et al., 2003). The producers of pantographs implement the results from these kinds of studies and have well defined models for their products. The pantograph model in the reference case is the WBL88 produced by Schunk Nordiska (sch, 2013) and the mathematical model used here was obtained from them, see appendix F.

The pantograph is modelled as two lumped masses with 2 DOF, where the pan-head is one mass and the frame is idealized as one mass. Between the frame and the roof of the train there is a friction force that acts in opposite direction to movement of the mass and a one-way damper that has a damping value for downwards motion but not upwards. For simplicity the model will assume the damper works in both ways. Two forces act on the mass, aerodynamic and static. The aerodynamic force is given as $5N$ given a train speed of $100km/h$, the force is dependent on speed but the variations is low and $5N$ will be assumed for all speeds. The static force is set to $60N$ but for Norwegian conditions $55N$ is used, therefore $55N$ will be used in this thesis. The top mass is actually split into two masses that will in reality experience different degrees of motion but they are considered negligible and therefore the masses are modelled as one. Between the top mass and the frame there are springs and dashpots. The adapted pantograph model is seen in figure 3.2. Equations of motion for the pantograph:

$$2m_1\ddot{v}_{tm} + 2c_1\dot{v}_{tm} + 2j_1v_{tm} - 2c_1\dot{v}_{fr} - 2k_1v_{fr} = -F(t) \tag{3.44}$$

$$m_2\ddot{v}_{fr} + (2c_1 + c_3)\dot{v}_{fr} + 2k_1v_{fr} - 2c_1\dot{v}_{tm} - 2k_1v_{tm} = ... \\ ... = F_{a2} + F_1 - sgn(v_{fr})U_1 \tag{3.45}$$

where v_{tm} and v_{fr} are vertical displacement for top mass and frame respectively, $F(t)$ is the contact force covered in section 3.1.4, $sgn(\cdot)$ is equal $+1$ if $\cdot$ is positive and -1 if $\cdot$ is negative and all other variables are defined in

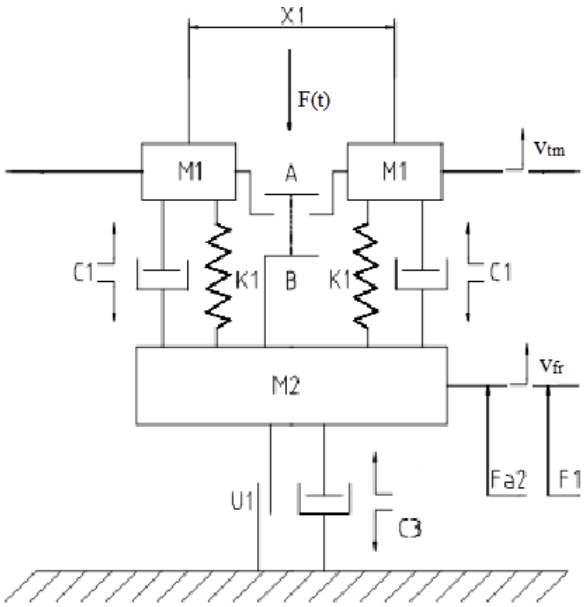

Figure 3.2: Adapted pantograph model after the one obtained from Schunsk Nordiska, (sch, 2013)

appendix F. The equations in matrix form:

$$\begin{bmatrix} 2m_1 & 0 \\ 0 & m_2 \end{bmatrix} \begin{Bmatrix} \ddot{v}_{tm} \\ \ddot{v}_{fr} \end{Bmatrix} + \begin{bmatrix} 2c_1 & -2c_1 \\ -2c_1 & (2c_1 + c_3) \end{bmatrix} \begin{Bmatrix} \dot{v}_{tm} \\ \dot{v}_{fr} \end{Bmatrix} + \ldots$$
$$\ldots + \begin{bmatrix} 2k_1 & -2k_1 \\ -2k_1 & 2k_1 \end{bmatrix} \begin{Bmatrix} v_{tm} \\ v_{fr} \end{Bmatrix} = \begin{bmatrix} -F(t) \\ F_{a2} + F_1 - sgn(v_{fr})U_1 \end{bmatrix} \tag{3.46}$$

or:

$$\mathbf{M}_{pg}\ddot{\mathbf{d}}_{pg} + \mathbf{C}_{pg}\dot{\mathbf{d}}_{pg} + \mathbf{K}_{pg}\mathbf{d}_{pg} = \mathbf{F}_{pg} \tag{3.47}$$

where the subscript pg stands for pantograph.

3.1.3 Damping

Formulating the damping matrix for vibrating structures is a key factor in accurately modelling it. Damping is the physical phenomenon of reducing oscillations that occur in a system, it is the dissipation of mechanical energy into another form of energy (e.g. heat). The catenary–pantograph system is

an oscillating system and therefore it is important to characterize its damping. Damping in the pantograph is well known, and the knowledge obtained on it from other research is implemented in the pantograph model described in section 3.1.2. Few studies have looked into damping in the catenary. This section focuses on how damping in the catenary has been treated and new ways of treating it.

The catenary is obviously a damped system as its response decreases gradually after it has been excited by the pantograph. Several papers state that the system can be assumed lightly damped (Cho et al., 2006; Arnold and Simeon, 2000; Poetsch et al., 1997) and furthermore (Wu and Brennan, 1998) states that the system can be assumed lightly damped for train speed up to $500km/h$. Due to the low damping in the system and the uplift of the wire, vibrations will occur over an area much bigger than the one near the pantograph location. That means that the system must be simulated as a whole. The choice of a time–step integration method has to take the low damping into account, for example it would be inaccurate to introduce numerical damping. The errors introduced by the integration method will be conserved in the system since the damping is low, that is why it is important to use small time steps to counteract that effect. The numerical model developed here uses a single pantograph and according to (Harell et al., 2005), which studies multiple pantograph setups, damping has a much greater effect on a a trailing pantograph than a leading one. Despite that, damping is still extremely important for any system if one wants to accurately predict its response.

The majority of studies on the catenary–pantograph system use mass and stiffness proportional damping (Rayleigh damping). A part of these studies, where it is mentioned specifically, are (Pombo and Ambrosio, 2012; Facchinetti and Bruni, 2012; Benet et al., 2007; Cho et al., 2010; Alberto et al., 2008; Seo et al., 2006; Sølvberg, 2008; Seo et al., 2005; Diana et al., 1998). In (Drugge, 2000), damping is proportional only to stiffness and is determined using the lowest eigenfrequency. The only damping model that is not proportional found in the literature survey is where an equivalent damping model is used for a 1 DOF analytical model in (Lopez-Garcia et al., 2007) and (Kia et al., 2010). Due to this commonly accepted practice, Rayleigh damping is used in the numerical model. The shortcomings

of Rayleigh damping is that damping is the same for each eigenmode. A method was proposed in (Wilson and Penzien, 1972), where each mode can have its own damping behaviour. This method is introduced here and the effect it has on the system behaviour is examined. Two other methods developed in (Adhikari, 2000; Pilkey, 1998) were also examined for use in this numerical method but measurement data was needed for their implementation. Measurements were performed on the reference system for this purpose among others, but the results could not be used.

Rayleigh damping Characterizing the global damping matrix using a linear combination of the global mass and stiffness matrices is called proportional damping or Rayleigh damping. In addition to these global matrices, eigenfrequencies of the system are needed along with critical damping ratios to formulate the damping matrix. Eigenfrequencies are obtained from the global mass and stiffness matrices by solving the undamped free vibration problem (Felippa, 2004):

$$\mathbf{M}\ddot{\mathbf{d}} + \mathbf{K}\mathbf{d} = 0 \tag{3.48}$$

where the variables were defined before in section 3.1.1. Introducing a solution $\mathbf{d}(t) = \sum_i \mathbf{v}_i e^{j\omega_i t}$ into equation 3.48:

$$(-\omega_i^2\mathbf{M} + \mathbf{K})\mathbf{v} = 0 \Rightarrow det[\mathbf{K} - \lambda_i\mathbf{M}] = 0 \tag{3.49}$$

where $\lambda_i = \omega_i^2$ is the i–th eigenfrequency and $\mathbf{v}$ is the eigenvector. Solving this problem for a multi DOF system can be quite cumbersome. MATLAB provides a built–in function that solves it automatically ($eig(\mathbf{K}, \mathbf{M})$).

The damping matrix, using Rayleigh damping:

$$\mathbf{C} = \alpha\mathbf{M} + \beta\mathbf{K} \tag{3.50}$$

where the coefficients α and β are dependent on eigenfrequencies (ω) and critical damping ratios(ξ), see figure 3.3. Critical damping ratios indicate if the system is underdamped ($\xi < 1$), critically damped ($\xi = 1$) or overdamped ($\xi > 1$) (Rönnquist, 2012). Choosing two values for critical damping ratios and two eigenfrequencies for the equations shown in figure 3.3 produces a set

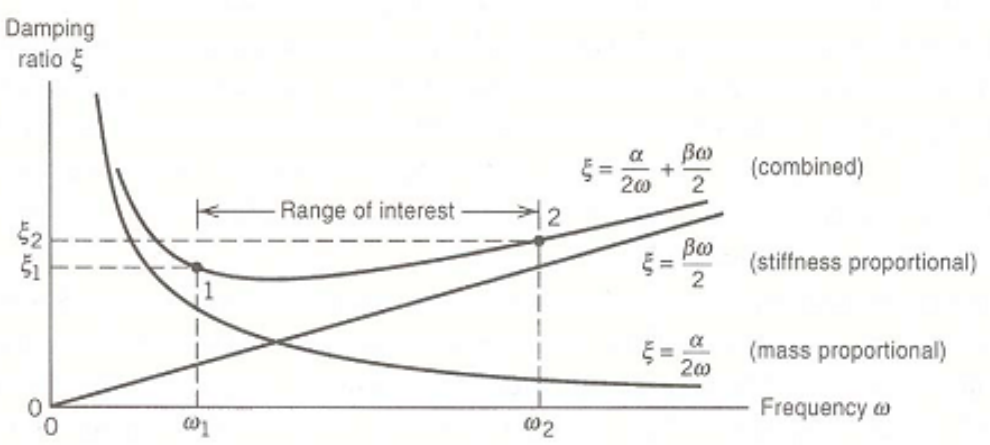

Figure 3.3: Fraction of critical damping necessary to obtain Rayleigh damping coefficients (Cook et al., 2001).

of linear equations, solving for α and β:

$$\alpha = \frac{2\omega_m\omega_n(\xi_m\omega_n - \xi_n\omega_m)}{\omega_n^2 - \omega_m^2} \quad n \neq m \tag{3.51}$$

$$\beta = \frac{2(\xi_n\omega_n - \xi_m\omega_m)}{\omega_n^2 - \omega_m^2} \quad n \neq m \tag{3.52}$$

Usually the first two eigenfrequencies are chosen to calculate the coefficients. According to (Poetsch et al., 1997) the critical damping ratio values for the wires are between $0,003$ and $0,01$ but a more recent experiment shows that these values may be overly conservative, the values should be between $0,01$ and $0,04$ (Cho et al., 2006). This is an important parameter and will be included in the parameter study, for the reference case $0,01$ is used for both wires. Finally the damping matrix can be formulated by using equation 3.50. Rayleigh damping is a good solution for the damping problem, but only if the system shows similar damping characteristics in different parts of it (Cook et al., 2001). This is important to consider, since damping can be quite different near registration arms and support brackets for example. To counteract that effect, the mass and stiffness matrices used to find the eigenfrequencies include the individual values from those parts.

Orthogonal damping matrix proposed in (Wilson and Penzien, 1972) The derivation method was done with the help of (Wilson, EL., Inc). Assume that the now known damping matrix satisfies the following criterion:

$$\mathbf{\Phi^T C \Phi} = \begin{bmatrix} \ddots & & \\ & 2\omega_n\xi_n & \\ & & \ddots \end{bmatrix} \tag{3.53}$$

where $\mathbf{\Phi}$ is the eigenvector matrix and the right hand side matrix contains only entries on the diagonal for every eigenfrequency and its corresponding critical damping ratio. It is important that the eigenvector matrix be normalized so that

$$\mathbf{\Phi^T M \Phi} = \mathbf{I} \tag{3.54}$$

where $\mathbf{I}$ is the entity matrix. Pre–multiply equation 3.53 by $\mathbf{\Phi M}$ and post–multiply it by $\mathbf{M\Phi^T}$:

$$\underbrace{\mathbf{\Phi M \Phi^T}}_{\mathbf{I}} \mathbf{C} \underbrace{\mathbf{\Phi M \Phi^T}}_{\mathbf{I}} = \mathbf{\Phi M}(2\omega_n\xi_n)\mathbf{M\Phi^T} = \sum_{n=1}^{N} C_n \tag{3.55}$$

where n is the number of node and N is the total number of nodes. That is how a damping matrix can be formulated for each specific mode separately. According to (Wilson, EL., Inc) this modal damping matrix is physically impossible and is simply a mathematical definition. The total damping matrix can finally be written as:

$$\mathbf{C} = \sum_{n=1}^{N} C_n = \sum_{n=1}^{N} 2\xi_n\omega_n \mathbf{M}\mathbf{v}_n\mathbf{v^T}_n\mathbf{M} \tag{3.56}$$

where as with Rayleigh damping, $\mathbf{v}_n$ is the n–th eigenvector.

Comparison between Rayleigh and Wilson–Penzien damping is presented in the results section.

3.1.4 Contact formulation

The contact formulation implemented here is based on the contact model presented in (Zhou and Zhang, 2011). Equations of motions for the catenary and pantograph have already been formulated along with the respective mass,

damping and stiffness matrices. The equation of motion for the whole system was stated in equation 3.1 where the matrices are defined as:

$$\mathbf{M} = \begin{bmatrix} \mathbf{M}_{cw} & \mathbf{0} \\ \mathbf{0} & \mathbf{M}_{pg} \end{bmatrix}, \mathbf{C} = \begin{bmatrix} \mathbf{C}_{cw} & \mathbf{0} \\ \mathbf{0} & \mathbf{C}_{pg} \end{bmatrix}, \mathbf{K} = \begin{bmatrix} \mathbf{K}_{cw} & \mathbf{0} \\ \mathbf{0} & \mathbf{K}_{pg} \end{bmatrix} \tag{3.57}$$

The zero notation in the matrices represent matrices full of zeros that fill up the space needed to complement the matrices. The vectors in equation 3.1 are similarly:

$$\mathbf{d} = \begin{Bmatrix} \mathbf{d}_{cw} \\ \mathbf{d}_{pg} \end{Bmatrix}, \dot{\mathbf{d}} = \begin{Bmatrix} \dot{\mathbf{d}}_{cw} \\ \dot{\mathbf{d}}_{pg} \end{Bmatrix}, \ddot{\mathbf{d}} = \begin{Bmatrix} \ddot{\mathbf{d}}_{cw} \\ \ddot{\mathbf{d}}_{pg} \end{Bmatrix}, \mathbf{F} = \begin{Bmatrix} \mathbf{F}_{cw} \\ \mathbf{F}_{pg} \end{Bmatrix} \tag{3.58}$$

The matrices and vectors presented above from equation 3.1 have all been defined before and nothing has changed except now they represent the whole catenary–pantograph system.

The coupling effect for the system is implemented by the contact force. As seen in section 3.1.2 the contact force is applied on the top mass with the direction pointing downwards. For the catenary wire, it is upwards pointing and at the same global location as the pantograph is supposed to be. The position of the pantograph is calculated by using the train's speed. For each time step the displacements of both catenary and pantograph are calculated, then the contact force is derived from them:

$$\text{If } \mathbf{v}_{cw} > \mathbf{v}_{pg}, \quad \text{then } \mathbf{F}(t) = 0 \tag{3.59}$$

$$\text{If } \mathbf{v}_{cw} < \mathbf{v}_{pg}, \quad \text{then } \mathbf{F}(t) = k_c|\mathbf{v}_{cw} - \mathbf{v}_{pg}| \tag{3.60}$$

where $\mathbf{v}_{cw}$ and $\mathbf{v}_{pg}$ are the vertical displacements of the catenary and pantograph respectively, $\mathbf{Fk}$ is the contact force and k_c is the contact stiffness. The contact stiffness is set to $50.000N/m$, according to (EN 50318:2002, 2002). Equation 3.59 states that if there is a gap between the catenary and pantograph the contact force is equal to zero and the program moves on to the next time step. If on the other hand, there is no gap, the contact force is calculated based on how far the pantograph penetrates the catenary wire. Once the force has been calculated it is implemented in the total force vector and the new displacements are calculated for the same time step using

the updated force vector, these displacements are then used in the next time step. Performing a check like this in every time step ensures that even though there is a detachment the model will attach again.

3.1.5 Time–stepping method

Due to low damping and wave propagation in the catenary, it is important to choose the right time–stepping solution method for the system for the reasons stated in section 3.1.3. The time–stepping solution method used in the numerical model is the constant average acceleration method, which is a special case of the Newmark method (see section E). This method is also used in several other studies, for example in (Zhou and Zhang, 2011). In (Cho, 2008) however, the HHT–α method (see (Cook et al., 2001)) is chosen based on a study between it and the constant average acceleration method. The HHT–α method is chosen because it does not undergo spurious oscillations, however it does introduce numerical damping that was not considered acceptable by (Poetsch et al., 1997). Beyond these two methods there are several more that have been used, for example central difference method (Benet et al., 2007), and all of them have their pros and cons so it is up to the user to weigh those against the goals of the study. This study aims for simplicity and a fast running model, that is why the constant average acceleration method is chosen.

According to the results from (Cho, 2008) the time step has to be maximum $\Delta t = 0,001s$ for the dispersive wave propagation to be included. The requirement made by the standard (EN 50119:2001, 2001) is that the catenary–pantograph must be modelled for at least every $0,2m$ of length, so the time step is dependent on the train's velocity. Considering the known sufficient time step of $\Delta t = 0,001s$, using the requirement from (EN 50119:2001, 2001) would yield a velocity of about $720km/h$. If velocity in the model exceeds that, the time step needs to be lowered. However it is unlikely that this study needs to check the response of the system for such great speeds and the time step is set constant to $\Delta t = 0,001s$.

3.2 Results

Results from the numerical model are presented here, they are based on the reference system and most values can be obtained from table 2.2. Values that are not given there are the time step implemented, contact stiffness, velocity of the train and element size. Choice of time step and contact stiffness was discussed in sections 3.1.5 and 3.1.4 and are $\Delta = 0,001s$ and $k_c = 50.000N/m$, respectively. The velocity chosen for the reference case is $100km/h$ which is reasonably below allowable design value for the span $130km/h$. Element size was chosen $0,5m$ because it has proven to be the optimal size for a numerical model of the system (Cho, 2008). Effects from axial degrees of freedom are considered negligible for the contact wire and a 4 DOF element is used, while the 6 DOF element is still used for the messenger wire. In addition, effects from coordinate transformation are negligible and will therefore be skipped. Four spans will be modelled in order to avoid reflection effects of the wave from the endpoints and most results will be obtained from the third span, i.e. third from the origin. After the results from the reference case have been covered, the results from the parameter study are presented. Note that more focus is put on examining the contact wire since its behaviour is more directly related to the dynamic behaviour of the system. Figure 3.4 shows initial geometry of the model.

3.2.1 Results for reference system

Static displacement of the system is calculated by:

$$\mathbf{d}_{static} = \mathbf{K}^{-1}\mathbf{F} \tag{3.61}$$

The global force vector used to calculate static displacement is assembled by element force vectors like the global mass and stiffness matrices, these vectors for the 6 and 4 DOF elements are expressed as:

$$\mathbf{f}_{e,6DOF} = \begin{bmatrix} P & -\frac{\rho g l_{el}}{2} & -\frac{\rho g l_{el}^2}{12} & -P & -\frac{\rho g l_{el}}{2} & \frac{\rho g l_{el}^2}{12} \end{bmatrix}^T \tag{3.62}$$

$$\mathbf{f}_{e,4DOF} = \begin{bmatrix} -\frac{\rho g l_{el}}{2} & -\frac{\rho g l_{el}^2}{12} & -\frac{\rho g l_{el}}{2} & \frac{\rho g l_{el}^2}{12} \end{bmatrix}^T \tag{3.63}$$

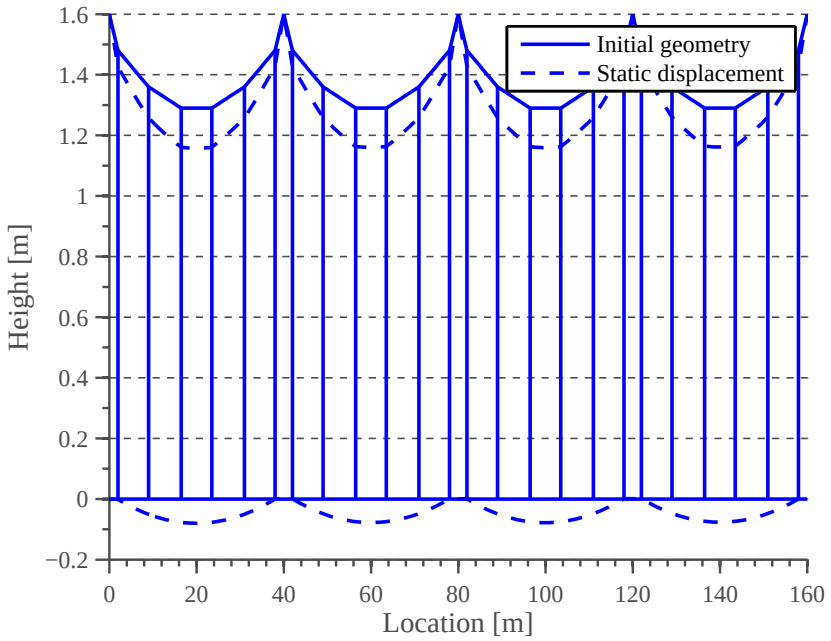

Figure 3.4: Static displacement of the four spans together with initial geometry.

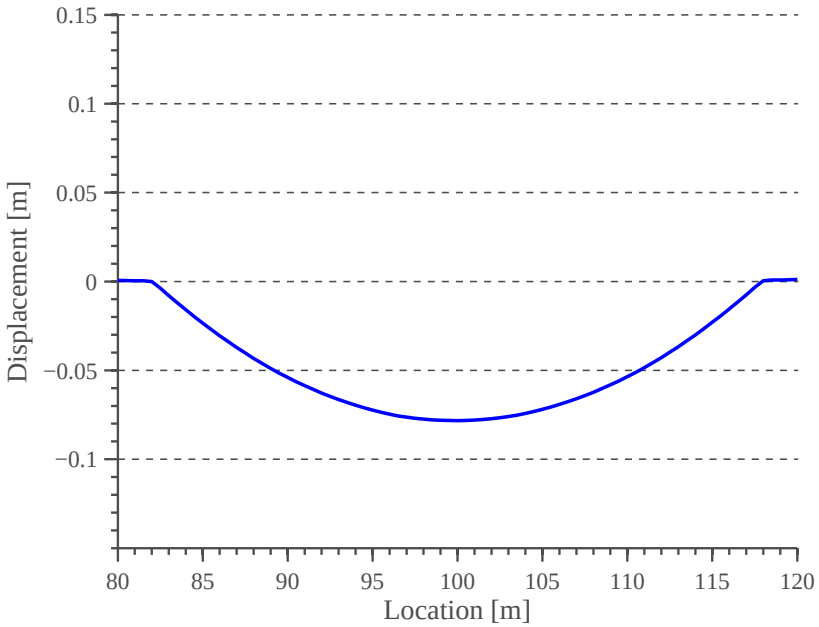

Figure 3.5: Static displacement of the contact wire in the third span.

Maximum static displacement in the contact wire obtained from the program is $\approx 8cm$, while the recommended value is $4cm$ using a ratio of $1:1000$ between pre–sag and span length. Error between calculated and recommended value is 50%. The error could be credited to the fact that out in the field the geometry is controlled and can deviate from what it is supposed to be. Modelling the support poles and droppers could reduce the error, but this would have to be checked in a further study. Having the static displacement of the contact wire correct is important to the dynamic behaviour of the system, as will be shown in the parameter study. Static displacement is shown together with initial geometry in figure 3.4 and figure 3.5 shows the static result of the contact wire in span 3.

Elasticity is obtained from the model and compared to the one obtained by measurements in figure 3.6. The modelled curve fits well with the measured one, although as mentioned in section 2.2 there are errors in the measured data. However, the curves show similar form and numbers while the modelled curve is more conservative. Uniformity of the modelled elasticity is $55,5\%$ and the midpoint value is $e = 0,77$, these numbers compare well to the

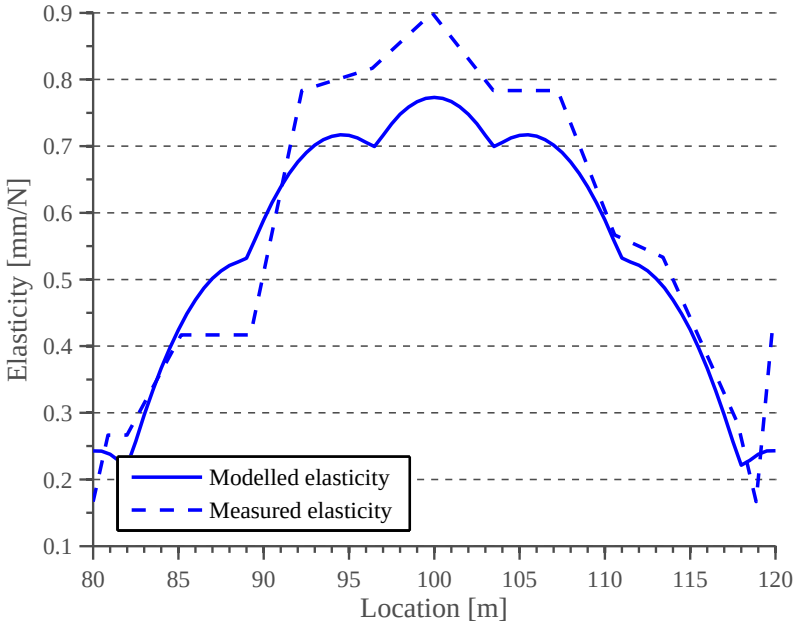

Figure 3.6: Elasticity of span 3 in the numerical model compared with measured elasticity for the reference span.

recommended values in table 2.3.

Eigenfrequencies for the four span system are shown in figure 3.7, modes are only shown for the contact wire but they are similar in the messenger wire. Both mode shapes and frequencies compare well with what other researchers have found for the system, such as in (Kiessling et al., 2012; Zhang et al., 2006). The lower modes dominate the system, as was observed out in the field for the reference system.

Wave propagation velocity for the contact wire in the reference span is:

$$c_{p,cw} = \sqrt{\frac{10e3}{0,94}} = 103,14m/s = 371km/h$$

Plotting up the displacement of a single point can help calculate the wave propagation velocity of the wire in the model. Figures 3.8, 3.9 and 3.10 show the displacement of three points in span 3. Matlab is used to accurately find the time when the point first starts to move, i.e. when the displacement first

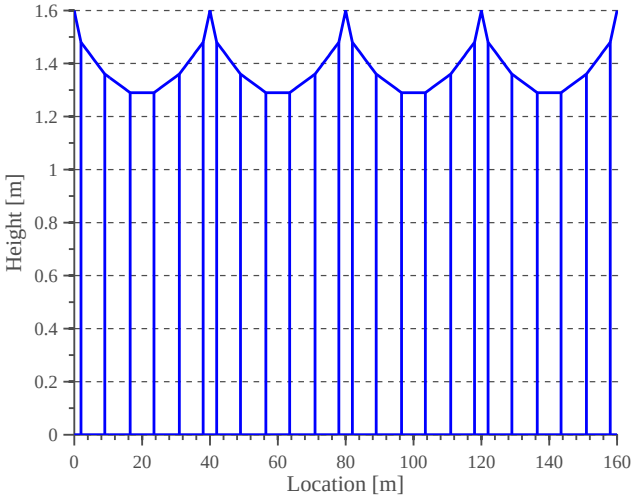

(a) The model

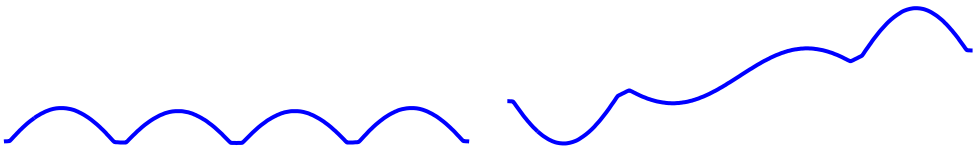

(b) Nr. 1, $f_1 = 1,06Hz$

(c) Nr. 2, $f_2 = 1,08Hz$

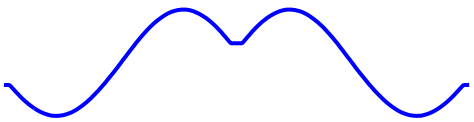

(d) Nr. 3, $f_3 = 1,14Hz$

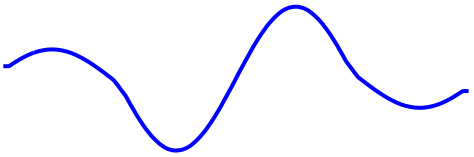

(e) Nr. 4, $f_4 = 1,21Hz$

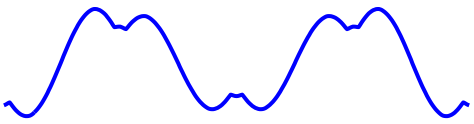

(f) Nr. 5, $f_5 = 2,09Hz$

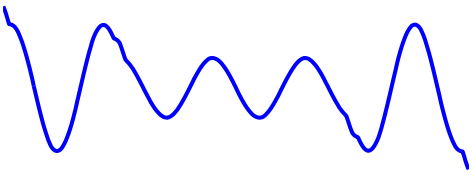

(g) Nr. 10, $f_{10} = 3,13Hz$

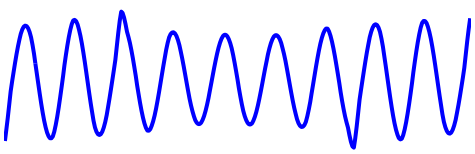

(h) Nr. 20, $f_{20} = 5,74Hz$

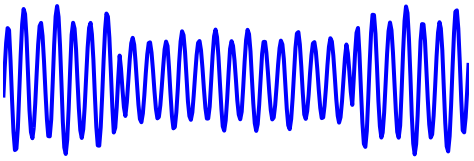

(i) Nr. 100, $f_{100} = 17,83Hz$

Figure 3.7: Eigenmodes of the contact wire for the four spans modelled. The number and frequency (f_i) of each mode, i, is given below each figure.

exceeds 1E+5m. The location of the point is known and the time when it first starts to move and from that wave propagation velocity is calculated. Table 3.1 shows the calculated wave propagation velocity for each point and the average. Average value is calculated and compared to the theoretical value, the error is $0,62\%$. Figure 3.8 shows the vertical displacement at a support pole, the maximum value is around $12mm$ which is way below the reference value presented in section 2.1.8 of around $50mm$. Those values were obtained for much higher speeds and should probably be lower, but $12mm$ is acceptable.

Table 3.1: Calculated wave propagation velocity values for chosen points in span 3

x [m]	c_p [km/h]
80	375,5
90	372,0
100	372,3
Average	373,3
Theoretical	371

Dropper slackening has been discussed and many researchers believe it to be important to the dynamic behaviour of the system. Figures 3.11 and 3.12 show how the height of droppers 15 and 18 in the model ($x = 96,5m$ and $x = 118m$). The figures show that the droppers experience compression before and after the train passes and it would be an improvement to the model if their mechanical properties were removed from the global matrices as they slacken.

Contact force is presented for all four spans in figure 3.13 and concentrated on span 3 in figure 3.14. Initial steps are required to reach equilibrium in the calculations and that is why span 3 is shown separately, no numerical disturbances should affect it. The contact force's mean and standard deviation are given in the figure captions. Comparing the results from the numerical model and the requirements it can be seen that the mean and generally the total range are fine, but the standard deviation is higher than it should be. That could be because dropper slackening is not modelled.

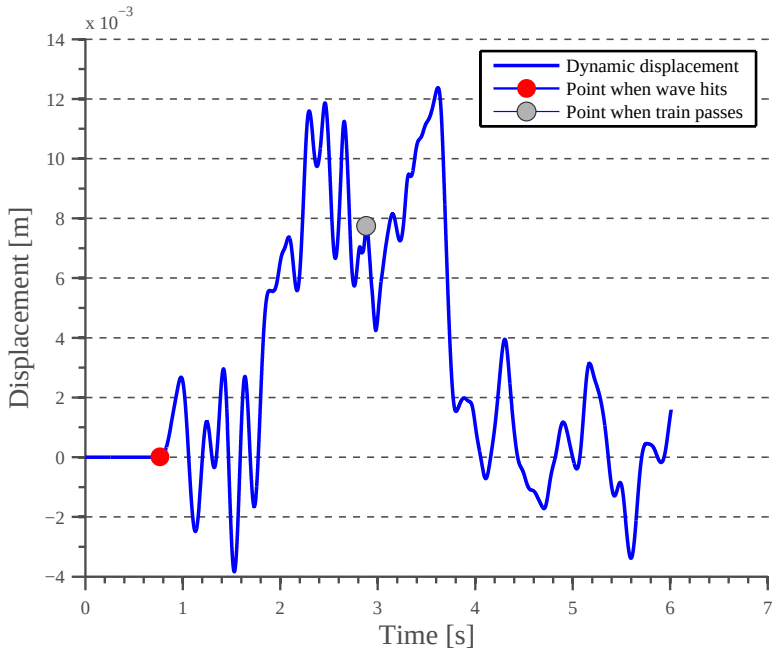

Figure 3.8: Vertical displacement of a point at support pole in span 3 ($x = 80m$) for the contact wire.

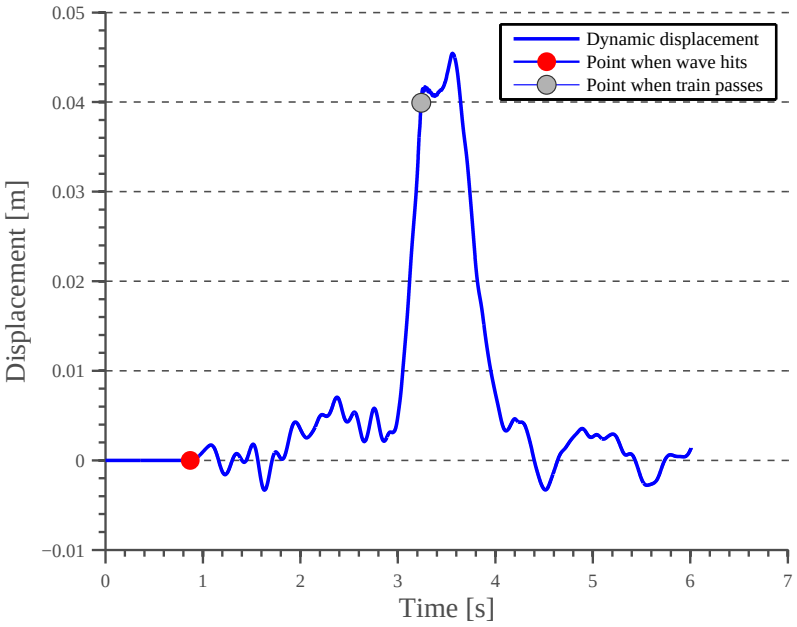

Figure 3.9: Vertical displacement of a point in span 3 ($x = 90m$) for the contact wire.

The statistical range recommended, see figure 2.10, says that for a velocity of $100km/h$ the contact force should be within $15 - 120N$. This range is violated six times, one above and five below. That being said, although the statistical range is violated no contact loss occurs in span 3. Displacement curves of the pantograph and contact wire at each point as the train passes by for span 3 is shown in figure 3.15. It clearly shows that problems arise as the pantograph nears the support pole, because that is where the biggest changes in elasticity occur.

3.2.2 Parameter study

Now that the dynamic behaviour of the system has been observed it is interesting to see what happens when some of the parameters are changed. A parameter study is accomplished by running the model several times, changing one parameter each time while the other remain unchanged. The following parameter study examines the effects of tension force, velocity of the train, critical damping ratio and the method of modelling damping. The system

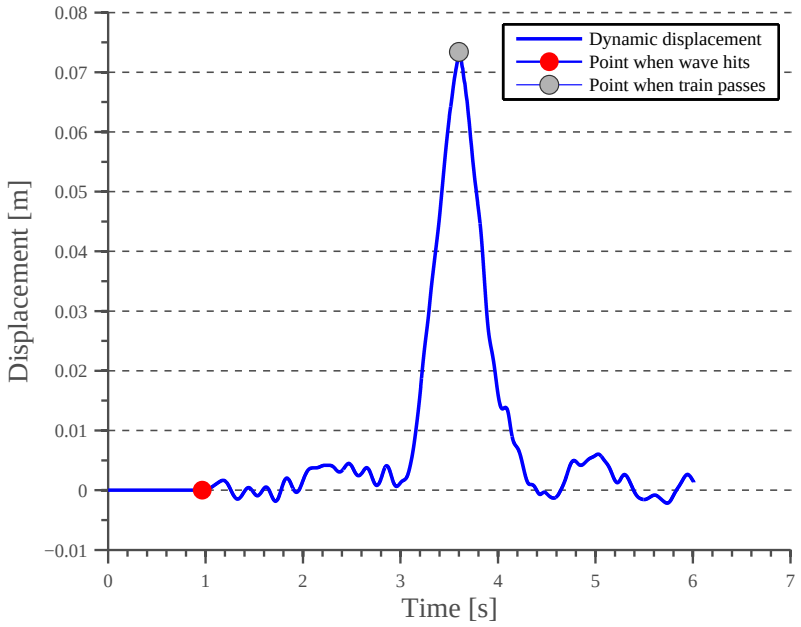

Figure 3.10: Vertical displacement of the midpoint of span 3 ($x = 100m$) for the contact wire.

which is examined is still the reference system, so that when the parameters that is being studied is changed all others are set to reference system values.

Tension force Reference values for tension forces in the system are $5kN$ and $10kN$ for the messenger and contact wire, respectively. An analysis was run were results for max. static displacement, max. dynamic displacement at chosen points, mean and standard deviation of contact force along with a count for contact loss were obtained for tension values of $2,5kN - 15kN$ with intervals of $500N$. Changing the tension had severe effects on the system as was expected, results are shown in figures 3.16-3.22.

As the tension force increases the dynamic behaviour of the system becomes more stable, the contact force's mean generally increases and the standard deviation of it decreases. Maximum static and dynamic displacements decrease as tension force is increased. Changes in dynamic displacement at the support point are more erratic than at midpoint, but so is the nature of its time history of displacement (see figure 3.8. For low tension force values there seem to be greater effects on the system, as can be seen from contact

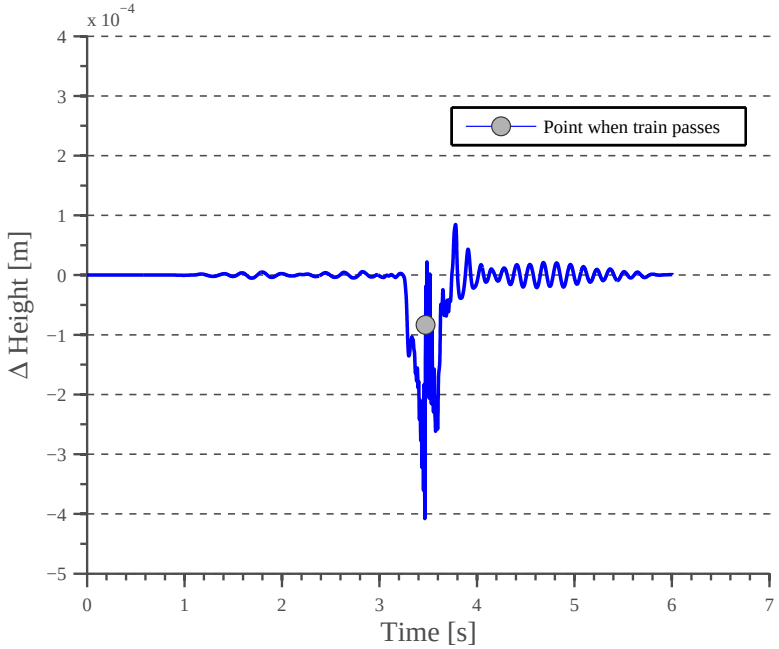

Figure 3.11: Height change of dropper number 15 in the model, span 3 ($x = 96, 5m$).

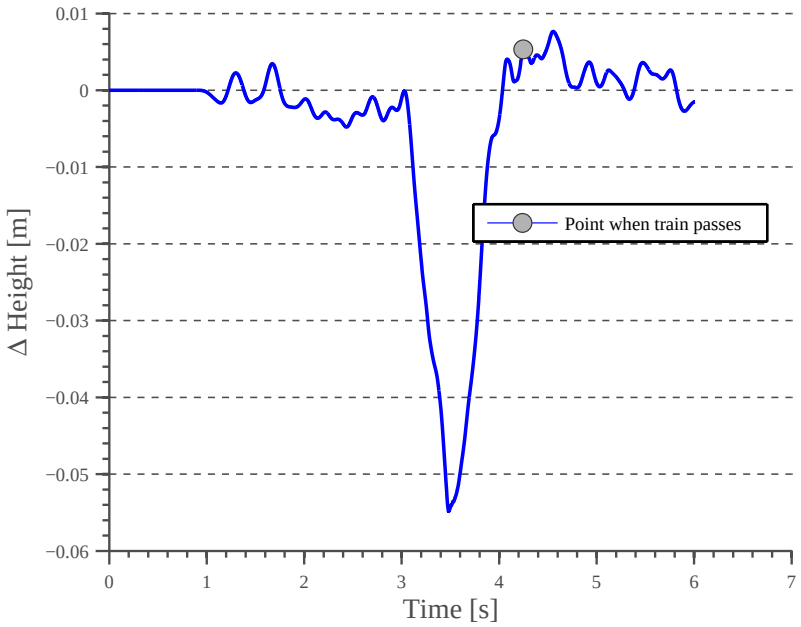

Figure 3.12: Height change of dropper number 18 in the model, span 3 ($x = 118m$).

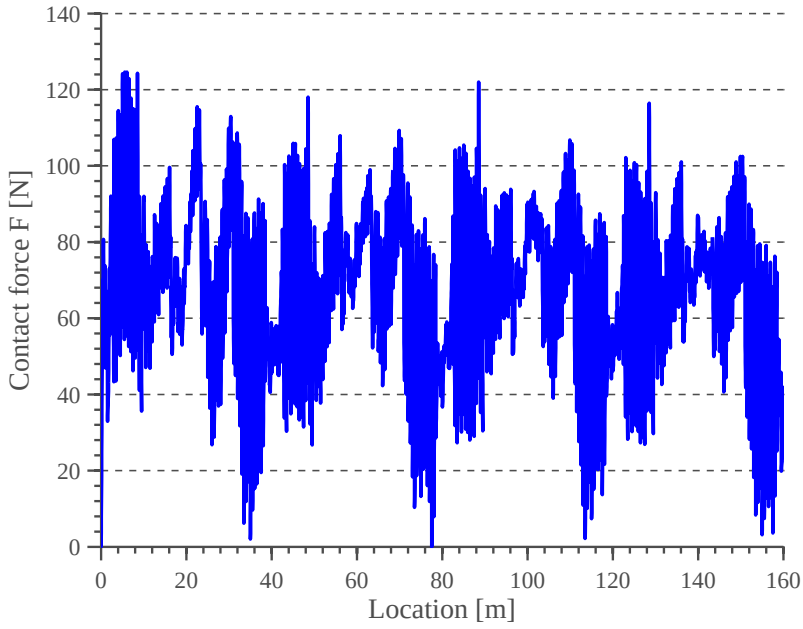

Figure 3.13: The contact force for all four spans. Mean contact force is $F_m = 65N$ and standard deviation of it is $\sigma_m = 23,8N$.

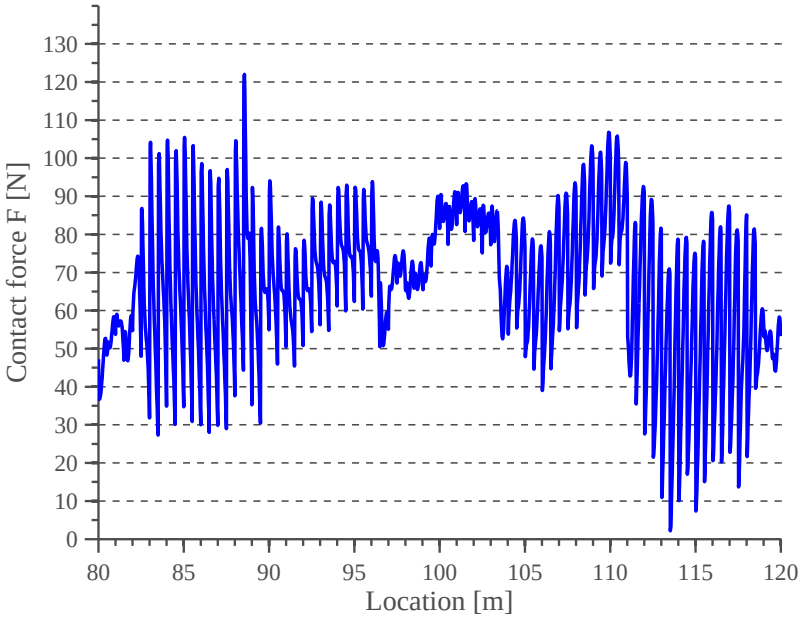

Figure 3.14: The contact force for span 3. Mean contact force is $F_m = 67,3N$ and standard deviation of it is $\sigma_m = 19N$.

loss and standard deviation, when it is low these values become dangerously large for the system's behaviour. The numerical model obviously captures the wave propagation velocity of the contact wire as can be seen from figure 3.22. As the tension increases, the theoretical value will increases obviously, but what is interesting to see is that the wave propagation velocity observed in the model also increases.

Damping Default value of critical damping ratio for both wires in the reference system is $0,01$. Other researchers have found that this value can be increased to $0,04$ for the messenger wire, but here it was deemed too high. That is why a parameter study was performed for this property, to see what effects it had to change the value. For completeness of the study, both values were varied between $0,01 - 0,04$ with an interval of $0,005$. The damping model proposed by Wilson and Penzien was implemented. Critical damping ratios were varied between $0,01 - -0,04$, where the ratio is $0,04$ for the first eigenfrequency and ascends down to the last one where the ratio is $0,01$. Implementing the damping model did not change much in

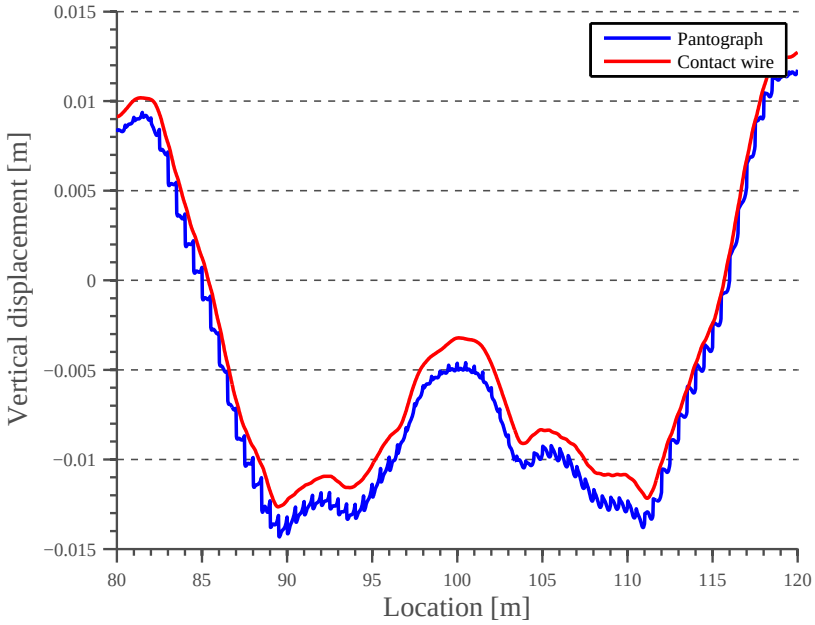

Figure 3.15: Displacement curves of pantograph and contact wire at points when the train passes by.

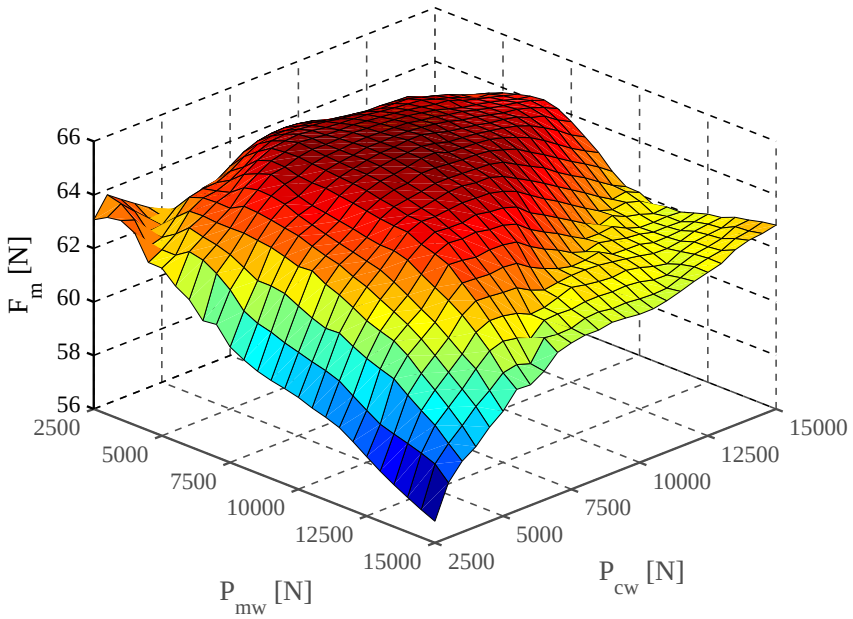

Figure 3.16: Mean contact force for different values of tension in the wires.

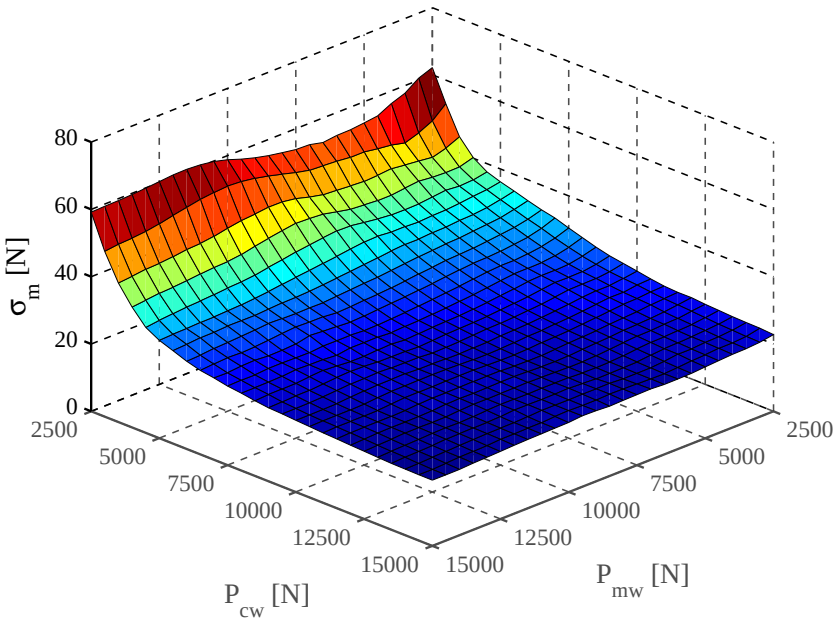

Figure 3.17: Standard deviation of contact force for different values of tension in the wires.

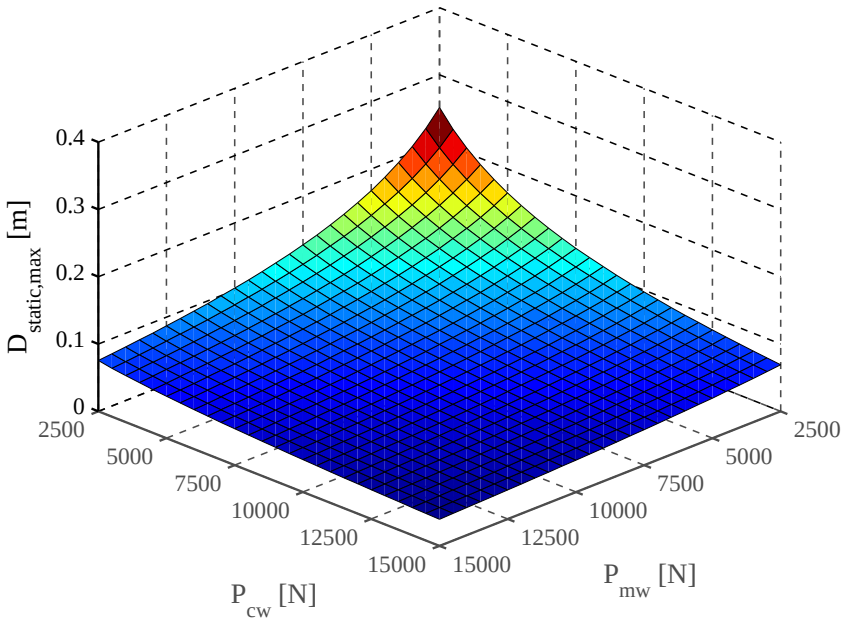

Figure 3.18: Maximum static displacement, which is always at midspan, for different values of tension in the wires.

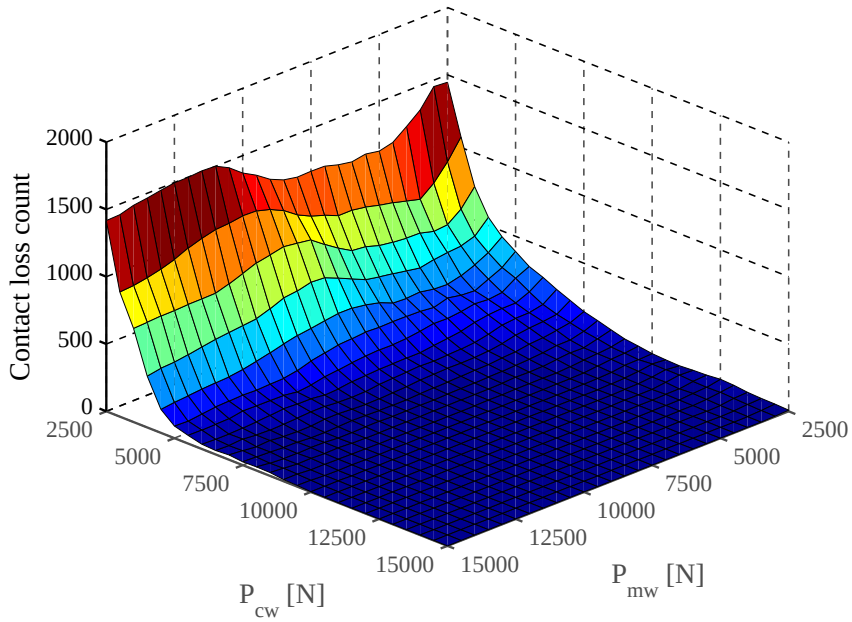

Figure 3.19: Number of times contact loss occurs for each run of the model, plotted with different values of tension in the wires.

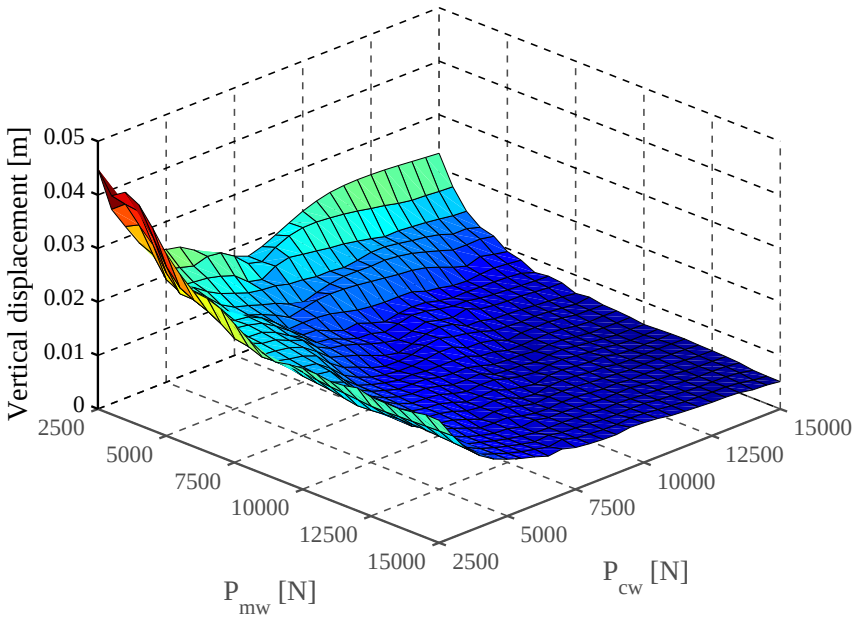

Figure 3.20: Maximum vertical displacement at support point $x = 80m$ for different values of tension in the wires.

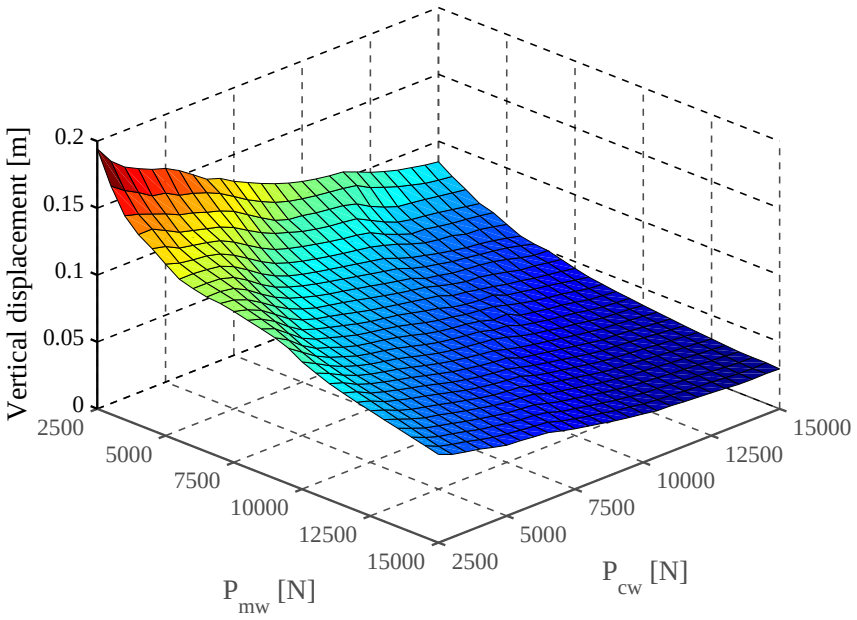

Figure 3.21: Maximum vertical displacement at midpoint of span 3 $x = 100m$ for different values of tension in the wires.

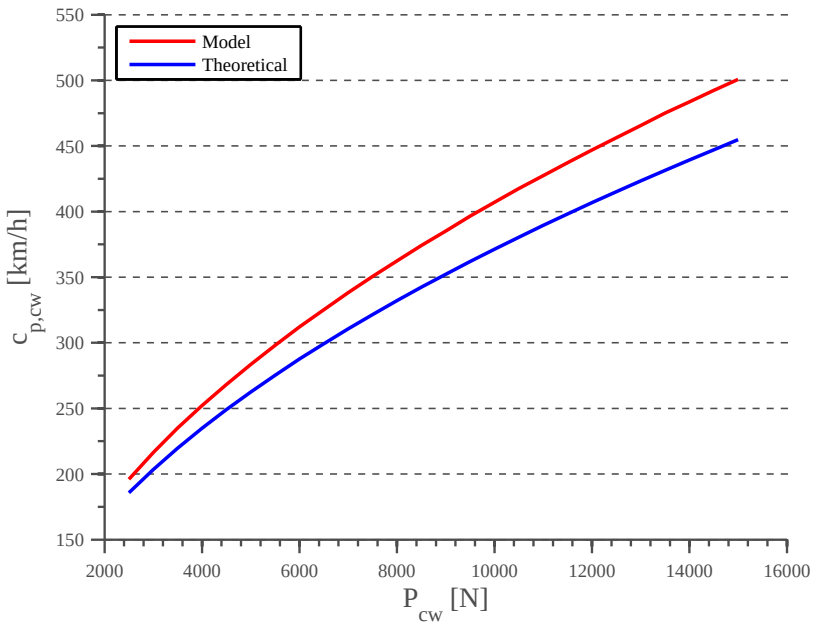

Figure 3.22: Wave propagation velocity ($c_{p,cw}$) of the contact wire for different tension force values, measured at midpoint of third span ($x = 90m$).

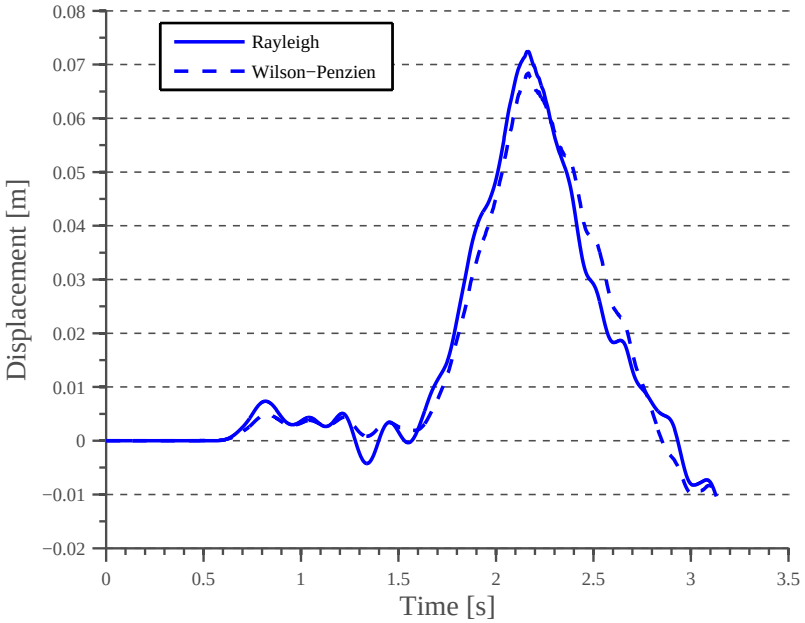

Figure 3.23: Vertical displacement time histories at midpoint of span 3 ($x = 100m$) for two different damping models, Rayleigh and Wilson–Penzien.

the system, see figure 3.23. More information is required about eigenmodes and eigenfrequencies for the system for that to be effective. Furthermore, effects from damping can be better researched when there are more than one pantographs in the system.

Varying the critical damping ratio between these boundaries had almost no effects on the mean or standard deviation of the contact force, which is why it is not displayed here. Figure 3.25 shows the vertical displacement time history of a chosen point (midpoint of span 3, $x = 90m$) as critical damping ratio is changed. The changes are not big but as the ratio is increased the time history curve becomes more smooth, as expected. Note that for figure 3.25 the critical damping ratio of the contact wire was varied but the one of the messenger wire was fixed at default value. Figure 3.24 shows the number of times contact loss happens with different values of damping ratios. Increasing the ratio for the messenger wire seems to increase contact loss, while increasing it for the contact wire decreases contact loss. Displacements occur at points in the contact wire before the pantograph reaches those points, due to the propagating wave. These displacement have a negative ef-

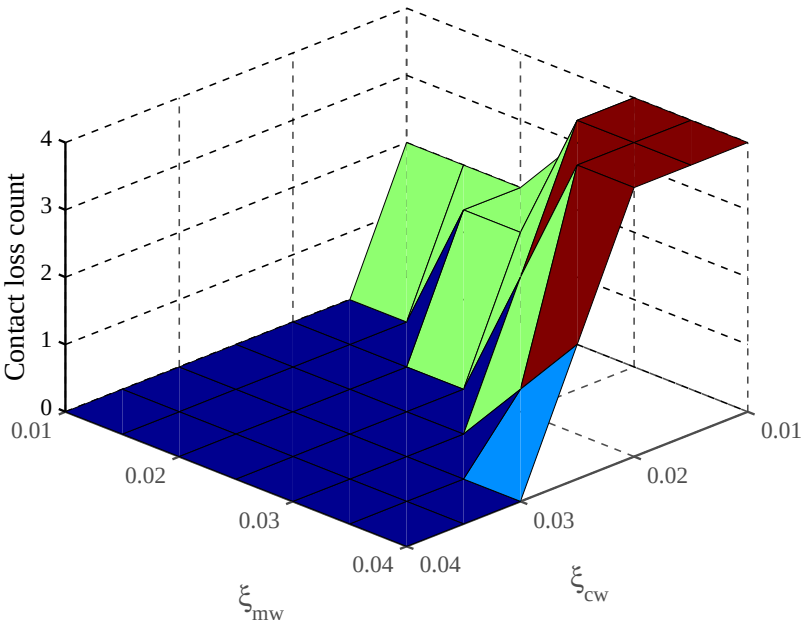

Figure 3.24: Contact loss count plotted up with respect to different damping ratio values for both contact and messenger wires.

fect on the dynamic behaviour of the system, but increasing the damping ratio decreases these displacements, and as the pantograph passes by these points they are closer to being where they are supposed to be. That being said, the damping ratio of the contact wire is obviously a governing factor, and even though the damping ratio of the messenger wire would be increased in the model it would not have much to say.

Train velocity The default value of train velocity is $100km/h$, velocities chosen for the parameter study are $50 - -500km/h$ with a $25km/h$ interval. There are two values of interest for the wire, that is wave propagation velocity and limiting velocity due to reflection in the system as described in sections 2.1.4 and 2.1.1, respectively. These velocities, calculated for the reference system, are $c_{p,cw} = 371km/h$ and $v_{\alpha,cw} = 122,7km/h$ and will be marked on the figures.

Figures 3.26-3.29 show the results from varying train velocity, these results are mean and standard deviation of contact force along with contact loss count and maximum vertical displacements of chosen points. The results

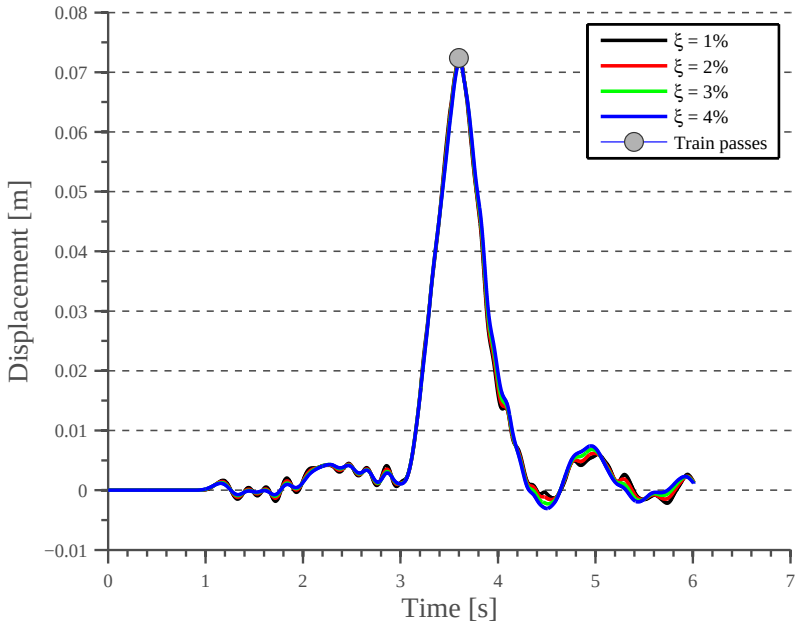

Figure 3.25: Vertical displacement time history of the midpoint of span 3, for different critical damping ratios.

clearly show that at velocities near $c_{p,cw}$ and $v_{\alpha,cw}$ the dynamic behaviour of the system is significantly affected. Peaks in contact force mean and standard deviation along with maximum vertical displacements are almost directly related to these velocities, although contact loss seems to occur near these values. In any case, the dynamic behaviour changes considerably around both velocities and they should be avoided. It is interesting to note that around $c_{p,cw}$ the standard deviation of the contact force is twice as large as the mean, which is unacceptable.

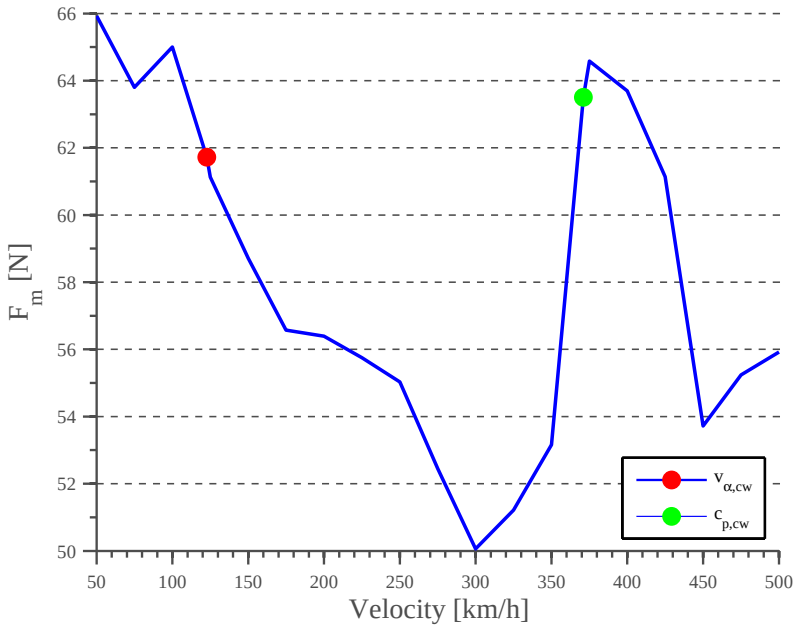

Figure 3.26: Mean of the contact force with different values for velocity of the train.

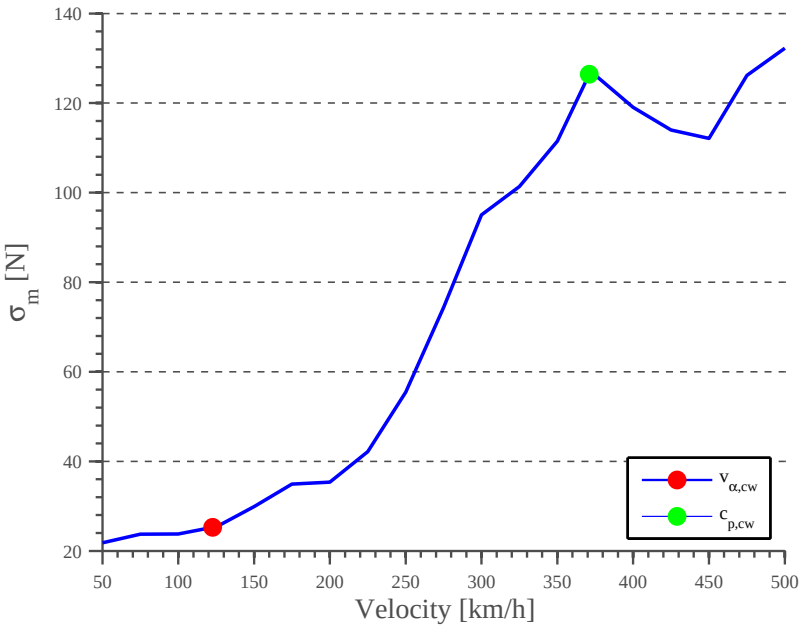

Figure 3.27: Standard deviation of the contact force with different values for velocity of the train.

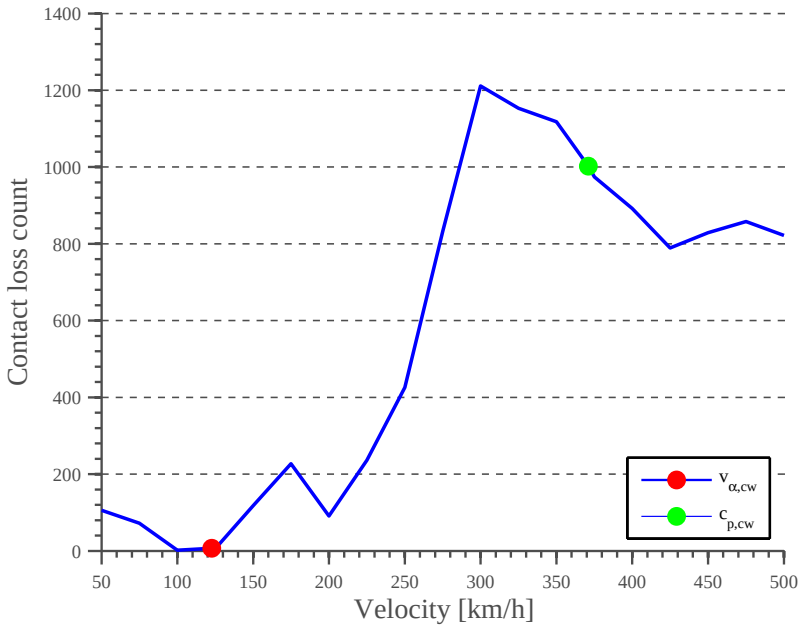

Figure 3.28: Contact loss count with different values for velocity of the train.

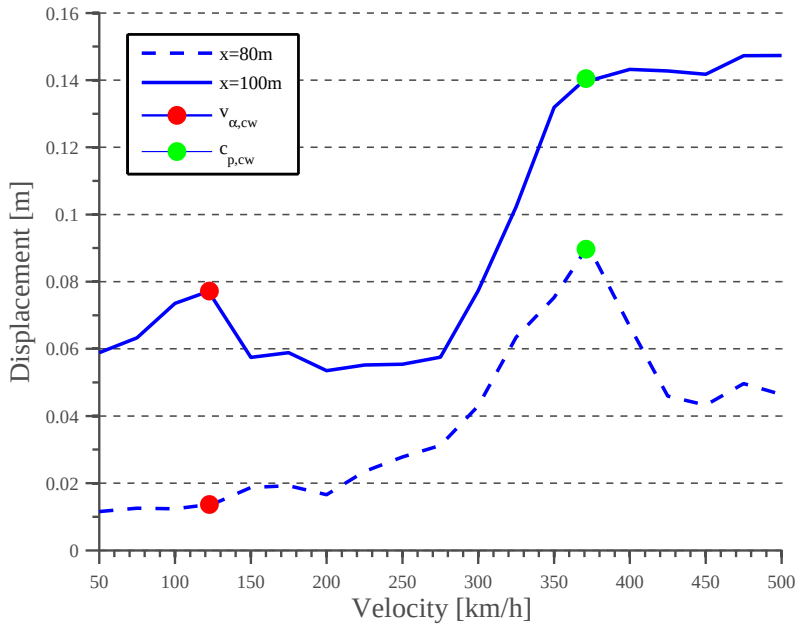

Figure 3.29: Maximum values of vertical displacement values at two different points, support pole in the beginning of span 3 and midpoint of span 3. These are plotted up with different values of train velocity.

4 Laboratory model

When they are built properly, scaled down models of structural systems can be valuable tools for examining its behaviour. For most systems, e.g. the catenary–pantograph, building a full–scale experimental model may be too expensive in terms of time and money. Therefore, it is preferable to scale the system down to a manageable size. Several scaled models have been built before and will be covered in this chapter (Farr et al., 1961; Willets and Edwards, 1966; Willets et al., 1966; Willets and Suddards, 1970; Manabe, 1989; Drugge, 2000). The aim of this chapter is to examine necessary steps for building a scaled model, what works and what does not.

Problems also arise when a scaled model is built. The following questions must be answered before embarking on such as mission. Are the efforts of building the model greater than what is gained by it? Is theoretical knowledge of the system sufficient for a complete study of its dynamic behaviour? Are the measuring devices available able to capture the properties and behaviour of the system? The aim of this chapter is also to try and answer these questions.

4.1 Previous work

4.1.1 Models based on the work from (Farr et al., 1961)

The following articles (Farr et al., 1961; Willets and Edwards, 1966; Willets et al., 1966; Willets and Suddards, 1970) all cover the same model originally built by (Farr et al., 1961) and will therefore be reviewed in the same section.

Only a handful of scaled laboratory models have been built and for studying the catenary–pantograph system. Reasons for that may be that it is a rather troublesome venture since it is a complex system, theoretical understanding has grown considerably over the years and measurement equipment for field testing has evolved significantly.

The earliest scaled model study found for this thesis is the one done by (Farr et al., 1961). In the study, two main reasons are listed for building a scaled model:

- Experimental tests and measurements may be practically and economically unfeasible.

- The system is too complex and theoretical knowledge is inadequate.

Despite advancements in the field of measuring equipment, it is still impractical to perform a complete study on the full–scale system. Most train tracks are used daily so it is difficult to make modification to the components of the system for a certain track. Special test tracks for full–scale studies have been built but are expensive and not worth the cost or effort in most cases. Some of the advancements in measuring equipment has been put to use in a special test train. JBV has one called the Roger1000 and measures variables such as the contact force and displacement of wires. The information obtained by Roger1000 is valuable but the measurements are only done for system checking, not for experimental purposes. Therefore, it is better to build a scaled model in a lab where environmental and system variables can be controlled. The second point mentioned is obsolete. Significant progress has been made in studying the system theoretically, directly and indirectly. With the increase in computational power and development of methods like the finite element method it has become easier to model structural systems in general. Furthermore, understanding of how the catenary–pantograph system works has increased through countless theoretical and experimental studies. Although insufficient theoretical understanding was a reason for them to build a scaled model, with that fixed today it could be a reason for building a model. Researchers armed with this theoretical understanding may have even more success than their predecessors in understanding the system behaviour based on a scaled model.

Setup of the model built in (Farr et al., 1961) is seen in figure 4.1. It is a simple catenary model representing a straight section with no gradients, curves or special sections. Scaled parameters are proposed for a auxiliary contact wire but no test are performed on a compound system. Curved sections are placed at the ends so the pantograph can run continuously and has space to accelerate, but the actual testing area is the straight part of the track. All components of the system are represented in a scaled version, such as supports, droppers (see figure 4(a)) and pantograph (see figure 4.2). One of the biggest problems faced by (Farr et al., 1961) is finding the appropriate material for representation of the wires. Scaling factors are chosen for the system, see section 4.2, and they are implemented for all system variables. Finding a suitable combination of every system variable can be troublesome.

The problem that arises with the wires is that, according to scaling chosen, they need to have the flexibility of a relatively thin wire and mass properties of a thicker wire. Several different approaches were tried like circular wires, stranded wires, non–metallic threads and etc. The best solution was found to be specially manufactured beaded tungsten wires. Maximum allowable speed on the model corresponds to a full–scale speed of $160km/h$ ($28km/h$ scaled).

The devices used to measure up the scaled model were relatively simple compared to what is available today. Basic behaviour of the system is observed, but the results in general are distorted because the system is too much scaled down (Kim, 2007).

In (Willets and Edwards, 1966), the aim was to increase the running speed of the pantograph. That is accomplished by changing the flat curved sections of the model's ends, see figure 4.1, and replacing them by ramps. The gradient of the ramps will slow the pantograph down as it tries to climb and accelerate it as it moves down the ramp. The new model is capable of modelling full–scale speeds up to $200km/h$ ($35km/h$ scaled). In addition the scaled pantograph model was replaced by a simpler model, see figure 4.3. Advanced measuring devices were installed that enabled the authors to extract more information from the model. The results from the model show that as speed is increased, more contact loss occurs, and contact loss happens mostly around the supports or if speed is high enough it happens at mid-span.

(Willets et al., 1966) introduce pre-sag into the model and also study what happens when the number of droppers per span is changed. These changes are implemented on the adjusted model by (Willets and Edwards, 1966). By introducing adjustable droppers, the pre-sag can be controlled in the model see figure 4.4. The results show that optimal pre-sag gives increased design speed, the same happens when the tension force in the wires is increased. Tension force affects the pre–sag, so if it is increased to much, it can have negative effects as seen before. The study also states that decreasing the amount of droppers in the model can have positive effects, when everything is taken into account (e.g. material cost and etc.). Maximum speed for the model is the same as in (Willets and Edwards, 1966).

The third and last study that uses the model from (Farr et al., 1961) is

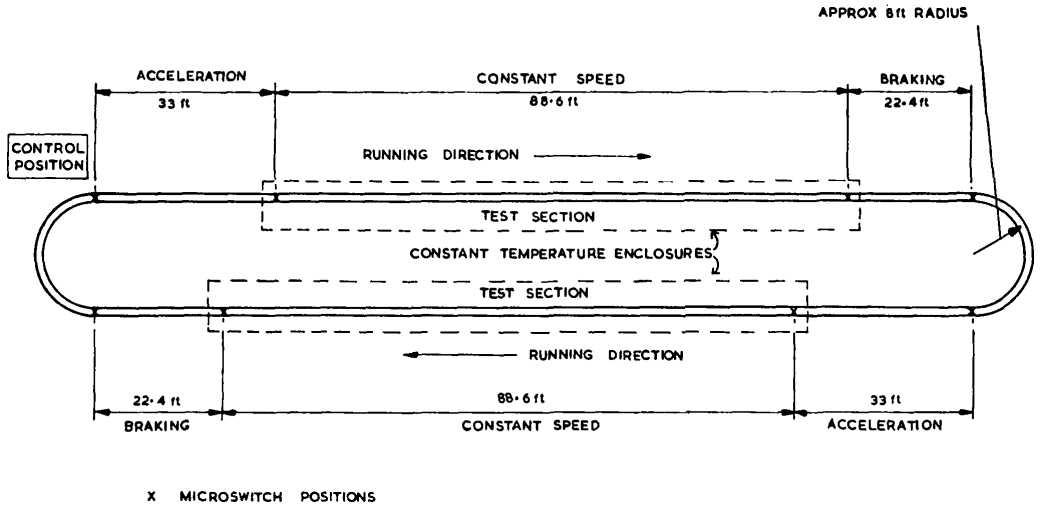

Figure 4.1: Scaled model setup from (Farr et al., 1961).

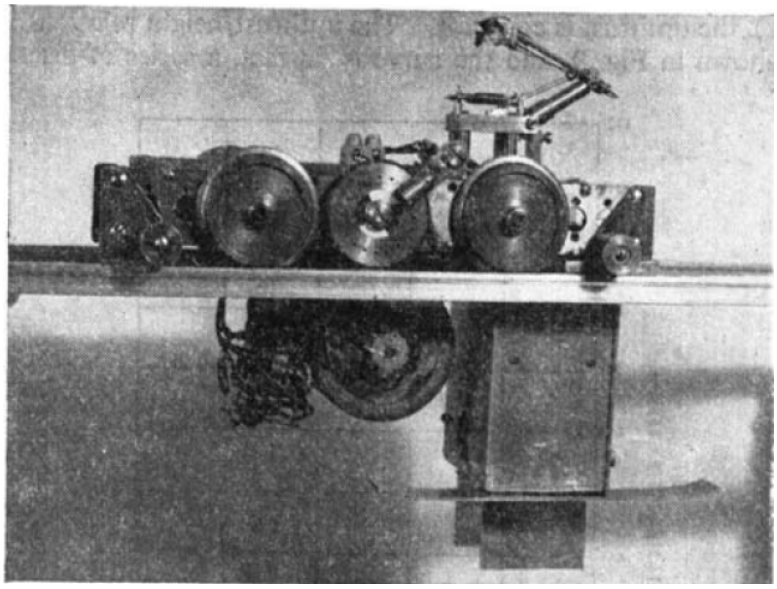

Figure 4.2: Scaled pantograph model from (Farr et al., 1961).

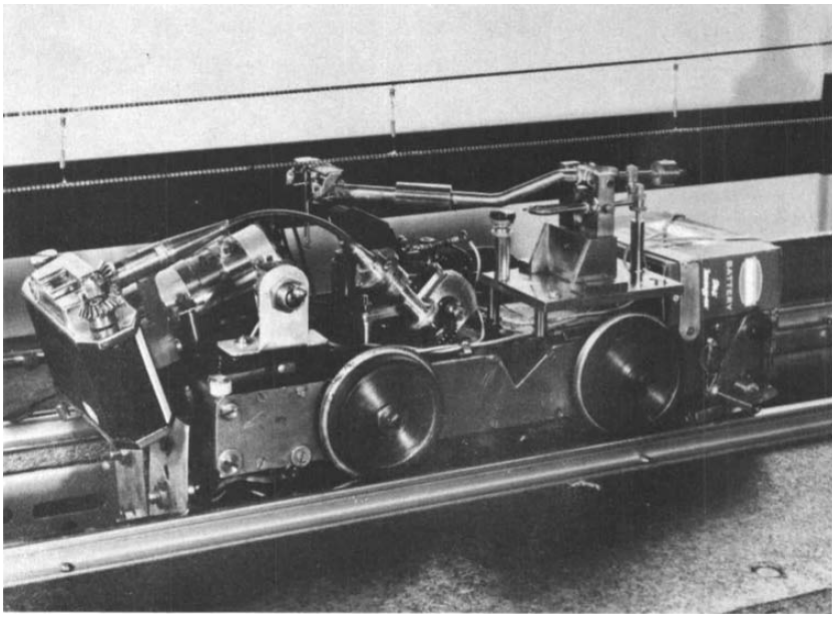

Figure 4.3: Scaled pantograph model from (Willets and Edwards, 1966).

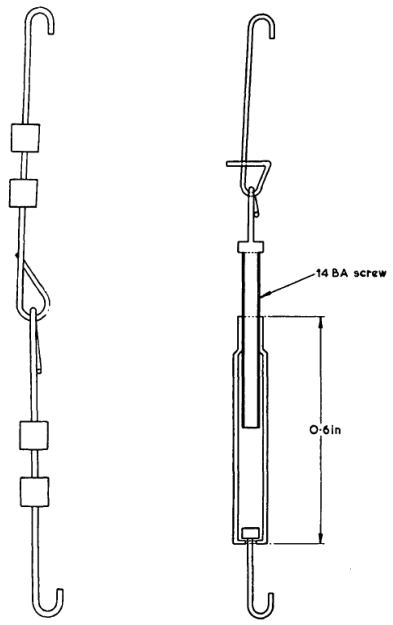

(a) (b)

Figure 4.4: These are two different setups for droppers. The one in 4(a) is the original dropper from (Farr et al., 1961) and the one in 4(b) is the adjustable dropper from (Willets and Edwards, 1966).

(Willets and Suddards, 1970). The changes they make are aimed to increase running speed, changing dropper lengths and testing different catenary systems. Running speed was increased by increasing the size of the ramps and introducing a improved trolley, on which the pantograph lies on. Changes in the pantograph trolley do nothing regarding the dynamic model of the pantograph itself. The final version of the model was able to model full–scale speeds of $320km/h$ ($56km/h$ scaled). Stitched wires and compound catenary setups were also introduced. Similar measurement methods are used as in the previous studies although they added a study of the contact wires elasticity. The study points out that errors can occur between design values and actual values for tension force and dropper lengths. Testing on the lab models reveals that these effects or not great if the errors are within described ranges, see (Willets and Suddards, 1970). Implementing stitched wires, using compound catenary and/or pre-sag improved the performance of the system and increased allowable speeds.

4.1.2 Manabe (1989)

The model built by (Manabe, 1989) builds upon the experience gained in studies covered in section 4.1.1. Manabe's however was to develop a more realistically scaled model, that could be used for quantitative measures.

The model of the catenary is a scaled version of a compound catenary system. Simple copper plate was used for the contact wire and stranded steel wires for messenger wire and auxiliary messenger wire. Due to more favourable scaling choices, finding materials is much easier than for (Farr et al., 1961). The pantograph model is a scaled version of the PS–200 A–type used by the Japanese Shinkansen lines, a comparison study was run with a different two low–mass pantograph model in the study Specially noted in (Manabe, 1989) is a defect in the model, says that the frictional force between pantograph and contact wire along with the aerodynamic force applied to the pantograph do not satisfy the similarity law. These same concerns were raised by (Farr et al., 1961).

Scaling used in the model is performed such that the system parameters (e.g. geometry, mass per unit length etc.) are more realistic. Reaching those realistic values meant instead that the scaled down speed was $50 - 170km/h$ instead of $28km/h$ in (Farr et al., 1961). Manabe's objective was to reach

speeds of $100 - 340km/h$, so his scaling factor for speed was $0,5$. This was accomplished by running the model on an existing pantograph equipment, $500m$ in length (compared to $\approx 40m$ in (Farr et al., 1961), capable of reaching those speeds.

Analysis for the scaled model is more sophisticated than the ones run in section 4.1.1. Importance of the wave propagation velocity is recognized and it plays a key role in the parameter study. Strain gauges are used to measure strain in the contact wire, results show that as the pantograph passes droppers the strain there becomes compressive as is expected. Results show, that as the pantograph's speed reaches the wave propagation velocity in the wire contact loss and stress in the wire increases.

4.1.3 Drugge (2000)

The most recent laboratory model to be built is by (Drugge, 2000). The aim of that model was to be simple yet descriptive of dynamic characteristics in the system. It was used to display the effects of running the pantograph at speeds near the wave propagation speed in the contact wire, multiple pantograph operation, different values for tension in the wire and changes in values for pantograph components.

The catenary part of the model consists of 8 rigid bars that form an octagon, see figure 4.5. In order to simulate a distributed stiffness system, the contact wire is suspended from springs that are fastened to the rigid bars at $25mm$ intervals (length of one rigid bar is $1,928m$). Tension in the wire is obtained by attaching a weight at support pole 1. Support poles are placed between bars and there is a horizontal arm at each one that holds the contact wire, making sure the model does not fall inwards to the center due to the tension force. Maximum allowable scaled down speed on the model is $\approx 30km/h$. Placed in the center of the octagon is a vertical pole, from which the pantograph model is extended on a rotating arm. The pantograph model is made up from a contact bar, a frame and a base see figure 4.6. Dynamic characteristics of a typical pantograph model are described by the one used here (e.g. torsional stiffness, translational stiffness, damping, moment of inertia etc.).

Displacements are measured in the contact wire at places between support poles 4 and 5, see figure 4.5. Vertical and angular motion are measured for

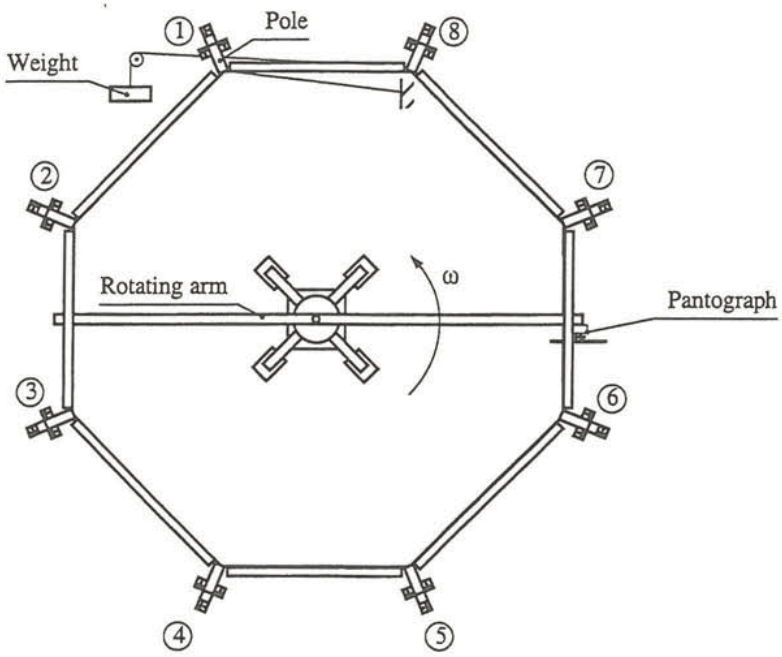

Figure 4.5: Drugge's laboratory model setup (Drugge, 2000).

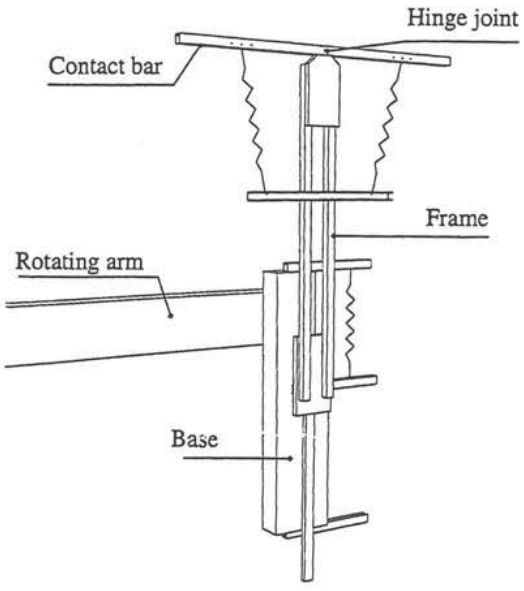

Figure 4.6: Drugge's pantograph model (Drugge, 2000).

the pantograph, and while the pantograph does not need power from the catenary to run there is a current running through that is measured and indicates if there is contact loss.

The noteworthy results from the study are that the lab model does describe the dynamic characteristics of the catenary–pantograph system. Spring distribution yields a stiffness variation in the system that is accurate, the stiffness at the support poles is $2,5$ times the stiffness in the middle of the span. Wave propagation velocities in the contact wire are between $8,1m/s$ and $10,3m/s$ for the different experimental setups proposed, velocities that are obtainable within the restrictions of a laboratory setup. Movement of the different system's parts increases and becomes more chaotic as the velocity of the pantograph reaches the wave propagation velocity.

All in all the modelling is successful, the model is simple and yet exhibits some important traits of the catenary–pantograph system. It is worth noting that some of these effects may be an effect from the laboratory model itself and are not reflective of real life situation.

4.1.4 Hybrid–in–the–loop (HIL)

Hybrid laboratory studies (HIL) are studies where there is a physical model of the pantograph connected to a mathematical model of the catenary. Several researchers have used this method (Bruni et al., 2012; Facchinetti and Bruni, 2012; Facchinetti and Mauri, 2009; Zhang et al., 2002). This is a clever method since no scaling is necessary, simple pantograph equipment can be used, models exhibit characteristic behaviours of the system and the model does not take up a lot of space (see figure 4.7). The biggest problem is obtaining and installing the equipment necessary to represent the interaction between the pantograph and catenary. If that equipment can be obtained it is worth it because so much different testing can be done, e.g. different catenary solutions can be implemented with a keystroke or adding/reducing the amount droppers. There are obviously many options and according to the studies mentioned this method has proven to be successful. Especially interesting is the results from (Facchinetti and Mauri, 2009) where they state that friction effects at contact point between pantograph and catenary along with aerodynamic effects are negligible for model studying of the system, this is confirmed by full–scale measurements. The finding erases concerns,

Figure 4.7: Hybrid–in–the–loop test stand (Bruni et al., 2012).

brought up by (Farr et al., 1961; Manabe, 1989), where they claimed these effects to be negative to their models.

4.1.5 Suggested model

What can be taken from the experience gained in these previous works are the following. Scaling the model too much down will yield distorted results like in (Farr et al., 1961). If the aim is to build a accurate model than it is best to use realistic scaling values and rather solve the problem of reaching high speeds in the model and finding a large enough space to store the model. For a simple model, were the numerical results do not need to be accurate, maybe it is better to come up with a clever solution like the one in (Drugge, 2000). Although that model had parameters similar in size to the model in (Farr et al., 1961) its setup was different which allowed for more realistic results.

It is the suggestion of the author that if a model were to be built it would use similar scaling as in (Manabe, 1989). Development of measuring equipment alone will make it worth it to build a model similar to that one. Equipment measures most of the same things as back then, but with a greater sampling rate which can be important to the system. The biggest problems will be, as mentioned before, finding a large enough storage space and having equipment that reaches high speeds. Large storage spaces are abundant and should not be hard to find in Trondheim or somewhere outside of the city. The speed range of interest for Norwegian rails is much lower than Manabe dealt with, although the same scaling factor were to be used it would scale down a smaller value. There are other things than those mentioned by Manabe that would be interesting to examine if a model existed. An area that has not been examined thoroughly is damping in the system, a scaled down laboratory model could give insight into the dissipative workings of the system. Building a track that ran in a curve would be especially interesting, since it has not been done with realistically scaled models. Other improvements of could be to build spans with different catenary system types and instead of using a copper plate it would be good to use the actual cross section shape. The model study should focus on the catenary, instead of a scaled down pantograph a simple equipment exerting constant force upwards could be used or the pantograph model used by (Drugge, 2000).

The numerical model developed in section 3 is intended to work also for scaled down models. To test that it will be implemented on the reference system scaled down by the factors used by Manabe. The scaling laws are presented in the next section and system parameters in terms of scaling factors are presented along with the scaled down values of the reference system.

4.2 Scaled model

Previous work of has been introduced and the model from (Manabe, 1989) was judged to be most feasible. This section will cover the scaling considerations needed if a scaled model is to be built. They are then used on the reference system to obtain a scaled system parameters, which will be implemented in the numerical model developed for this thesis. One of the objectives of the numerical model is to be able to simulate scaled down models, and in this way the model is being checked if it works in that way..

4.2.1 Scaling laws

Scaling down a structural system can be tricky. The scaled model should be as small as possible without losing dynamic characteristics of the full–scale system or so small that measuring displacements and forces becomes difficult. It is important to know what quantities need to be scaled down, they are obtained by realizing the forces affecting the system. These forces include the gravity force on system mass, forces from the pantograph, tension in the wires and forces derived from wind conditions (Farr et al., 1961).

The three basic properties of the system, from which all other values that need to be scaled can be derived from, are length $[L]$, mass $[M]$, and time $[t]$. Let the scaling factors for these values be λ for length, μ for mass and τ for time. The scaling laws for the catenary–pantograph system are presented in (Farr et al., 1961) and improved upon in (Manabe, 1989), the latter is derived here.

In order to make the model manufacturing easier, it is clever to introduce two different scaling factor for horizontal and vertical length (λ_h and λ_v). There are four scaling factors that have to be considered, by a little manipulation these can be reduced to three. The scaled model is operated in the

same gravitational field as the full–scale one, so acceleration should be scaled to unity:

$$\frac{\lambda_v}{\tau^2} = 1 \tag{4.1}$$

introducing a scaling factor for velocity:

$$\frac{\lambda_h}{\tau} = \alpha_s \tag{4.2}$$

Now there are only three scaling factors that have to carefully chosen, λ_h, μ and α_s. As stated above, other necessary system parameters can be obtained from these factors. For example, Young's modulus:

$$E = \frac{[m][L]}{[t]^2[L]^2} = \frac{[m]}{[t]^2[L]} = \frac{\mu\alpha_s^2}{\lambda_h^3} \tag{4.3}$$

it is customary to represent fundamental variables, when studying lab models and calculating units, by [] (e.g. length-[L], mass-[m] and time [t]) as can be seen from the equation above.

4.3 Scaled model results

The scaling factors used by Manabe (1989) will be used here and they are:

$$\lambda_h = 1 \quad \mu = 2 \quad \alpha_s = 0,5 \tag{4.4}$$

Table 4.1 lists up most of the system parameters expressed by the scaling factors, their reference system values and corresponding scaled down values. The mass, stiffness and damping scaling values for the pantograph are also applicable to the droppers, registration arms and support brackets. Contact stiffness is also scaled in the same way as pantograph stiffness but the critical damping ratios remain unchanged, the reason for that is that they are ratios. Damping in the wires will scale down due to other factors that it is dependent on: mass, stiffness and eigenfrequencies (see section 3.1.3). Some system parameters are scaled to unity and are therefore not listed in the table, these are: horizontal displacements/lengths (L), damping (c), cross sectional area (A) and moment of inertia (I). Since horizontal length is scaled to unity, the span length and arrangement of droppers will not be changed. Same

rules apply for the time step needed for the integration method, the system must be modelled every $0,2m$ and is therefore dependent on train velocity. Velocity is scaled by $0,5$, so given a reference case velocity of $100kmk/h$ the scaled down velocity must be $50km/h$. That means that the time step must be below:

$$\Delta t = \frac{0,2}{50e3/3600} = 0,0144 \tag{4.5}$$

Obviously the previous known optimal time step of $0,001s$ will be sufficient. Applying all of these scaling values to the reference system, the results can be obtained. For the purposes of showing some of the results there are two other system parameters that need to be derived in terms of scaling factors, frequency (f) and elasticity (e).

$$f = \frac{1}{[t]} = \frac{\alpha_s}{\lambda_h} = 0,5 \tag{4.6}$$

$$e = \frac{[L]_v}{[m]\frac{[L]_v}{[t]^2}} = \frac{\lambda_h^2}{\mu\alpha_s^2} = 2 \tag{4.7}$$

where the subscript v stands for vertical.

Figures 4.8–4.11 show the results from the scaled model. Comparing them to their full–scale identical figures (3.7,3.6,3.10 and 3.14) it is easily seen if the scaled down values are implemented in the numerical model it will yield results with similar scaling. Some of the key results parameters were obtained from the scaled model and compared with results from the reference case, these can be seen in table 4.2. The columns in table 4.2 represent from the first; parameter, parameter value in the reference system, scaling factor, what the scaled model results should be, what the scaled result is and finally error between them. The largest error between scaled and full–scale results is $7,81\%$ for the standard deviation of the contact force, but all others are within 2%. Errors within 2% are acceptable and it shows that the numerical model can be used on scaled models. Standard deviation is a difficult parameter to control, but since the scaled model results are smaller than what was expected, and it is preferable that standard deviation is small, it is also acceptable.

Table 4.1: Scaling expressions and some of the scaled down system parameters

	System parameter						Kinematic quantities		
	Catenary			Pantograph			Vertical		Horizontal
	$\rho[kg/m]$	$P[kN]$	$E[N/m^2]$	$m_i[kg]$	$k_i[N/m]$	$F_1[N]$	Displ.	Force	Force
Expr.	μ/λ_h	$\alpha_s^2\mu/\lambda_h$	$\alpha_s^2\mu/\lambda_h$	μ	$\alpha_s^2\mu/\lambda_h$	μ	λ_h^2/α_s^2	μ	$\alpha_s^2\mu/\lambda_h$
Values	2	0,5	0,5	2	0,5	2	4	2	0,5
Ref. model	0,94/0,46	10/5	124e9/113e9	4,6/16,5	3100/-	55 ± 17	-	-	-
Sc. model	1,88/0,92	5/2.5	62e9/56,5e9	9,2/33	1550/-	110 ± 34	-	-	-

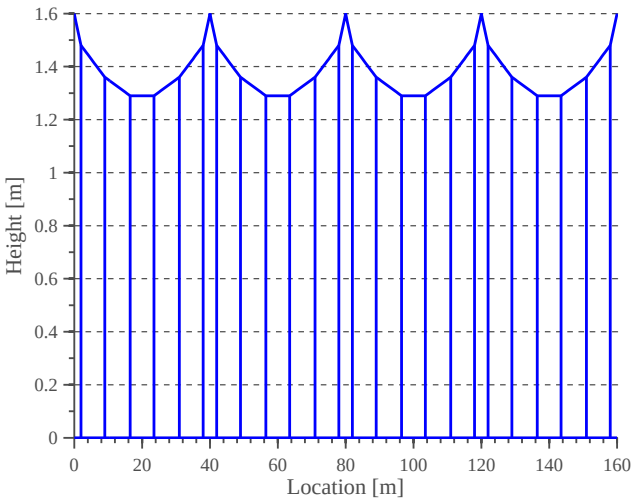

(a) The model

(b) Nr. 1, $f_1 = 0,53Hz$

(c) Nr. 2, $f_2 = 0,54Hz$

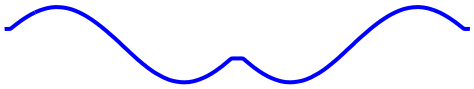

(d) Nr. 3, $f_3 = 0,57Hz$

Figure 4.8: Eigenmodes of the contact wire for scaled model. The number and frequency (f_i) of each mode, i, is given below each figure.

Table 4.2: Comparison between running the numerical model with full–scale parameters and scaled down ones.

Parameter	Ref. System	Scaling	Scal. System	Scal. Model	Error [%]
F_m [N]	65,00	2,00	130,00	132,72	2,05
σ_m [N]	23,80	2,00	47,60	44,15	-7,81
$d_{stat,max}$ [m]	0,08	4,00	0,32	0,32	0,00
e_{max} [mm/N]	0,77	2,00	1,54	1,55	0,65
$e - unif$ [%]	55,50	1,00	55,50	55,50	0,00
$c_{p,cw}$ [km/h]	373,30	0,50	186,65	190,63	2,09
f_1 [Hz]	1,06	0,50	0,53	0,53	0,00
f_2 [Hz]	1,08	0,50	0,54	0,54	0,00
f_3 [Hz]	1,14	0,50	0,57	0,57	0,00
f_4 [Hz]	1,21	0,50	0,61	0,61	0,82
f_5 [Hz]	2,09	0,50	1,05	1,05	0,48
f_10 [Hz]	3,13	0,50	1,57	1,57	0,32
f_20 [Hz]	5,74	0,50	2,87	2,87	0,00
f_100 [Hz]	17,83	0,50	8,92	8,91	-0,06

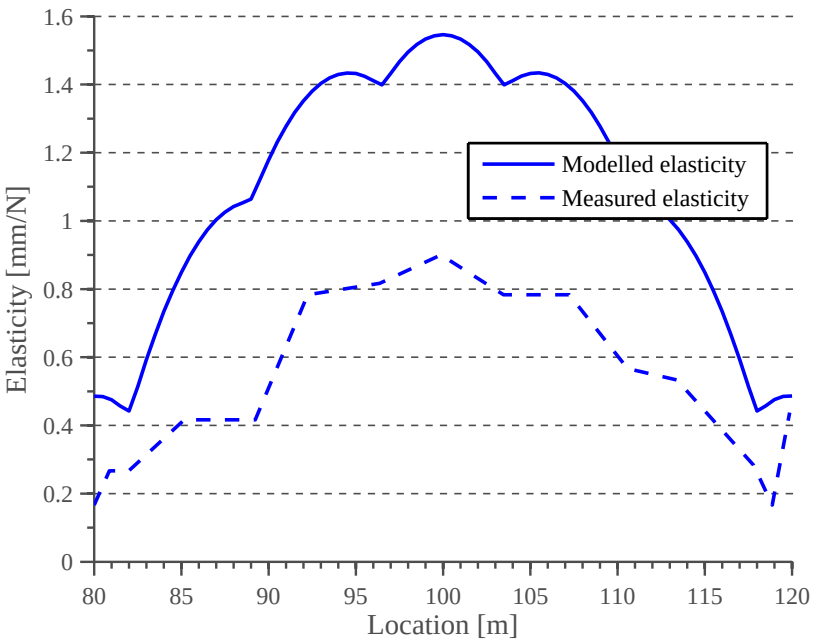

Figure 4.9: Elasticity curve of the scaled model.

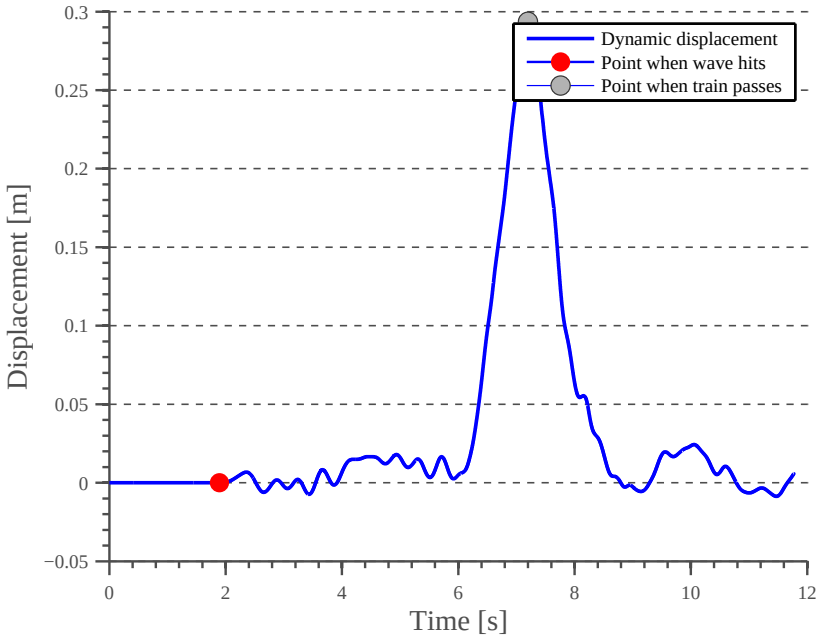

Figure 4.10: Vertical displacement of the midpoint in span 3.

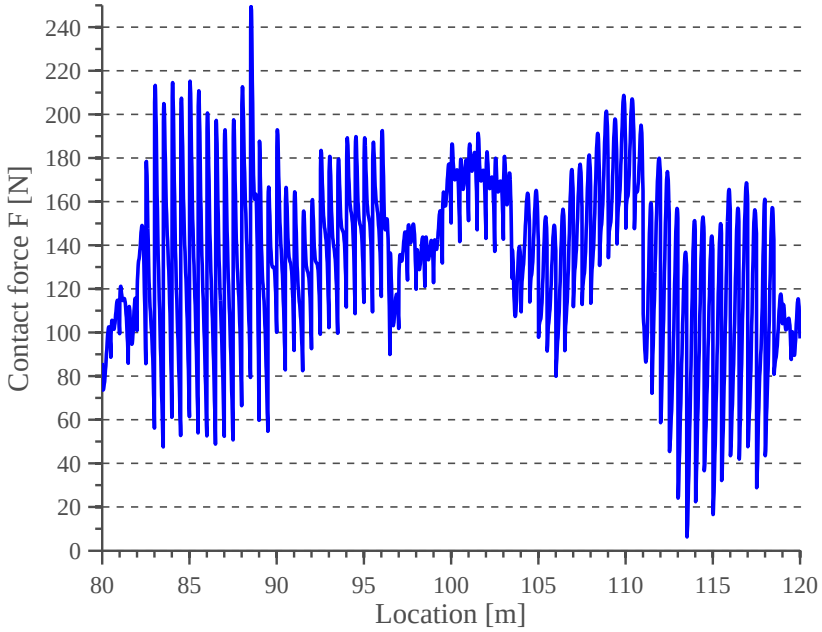

Figure 4.11: Contact force for span 3 of the scaled model.

5 Conclusions

Dynamic behaviour of the catenary–pantograph system has been examined, by a literature survey and by modelling it numerically. More focus was put into examining the catenary system instead of the pantograph. The reason for that is that important parameters and behaviour of the pantograph are already well known and documented, a mathematical model of it was implemented in the numerical model based on this knowledge. Suggested articles that present findings on pantograph behaviour are (Pombo and Ambrosio, 2012; Lee et al., 2012; Pombo et al., 2009). Properties found to be critical for the dynamic behaviour of the catenary are wave propagation velocity, speed of the train, limiting speed due to reflection in the system and the critical damping ratio.

Parameters of the system controlling the first two properties are tension in the wires and their mass per unit length. Wave propagation velocity proved to be a critical factor to the system, it is controlled by mass per unit length and tension force in the wire. Behaviour of the system becomes chaotic as the train's speed nears this velocity limit and the parameters controlling it should be set so that the limit is high. The further the train's velocity is from the wave propagation velocity, the better the system behaves. Same effects were observed when the velocity of the train was around the limiting speed due to reflection in the system.

Damping is an area of this system that has not been researched enough and has room for improvement. Large part of the literature for the system was examined and proportional damping models seem to be the only ones used to represent this phenomena in the system. Motion at low frequencies dominates the system and it was interesting to see the change in the system as the damping model obtained from (Wilson, EL., Inc) that has the option for different damping at different frequencies. That being said, effects from damping are not important to systems with a single pantograph.

Work that has been done previously on scaled laboratory models for the system was reviewed. Valuable insight was obtained to what could be done and what could not be done. Building scaled models that are scaled down considerably will give distorted results and it is recommended that if a laboratory model were to be built, that it would be done in large scale. The biggest factor for building the actual model is the chance to study damping

or the effects of curvature in the system or the effects curvature. The numerical model proved to be a good tool for checking scaled down models as expected.

5.1 Future work

The numerical model developed here proved to be descriptive of the system while also being simple and having low run time. If improvements are to be made for the model in the future it is important that these characteristics should not be lost. The ideas for future work improvements on the model are presented given that criteria. If these improvements yield increased complexity in the model and a long calculation time it would perhaps be better to turn to commercial finite element software such as ABAQUS or ANSYS. Improvements that could be beneficial to the numerical model are:

- Changing the model from 2D to 3D would allow for effects such as curvature and zig–zag to be included. These effects are important to the system's behaviour and should be included, but it would be risky since the calculation time could increase.

- Adding nonlinear effects of dropper slackening. Many studies have shown the importance of this property to the systems behaviour and adding it should be included (Cho, 2008). That would mean that for every time step the geometry of the droppers need to be checked and if they are in compression the global stiffness and damping matrices need to be updated. This operation could be time consuming, but since the matrices in whole are not being changed, this could be a possibility for improvement.

- Changing the program code so that spans of different lengths and with different dropper arrangement could be modelled together. In reality different span arrangements are often built side by side and full–scale measurement data does exist for these lines that could be used for validating the model. Validation is possible for the model as it is today but this could give more accuracy in the results. This improvement would not result in increased calculation time.

- Implementing the option of having multiple pantographs. If damping is to be studied for the system, including multiple droppers is essential. Damping does not affect the system to a great degree when there is only one pantograph. Increase in calculation time should not be significant, and for simplicity the same mathematical model could be used for both pantographs.

- Different contact formulation methods should be tested. The one used in this thesis proved successful, but there are many formulations that have been implemented and it would be interesting to see if any of them gives better results.

- Making the computer code more user friendly, i.e. commercializing it. Setting up a simple graphical user interface could make the model more accessible. Checking dynamic performances of a system with a model that requires only minutes in calculation time and can easily change system parameters is good to have.

Building a scaled laboratory model is obviously suggested as well for future work. As mentioned before, damping in the system is underdeveloped and future work should include a study of damping. Work on damping was initiated during the course of this study but could not be completed due to bad measurement results. Two different PhD theses were studied for this purpose where different methods for modelling damping in a structural system are proposed (Adhikari, 2000; Pilkey, 1998). Both methods require measurements of eigenmodes and frequencies, which were almost retrieved for the reference system with a model hammer, but problems arose with the measurements and ultimately could not be retrieved. For future work, this measurement should be repeated and the results used to model damping in the system. The numerical model developed here can be used to try out different formulations of damping.

6 References

References

(2013). Website: http://www.schunk.se. Schunk Nordiska website.

Adhikari, S. (2000). *Damping models for structural vibration*. PhD thesis, Cambridge University.

Aftenbladet (2011). De meste populære flyrutene. Website: http://reise.aftenbladet.no/reise/De-mest-populare-flyrutene-35576.html. Retrieved from web: 02.06.2013.

Alberto, A., Benet, J., Arias, E., Cebrian, D., Rojo, T., and Cuartero, F. (2008). A high performance tool for the simulation of the dynamic pantograph-catenary interaction. *MATHEMATICS AND COMPUTERS IN SIMULATION*, 79(3):652–667.

Arias, E., Alberto, A., Montesinos, J., Rojo, T., Cuartero, F., and Benet, J. (2009). A mathematical model of the static pantograph/catenary interaction. *INTERNATIONAL JOURNAL OF COMPUTER MATHEMATICS*, 86(2):333–340.

Arnold, M. and Simeon, B. (2000). Pantograph and catenary dynamics: A benchmark problem and its numerical solution. *APPLIED NUMERICAL MATHEMATICS*, 34(4):345–362.

Benet, J., Alberto, A., Arias, E., and Rojo, T. (2007). A mathematical model of the pantograph-catenary dynamic interaction with several contact wires. *INTERNATIONAL JOURNAL OF APPLIED MATHEMATICS*, 37(2).

Brown, D. (2010). By the numbers, flying is a lot safer than driving or taking the train. Website: http://www.airlinereporter.com/2010/09/flying-is-safe-and-i-am-going-to-prove-it/. Retrieved from web: 7.12.2012.

Bruni, S., Bucca, G., Collina, A., and Facchinetti, A. (2012). Numerical and hardware-in-the-loop tools for the design of very high speed pantograph-catenary systems. *JOURNAL OF COMPUTATIONAL AND NONLINEAR DYNAMICS*, 7(4).

Cho, Y. (2008). Numerical simulation of the dynamic responses of railway overhead contact lines to a moving pantograph, considering a nonlinear dropper. *JOURNAL OF SOUND AND VIBRATION*, 315:433–454.

Cho, Y., Lee, J., Park, S., and Lee, E. (2006). Robust measurement of damping ratios of a railway contact wire using wavelet transforms. In Lee, SS. and Lee, JH. and Park, IK. and Song, SJ. and Choi, MY., editor, *ADVANCED NONDESTRUCTUVE EVALUATION I, PTS 1 AND 2, PROCEEDINGS*, volume 321-323 of *KEY ENGINEERING MATERIALS*, pages 1629–1635.

Cho, Y., Lee, K., Park, Y., Kang, B., and Kim, K. (2010). Influence of contact wire pre-sag on the dynamics of pantograph-railway catenary. *INTERNATIONAL JOURNAL OF MECHANICAL SCIENCES*, 52(11, SI):1471–1490.

Chopra, A. (2007). *Dynamics of structures: theory and applications to earthquake engineering*. Pearson Prentice Hall, 3rd edition.

Clarke, F. (2013). *Functional Analysis, Calculus of Variations and Optimal Control*. Springer London, Limited.

Cook, R.D.and Malkus, D., Plesha, M., and Witt, R. (2001). *Concepts and applications of finite element analysis*. Wiley, 4th edition.

Design tables (2013). *Design tables obtained from Jernbaneverket*. Jernbaneverket.

Diana, G., Bruni, S., Collina, A., Fossati, F., and Resta, F. (1998). High speed railways: pantograph and overhead lines modelling and simulation. In Mellitt, B. and Hill, RJ. and Allan, J. and Sciutto, G. and Brebbia, CA., editor, *COMPUTERS IN RAILWAYS VI*, volume 2 of *ADVANCES IN TRANSPORT*, pages 847–856. Wessex Inst Technol.

Drugge, L. (2000). *Modelling and Simulation of Pantograph–Catenary Dynamics*. PhD thesis, Luleå tekniska universitet, Luleå, Sweden.

EN 50119:2001 (2001). *Railway aplications–fixed installations–electric traction overhead vontact lines*. European Committee for Electrotechnical Standardization.

EN 50318:2002 (2002). *Railway applications–current collection systems–current collection systems validation of simulation of the dynamic interaction between pantograph and overhead contact line*. European Committee for Electrotechnical Standardization.

Facchinetti, A. and Bruni, S. (2012). Hardware-in-the-loop hybrid simulation of pantograph-catenary interaction. *JOURNAL OF SOUND AND VIBRATION*, 331(12):2783–2797.

Facchinetti, A. and Mauri, M. (2009). Hardware-in-the-loop overhead line emulator for active pantograph testing. *IEEE TRANSACTIONS ON INDUSTRIAL ELECTRONICS*, 56(10):4071–4078.

Farr, D., Hall, H., and Williams, A. (1961). A Dynamic Model for Studying the Behaviour of the Overhead Equipment Used in Electric Railway Traction. *THE INSTITUTION OF ELECTRICAL ENGINEERS*, Vol. 108(Paper No. 3530 U):pp. 421–434.

Felippa, C. (2004). *Introduction to finite element methods*, chapter 31. University of Colorado.

Hallgrimsson, A. (2012). Modelling dynamic responses of overhead contact lines. Project report.

Harell, P., Drugge, L., and Reijm, M. (2005). Study of critical sections in catenary systems during multiple pantograph operation. *PROCEEDINGS OF THE INSTITUTION OF MECHANICAL ENGINEERS PART F-JOURNAL OF RAIL AND RAPID TRANSIT*, 219(4):203–211.

JBV and Railconsult AS (2012). Konklusjoner og oppsummering av arbeidet i Fase 3, Del 1.

JD 542 (2004). *Regler for vedlikehold–Kontaktledning og krav til krefter mellom strømavtaker og kontakttråd (https://trv.jbv.no/wiki/Kontaktledning)*. Norwegian national rail administration.

Jensen, C. and True, H. (1998"). Dynamics of an electrical overhead line system and moving pantographs. *VEHICLE SYSTEM DYNAMICS*, 29(1):104–113.

Jung, S., Kim, Y., Paik, J., and Park, T. (2012). Estimation of dynamic contact force between a pantograph and catenary using the finite element method. *JOURNAL OF COMPUTATIONAL AND NONLINEAR DYNAMICS*, 7(4).

Kia, S., Bartolini, F., Mpanda-Mabwe, A., and Ceschi, R. (2010). Pantograph-catenary interaction model comparison. In *IECON 2010 - 36TH ANNUAL CONFERENCE ON IEEE INDUSTRIAL ELECTRONICS SOCIETY*, IEEE Industrial Electronics Society.

Kiessling, F., Puschmann, R., Schmieder, A., and Schneider, E. (2012). *Contact lines for electric railways: planning, design, implementation, maintenance*. Publicis Publishing, 2nd edition.

Kim, J. (2007). An experimental study of the dynamic characteristics of the catenary-pantograph interface in high speed trains. *JOURNAL OF MECHANICAL SCIENCE AND TECHNOLOGY*, 21(12):2108–2116.

Kim, J., Chae, H., Park, B., Lee, S., Han, S., and Jang, J. (2007). State sensitivity analysis of the pantograph system for a high-speed rail vehicle considering span length and static uplift force. *JOURNAL OF SOUND AND VIBRATION*, 303(3-5):405–427.

Koerner, B. (2004). Which are safer, trains or planes? Website: http://www.slate.com/articles/news_and_politics/explainer/2004/04/–which_are_safer_trains_or_planes.html. Retrieved from web: 7.12.2012.

Kreyszig, E. (2010). *Advanced Engineering Mathematics*. John Wiley & Sons.

Langen, I. and Sigbjörnsson, R. (1979). *Dynamisk analyse av konstruksjoner: Dynamic analysis of structures*. Tapir.

Larsson, T. and Drugge, L. (1998). Dynamic behaviour of pantographs due to different wear situations. In Mellitt, B. and Hill, RJ. and Allan, J. and Sciutto, G. and Brebbia, CA., editor, *COMPUTERS IN RAILWAYS VI*, volume 2 of *ADVANCES IN TRANSPORT*, pages 869–880. Wessex Inst Technol.

Lavprisekspressen (2013). Web page of bus company Lavprisekspressen. Website: http://www.lavprisekspressen.no. Retrieved from web: 03.05.2013.

Lee, J., Kim, Y., Paik, J., and Park, T. (2012). Performance evaluation and design optimization using differential evolutionary algorithm of the pantograph for the high-speed train. *JOURNAL OF MECHANICAL SCIENCE AND TECHNOLOGY*, 26(10):3253–3260.

Lopez-Garcia, O., Carnicero, A., and Marono, J. (2007). Influence of stiffness and contact modelling on catenary-pantograph system dynamics. *JOURNAL OF SOUND AND VIBRATION*, 299(4-5):806–821.

Lopez-Garcia, O., Carnicero, A., and Torres, V. (2006). Computation of the initial equilibrium of railway overheads based on the catenary equation. *ENGINEERING STRUCTURES*, 28(10):1387–1394.

Lopez-Garcia, O., Carnicero, A., Torres, V., and Jimenez-Octavio, J. (2008). The influence of cable slackening on the stiffness computation of railway overheads. *INTERNATIONAL JOURNAL OF MECHANICAL SCIENCES*, 50(7):1213–1223.

Manabe, K. (1989). High–Speed Contact Performance of a Catenary–Pantograph System (An Experimental Study Using a Dynamically Scaled Model). *JSME INTERNATIONAL JOURNAL SERIES III*, Vol. 32(No. 2):pp. 200–205.

NSB (2013). Web page of Norwegian State Railways, NSB. Website: http://www.nsb.no. Retrieved from web: 03.05.2013.

Nåvik, P. (2013). Cross section properties obtained via private communication with Petter through email. Nåvik email.

Park, T., Han, C., and Jang, J. (2003). Dynamic sensitivity analysis for the pantograph of a high-speed rail vehicle. *JOURNAL OF SOUND AND VIBRATION*, 266(2):235–260.

Pilkey, D. F. (1998). *Computation of a damping matrix for finite element model updating*. PhD thesis, Virginia Polytechnic Institute and State University.

Poetsch, G., Evans, J., Meisinger, R., Kortum, W., Baldauf, W., Veitl, A., and Wallaschek, J. (1997). Pantograph/catenary dynamics and control. *VEHICLE SYSTEM DYNAMICS*, 28(2-3):159–195.

Pombo, J. and Ambrosio, J. (2012). Influence of pantograph suspension characteristics on the contact quality with the catenary for high speed trains. *COMPUTERS & STRUCTURES*, 110:32–42.

Pombo, J., Ambrosio, J., Pereira, M., Rauter, F., Collina, A., and Facchinetti, A. (2009). Influence of the aerodynamic forces on the pantograph-catenary system for high-speed trains. *VEHICLE SYSTEM DYNAMICS*, 47(11):1327–1347.

Quek, S. and Liu, G. (2003). *Finite Element Method: A Practical Course*. Elsevier Science.

Rönnquist, A. (2012). Lecture notes from the course tkt4201 konstr dynamikk at ntnu.

SAS (2013). Web page of airliner SAS. Website: http://www.sas.no. Retrieved from web: 03.05.2013.

Schaub, M. and Simeon, B. (2001). Pantograph-catenary dynamics: An analysis of models and simulation techniques. *MATHEMATICAL AND COMPUTER MODELLING OF DYNAMICAL SYSTEMS*, 7(2):225–238.

Seo, J., Jung, I., Park, T., and Chai, J. (2005). Dynamic analysis of a multibody system including a very flexible beam element. *JSME INTERNATIONAL JOURNAL SERIES C-MECHANICAL SYSTEMS MACHINE ELEMENTS AND MANUFACTURING*, 48(2):224–233.

Seo, J., Kim, S., Jung, I., Park, T., Mok, J., Kim, Y., and Chai, J. (2006). Dynamic analysis of a pantograph-catenary system using absolute nodal coordinates. *VEHICLE SYSTEM DYNAMICS*, 44(8):615–630.

Sølvberg, J. (2008). Matematisk modellering av strømavtager og kontaktledning. Master's thesis, Universitet i Oslo.

Sture, P., Backer, A., Jahre, R., Telle, O., Løken, O., and Nørbech, S. (1982). *Ombygging av kontaktledningsanlegg tilpasset fremtidig belastningsforhold og kjørehastigheter*. Norges Statsbaner AS.

Vestlandsforskning (2013). Environmental information for a variety of trips within Norway. Website: http://vfp1.vestforsk.no/nsb/person1.asp. Retrieved from web: 03.05.2013.

Willets, T., Allen, C., and Edwards, D. (1966). Dynamic–Model Studies of Overhead Equipment for Electric Railway Traction. Part 2. Sagged Simple Catenary Equipment. volume 113. Proc. IEE. pp. 697–703.

Willets, T. and Edwards, D. (1966). Dynamic–Model Studies of Overhead Equipment for Electric Railway Traction. Part 1. Sagged Simple Catenary Equipment. volume 113. Proc. IEE. pp. 690–696".

Willets, T. and Suddards, A. (1970). Dynamic–Model Studies of Overhead Equipment for Electric Railway Traction. Sagged Stitched– and Compound–Catenary Equipment and Further Tests on Sagged Simple–Catenary Equipment. volume 117. Proc. IEE. pp. 1815–1828.

Wilson, E. and Penzien, J. (1972). Evaluation of orthogonal damping matrices. *INTERNATIONAL JOURNAL FOR NUMERICAL METHODS IN ENGINEERING*, 4(1):5–10.

Wilson, EL. (1997, Publisher= Computers and Structures Inc.,). *Three dimensional dynamic analysis of structures: with emphasis on earthquake engineering*.

Wu, T. and Brennan, M. (1998). Basic analytical study of pantograph-catenary system dynamics. *VEHICLE SYSTEM DYNAMICS*, 30(6):443–456.

Wu, T. and Brennan, M. (1999). Dynamic stiffness of a railway overhead wire system and its effect on pantograph-catenary system dynamics. *JOURNAL OF SOUND AND VIBRATION*, 219(3):483–502.

Zhang, W., Liu, Y., and Mei, G. (2006). Evaluation of the coupled dynamical response of a pantograph-catenary system: contact force and stresses. *VEHICLE SYSTEM DYNAMICS*, 44(8):645–658.

Zhang, W., Mei, G., Wu, X., and Shen, Z. (2002). Hybrid simulation of dynamics for the pantograph-catenary system. *VEHICLE SYSTEM DYNAMICS*, 38(6):393–414.

Zhou, N. and Zhang, W. (2011). Investigation on dynamic performance and parameter optimization design of pantograph and catenary system. *FINITE ELEMENTS IN ANALYSIS AND DESIGN*, 47(3):288–295.

A Contact wire cross section

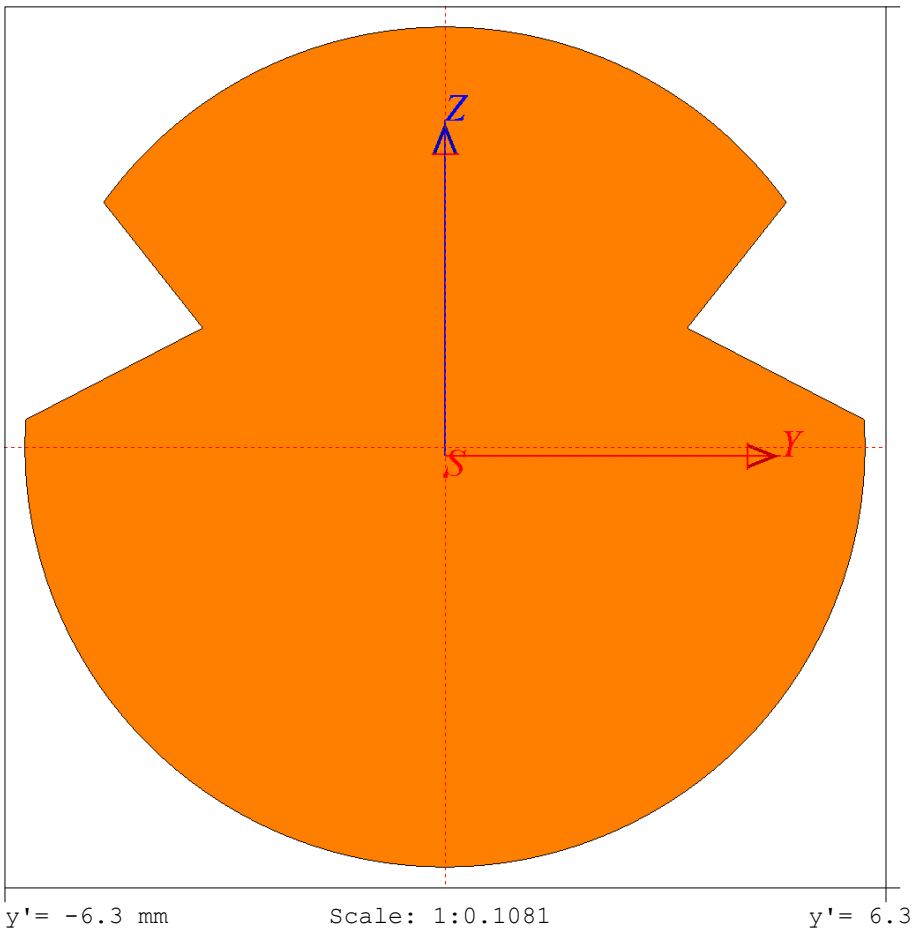

z'= 6.3 mm

Base material:

Name: Contactwire
E = 1.240e+005 N/mm²
G = 4.470e+004 N/mm²
ν = 0.34
ρ = 8930.00 kg/m³

C = center of gravity
S = shear center

Angle (y',y) =-0.00 deg

y'_c = 0.0 mm
z'_c = -0.1 mm
y'_s = 0.0 mm
z'_s = -0.4 mm
y_s = 0.0 mm
z_s = -0.3 mm

True area
1.0567e+002 mm²

Weight per unit length
0.01 kN/m

Mass per unit length
0.94 kg/m

z'= -6.3 mm

y'= -6.3 mm Scale: 1:0.1081 y'= 6.3 mm

PARAMETER*	VALUE	
A	1.0567e+002	mm²
I_y	9.8650e+002	mm⁴
I_z	8.3921e+002	mm⁴
I_t	1.5115e+003	mm⁴
S_y	1.6089e+002	mm³
S_z	1.3987e+002	mm³
r_y	3.0554e+000	mm
r_z	2.8181e+000	mm
κ_y	1.13699	
κ_z	1.26461	
$I_{y'}$ (y' at C)	9.8650e+002	mm⁴
$I_{z'}$ (z' at C)	8.3921e+002	mm⁴
$I_{y'z'}$ (at C)	0.0000e+000	mm⁴

STIFFNESS	VALUE	
EA	1.3104e+004	kN
EI_y	1.2233e-001	kN·m²
EI_z	1.0406e-001	kN·m²
GI_t	6.7562e-002	kN·m²
GA_{sy}	4.1545e+003	kN
GA_{sz}	3.7353e+003	kN
GA	4.7237e+003	kN
$EI_{y'}$	1.2233e-001	kN·m²
$EI_{z'}$	1.0406e-001	kN·m²
$EI_{y'z'}$	5.7744e-018	kN·m²

* Apply to an equivalent cross section of base material

B Application of calculus of variations

From section 3.1.1 there is a derivation of the Hamilton principle where principles from calculation of variations are used. These derivations are shown here. The main principle used is that the variation and integration operators can be interchangeable. Some of the derivations are from (Quek and Liu, 2003) and the principles of variation calculations are taken from (Clarke, 2013).

In order to get from equation 3.23 to 3.24 the following derivations are made, starting with the first term:

$$\begin{aligned}
\underline{\delta\left(\frac{1}{2}\mathbf{d_e^T k_e d_e}\right)} &= \delta\left(\frac{1}{2}\{d_1 \quad d_2\}\begin{bmatrix}k_{11} & k_{12}\\ k_{21} & k_{22}\end{bmatrix}\begin{Bmatrix}d_1\\ d_2\end{Bmatrix}\right)\\
&= \frac{1}{2}\delta\left(\{d_1k_{11}+d_2k_{12}\ \ d_1k_{12}+d_2k_{22}\}\begin{Bmatrix}d_1\\ d_2\end{Bmatrix}\right)\\
&= \frac{1}{2}\delta(d_1^2k_{11}+2d_1d_2k_{12}+d_2^2k_{22})\\
&= \frac{1}{2}\left[\frac{\partial(d_1^2k_{11}+2d_1d_2k_{12}+d_2^2k_{22})}{\partial d_1}\delta d_1+\frac{\partial(d_1^2k_{11}+2d_1d_2k_{12}+d_2^2k_{22})}{\partial d_2}\delta d_2\right]\\
&= (d_1k_{11}+d_2k_{12})\delta d_1+(d_1k_{12}+d_2k_{22})\delta d_2\\
&= \{\delta d_1 \quad \delta d_2\}\begin{Bmatrix}d_1k_{11}+d_2k_{12}\\ d_1k_{12}+d_2k_{22}\end{Bmatrix}=\{\delta d_1 \quad \delta d_2\}\begin{bmatrix}k_{11} & k_{12}\\ k_{21} & k_{22}\end{bmatrix}\begin{Bmatrix}d_1\\ d_2\end{Bmatrix}\\
&= \underline{\delta\mathbf{d_e^T k_e d_e}}
\end{aligned} \tag{B.1}$$

where $k_{12}=k_{21}$. Applying similar derivations the rest of the terms in equation 3.23 become:

$$\delta\left(\frac{1}{2}\dot{\mathbf{d}}_\mathbf{e}^\mathbf{T}\mathbf{m_e}\dot{\mathbf{d}}_\mathbf{e}\right) = \delta\dot{\mathbf{d}}_\mathbf{e}^\mathbf{T}\mathbf{m_e}\dot{\mathbf{d}}_\mathbf{e} \tag{B.2}$$

$$\delta\left(\frac{1}{2}\mathbf{d_e^T c_e}\dot{\mathbf{d}}_\mathbf{e}\right) = \delta\mathbf{d_e^T c_e}\dot{\mathbf{d}}_\mathbf{e} \tag{B.3}$$

$$\delta(\mathbf{d_e^T f_e}) = \delta\mathbf{d_e^T f_e} \tag{B.4}$$

C Strain–displacement equations

The strain–displacement relations can be expressed as follows, the second order nonlinear terms added for the geometric stiffness are shown in parenthesis:

$$\begin{aligned}
\varepsilon_x &= \frac{\partial u}{\partial x} + \left(\frac{1}{2}\overline{\mathbf{u}}_{,x}^T\overline{\mathbf{u}}_{,x}\right) \\
\varepsilon_y &= \frac{\partial v}{\partial y} + \left(\frac{1}{2}\overline{\mathbf{u}}_{,y}^T\overline{\mathbf{u}}_{,y}\right) \\
\varepsilon_z &= \frac{\partial w}{\partial z} + \left(\frac{1}{2}\overline{\mathbf{u}}_{,z}^T\overline{\mathbf{u}}_{,z}\right) \\
\gamma_{xy} &= \frac{\partial u}{\partial y} + \frac{\partial v}{\partial x} + \left(\frac{1}{2}\overline{\mathbf{u}}_{,x}^T\overline{\mathbf{u}}_{,y} + \frac{1}{2}\overline{\mathbf{u}}_{,y}^T\overline{\mathbf{u}}_{,x}\right) \\
\gamma_{xz} &= \frac{\partial u}{\partial z} + \frac{\partial w}{\partial x} + \left(\frac{1}{2}\overline{\mathbf{u}}_{,x}^T\overline{\mathbf{u}}_{,z} + \frac{1}{2}\overline{\mathbf{u}}_{,z}^T\overline{\mathbf{u}}_{,x}\right) \\
\gamma_{yz} &= \frac{\partial v}{\partial z} + \frac{\partial w}{\partial y} + \left(\frac{1}{2}\overline{\mathbf{u}}_{,y}^T\overline{\mathbf{u}}_{,z} + \frac{1}{2}\overline{\mathbf{u}}_{,z}^T\overline{\mathbf{u}}_{,y}\right)
\end{aligned} \tag{C.1}$$

where e.g. $\overline{\mathbf{u}}_{,x}^T = \begin{bmatrix} u_{,x} & v_{,x} & w_{,x} \end{bmatrix}$ and: u, v and w are displacements in x, y, z direction respectively. These relations are identical to the classical Green–Lagrange strain (Wilson, EL., Inc)

D Element matrices

The two node Euler–Bernoulli beam element with 2 DOF at each node has the following element matrices (Rönnquist, 2012):

$$m_e = \frac{\rho l_{el}}{420} \begin{pmatrix} 156 & 22l_{el} & 54 & -13l_{el} \\ 22l_{el} & 4l_{el}^2 & 13l_{el} & -3l_{el}^2 \\ 54 & 13l_{el} & 156 & -22l_{el} \\ -13l_{el} & -3l_{el}^2 & -22l_{el} & 4l_{el}^2 \end{pmatrix} \tag{D.1}$$

$$k_{em} = \frac{EI}{l_{el}^3} \begin{pmatrix} 12 & 6l_{el} & -12 & 6l_{el} \\ 6l_{el} & 4l_{el}^2 & -6l_{el} & 2l_{el}^2 \\ -12 & -6l_{el} & 12 & -6l_{el} \\ 6l_{el} & 2l_{el}^2 & -6l_{el} & 4l_{el}^2 \end{pmatrix} \tag{D.2}$$

$$k_{eg} = \frac{P}{30l_{el}} \begin{pmatrix} 36 & 3l_{el} & -36 & 3l_{el} \\ 3l_{el} & 4l_{el}^2 & -3l_{el} & -l_{el}^2 \\ -36 & -3l_{el} & 36 & -3l_{el} \\ 3l_{el} & -l_{el}^2 & -3l_{el} & 4l_{el}^2 \end{pmatrix} \tag{D.3}$$

where ρ is the mass density per unit length, l_{el} is the element length, E is Young's modulus of elasticity, I is the moment of inertia and P is the pretensioned axial force.

The two node Euler–Bernoulli beam element with 3 DOF at each node has the following element matrices (Quek and Liu, 2003):

$$m_e = \frac{\rho l_{el}}{420} \begin{pmatrix} 140 & 0 & 0 & 70 & 0 & 0 \\ 0 & 156 & 22l_{el} & 0 & 54 & -13l_{el} \\ 0 & 22l_{el} & 4l_{el}^2 & 0 & 13l_{el} & -3l_{el}^2 \\ 70 & 0 & 0 & 140 & 0 & 0 \\ 0 & 54 & 13l_{el} & 0 & 156 & -22l_{el} \\ 0 & -13l_{el} & -3l_{el}^2 & 0 & -22l_{el} & 4l_{el}^2 \end{pmatrix} \tag{D.4}$$

$$k_{em} = \frac{EI}{l_{el}^3} \begin{pmatrix} \frac{Al_{el}^2}{I} & 0 & 0 & -\frac{Al_{el}^2}{I} & 0 & 0 \\ 0 & 12 & 6l_{el} & 0 & -12 & 6l_{el} \\ 0 & 6l_{el} & 4l_{el}^2 & 0 & -6l_{el} & 2l_{el}^2 \\ -\frac{Al_{el}^2}{I} & 0 & 0 & \frac{Al_{el}^2}{I} & 0 & 0 \\ 0 & -12 & -6l_{el} & 0 & 12 & -6l_{el} \\ 0 & 6l_{el} & 2l_{el}^2 & 0 & -6l_{el} & 4l_{el}^2 \end{pmatrix} \tag{D.5}$$

$$k_{eg} = \frac{P}{30l_{el}} \begin{pmatrix} 0 & 0 & 0 & 0 & 0 & 0 \\ 0 & 36 & 3l_{el} & 0 & -36 & 3l_{el} \\ 0 & 3l_{el} & 4l_{el}^2 & 0 & -3l_{el} & -l_{el}^2 \\ 0 & 0 & 0 & 0 & 0 & 0 \\ 0 & -36 & -3l_{el} & 0 & 36 & -3l_{el} \\ 0 & 3l_{el} & -l_{el}^2 & 0 & -3l_{el} & 4l_{el}^2 \end{pmatrix} \tag{D.6}$$

where A is the elements cross section and all other variables are the same as above. Transformation matrix used for the element with 3 DOF at each node (Quek and Liu, 2003):

$$\mathbf{T} = \begin{pmatrix} C & S & 0 & 0 & 0 & 0 \\ -S & C & 0 & 0 & 0 & 0 \\ 0 & 0 & 1 & 0 & 0 & 0 \\ 0 & 0 & 0 & C & S & 0 \\ 0 & 0 & 0 & -S & C & 0 \\ 0 & 0 & 0 & 0 & 0 & 1 \end{pmatrix} \tag{D.7}$$

where C and S represent the cosines and sines of each elements angle between local and global coordinate systems.

E Time–stepping solution method

The following is an algorithm for Newmark's time–stepping solution method (Chopra, 2007). Different values for γ and β control which method it is. The method used here is the average–acceleration method, where $\gamma = \frac{1}{2}$ and $\beta = \frac{1}{4}$. All variables used in the algorithm have been defined in the text above and have the same meaning here, subscript zero means initial values.

1.0 Initial calculations

1.1 $\ddot{\mathbf{r}}_0 = \mathbb{M}^{-1}(\mathbb{F}_0 - \mathbb{C}\dot{\mathbf{r}}_0 - \mathbb{K}\mathbf{r}_0)$.

1.2 Select Δt.

1.3 $\hat{\mathbb{K}} = \mathbb{K} + \frac{\gamma}{\beta\Delta t}\mathbb{C} + \frac{1}{\beta(\Delta t)^2}\mathbb{M}$.

1.4 $\mathbf{a} = \frac{1}{\beta\Delta t}\mathbb{M} + \frac{\gamma}{\beta}\mathbb{C}$; and $\mathbf{b} = \frac{1}{2\beta}\mathbb{M} + \Delta t\left(\frac{\gamma}{2\beta} - 1\right)\mathbb{C}$.

2.0 Calculations for each time step, i

2.1 $\Delta\hat{\mathbb{F}}_i = \Delta\mathbb{F}_i + \mathbf{a}\dot{\mathbf{r}}_i + \mathbf{b}\ddot{\mathbf{r}}_i$. Where $\Delta\mathbb{F}_i = \mathbb{F}_i - \mathbb{F}_{i-1}$.

2.2 $\Delta\mathbf{r}_i = \hat{\mathbb{K}}^{-1}\Delta\hat{\mathbb{F}}_i$.

2.3 $\Delta\dot{\mathbf{r}}_i = \frac{\gamma}{\beta\Delta t}\Delta\mathbf{r}_i - \frac{\gamma}{\beta}\dot{\mathbf{r}}_i + \Delta t\left(1 - \frac{\gamma}{2\beta}\right)\ddot{\mathbf{r}}_i$.

2.4 $\Delta\ddot{\mathbf{r}}_i = \frac{1}{\beta(\Delta t)^2}\Delta\mathbf{r}_i - \frac{1}{\beta\Delta t}\dot{\mathbf{r}}_i - \frac{1}{2\beta}\ddot{\mathbf{r}}_i$.

2.5 $\mathbf{r}_{i+1} = \mathbf{r}_i + \Delta\mathbf{r}_i$, $\dot{\mathbf{r}}_{i+1} = \dot{\mathbf{r}}_i + \Delta\dot{\mathbf{r}}_i$, $\ddot{\mathbf{r}}_{i+1} = \ddot{\mathbf{r}}_i + \Delta\ddot{\mathbf{r}}_i$.

3.0 Replace i by $i + 1$ and repeat steps $2.1 - 2.5$.

F Pantograph specs

1.1 Tekniska data för simulering WBL 88 AT ,Flygtoget BM73

Benämning	Del	Data	Enhet	Anmärkning
Toppbygel massa	M_1	2x2,3	Kg	primär massa
Avstånd mellan kolslitskenor	X_1	595	mm	
Effektiv dynamisk sax massa	M_2	16.5	Kg	sekundär massa
Toppbygelns dämpnings konstant	C_1	10	Ns/m	primär
Saxens dämpnings konstant	C_2	0	Ns/m	sekundär
Saxens dämpnings konstant	C_3	63,5	Ns/m	sekundär
Saxens fiktion	U_1	17	N	
Fjäderkonstant för toppbygel	K_1	3100	N/m	
Statiskt upptryck	F_1	60	N	
Fjäderväg från A till B	-	35	mm	för primär massan
Fjäderväg vid statiskt upptryck (F1)	-	12	mm	
Max höjd	-	2,0	m	maximal höjd för strömavtagaren(från viloläge)
Toppbygelbredd		1.8	m	
Längd kolslitskena	-	1,03	m	
Höjd kolslitskena	-	0,039	m	i mitten av kolslitskenan i förhållande till dess ändar
Aerodynamisk uppkraft på toppbygel	F_{a1}	0	N	vindstilla vid 100 km/h
Aerodynamisk uppkraft på saxen	F_{a2}	5	N	vindstilla vid 100 km/h

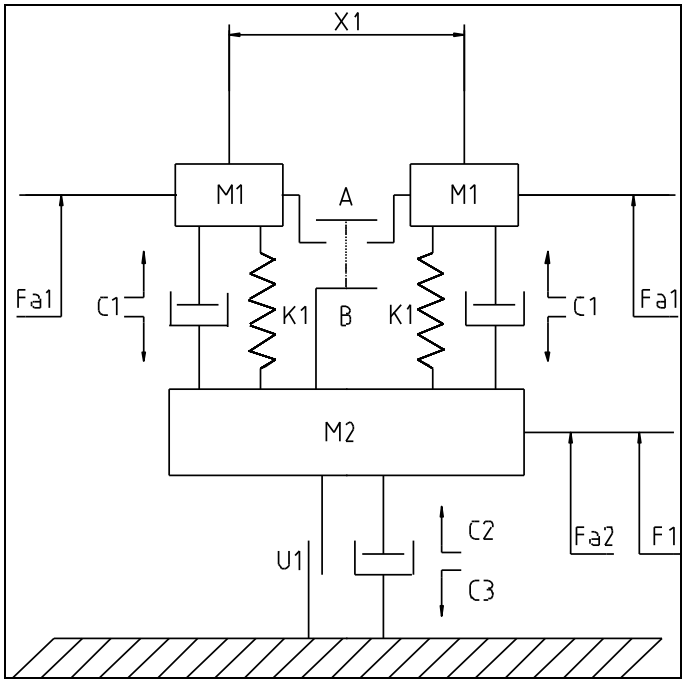

G Zip–file

The thesis is handed in on an electronic format, where there is an option for attachments. The electronic attachment for this thesis is a zip–file containing Matlab program necessary to run the numerical model and a movie file that displays a run of the model. The programs attached are:

- PCrun.m
- Geometry.m
- assembleCat.m
- indadd.m
- Rayleighdamping.m
- WilsonPenziendamping.m
- WBL88.m
- Newmarkint.m
- Themodel.m
- Staticdisplacement.m
- Eigenfrequencies.m
- Elasticity.m
- Dropperdisplacement.m
- PantographPosition.m
- Dynamicthreepoints.m
- Contactforce.m
- Motion.m
- movie.avi